Chapter 2
Presentation of common non destructive techniques

Many experts contributed to Chapter 2. Their list is following

  1 Ultrasounds through transmission Vincent Garnier
  2 Ultrasonic Echo   Martin Krause and Franck Mielentz
  3 Surface waves methods   John Popovics and Odile Abraham
  4 Impact echo   Andrzej Moczko
  5 Impulse response   Andrzej Moczko and Claus Germann Petersen
  6 Acoustic emission   Jean-Paul Balayssac and Masayasu Ohtsu
  7 Ground Penetrating Radar   Johannes Hugenschmidt and Jean-Paul Balayssac
  8 Capacitive technique   Xavier Dérobert
  9 Electrical resistivity measurement Jean-François Lataste
 10 Infrared thermography   Didier Defer and Christiane Maierhofer
 11 Radiography   Jean-Paul Balayssac
 12 Rebound hammer   Markus Fischli and Andrzej Moczko
 13 Pull-out testing   Andrzej Moczko

1 Ultrasounds through transmission

Vincent Garnier

1.1 Physical principles and theory

The ultrasonic method can be applied by the reflection or the transmission of elastic waves in the concrete or on its surface. The first method, called "ultrasonic echo" or "pulse echo" is explained in the next section (§2).

The second is the ultrasonic transmission method (also named "sonic pulse velocity" measurement). It is a common technique used by many companies to

evaluate the concrete in situ and to provide information on the quality of the concrete element. It allows measuring the velocity and attenuation of elastic waves. It consists to send the ultrasonic wave from a transducer "emitter" and to record the signal with a separate transducer "receiver". Typical transducers generate the wave by exciting a piezoelectric disk.

The two transducers are generally identical in geometry and wave frequency range. The typical frequency range used for the concrete is from 20 kHz to 300 kHz. A usual device is proposed with 24 or 54 kHz transducers. The new devices propose higher frequency transducers but their attenuation is important. Pressure waves (P-waves, longitudinal waves) and surface waves (Rayleigh waves) are generally used. Shear waves (S-waves, transverse waves) are exploited only in specific cases.

The velocity C is the most currently and easily evaluated parameter by transmission technique. C is deduced from the measurement of the time of flight t and the distance L that the wave covers in the concrete.

$$C = \frac{L}{t}$$

The attenuation α is deduced from the decrease of the amplitude A_1 and A_2 of the received signal for two paths with two different lengths L_1 and L_2.

$$\alpha = \frac{20}{L_2 - L_1} * \log\left(\frac{A_1}{A_2}\right)$$

The current unit for attenuation is dB/m.

The attenuation measurement is not very easy because the contact conditions between the transducer and the concrete are not fully repeatable. Some new air coupling transducers (avoiding any contact) are in development today.

1.2   Correlation with the mechanical properties

Because the wave propagation is depending on the material mechanical properties, many tests are developed to link the compressive strength f_c or elasticity modulus E with the ultrasonic velocity. Since the propagation is modified by any defect in the material, the measurements can also inform about these defects.

The correlation with material properties can be calibrated with cores extracted from the structure or on a cubic specimen from the same concrete as the structure. For instance, ACI 228 1.R considers that V^4 is proportional to E^2 and to concrete strength. It is however not possible to define a general law. European standard EN13791 considers a polynomial relationship of order 2 between concrete strength and velocity. In a literature study [Evangelista et al., 2003] registered, without being exhaustive, 12 different laws (linear, exponential or power), from 1988 to 2000, establishing a relationship between the compressive strength f_c and the P-waves.

Table 2.1 Usual values of velocity and attenuation of the P-wave in a concrete

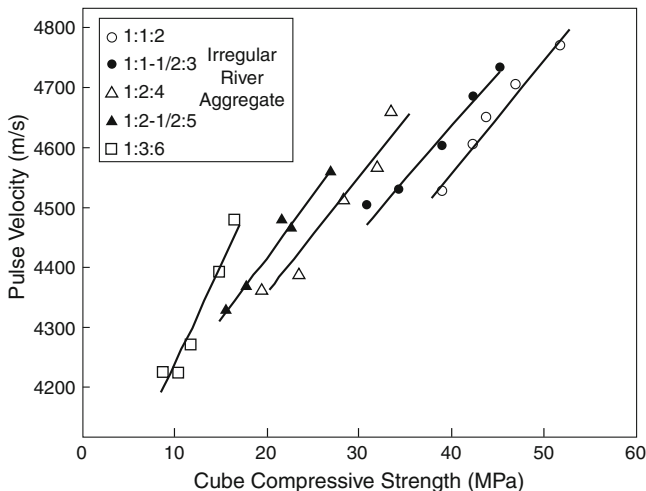| Concrete condition	P-wave velocity (100 kHz)	P-wave attenuation (100 kHz)
Damaged	velocity < 3000 m/s	> 90 dB/m
Sound	velocity > 4500 m/s	< 30 dB/m

Fig. 2.1 Effect of aggregate to cement ratio on the relationship between pulse velocity and compressive strength (after [Naik et al., 2004])

[Popovics, 2006] explains the problem and proposes to work with the surface waves to get an accuracy better than ± 20 percent.

It is suggested to estimate material properties after having fitted a specific correlation with velocity by using multiple regression techniques. One must keep in mind that a lot of parameters influence the ultrasonic velocities: the aggregate size, nature and rate, the ratio aggregate on cement or water on cement, the cement nature, the age of the concrete, the geometry of the tested structure or beam, the curing conditions, the porosity rate, the water contained in the pores and the cracks, the damage and also the rebar.

Typical values of velocity and attenuation are plotted on Table 2.1. These values depend on the wave frequency. So the transducers choice for a test can be very important.

An example of laws depending on the ratio aggregate to cement is given by Fig. 2.1. The figure shows that for a given value of pulse velocity, the higher the aggregate to cement ratio, the lower the compressive strength.

A solution exploited in situ is not to give the absolute value of the velocity but to compare the different zones (damaged or not). That allows defining the most suspect zones of the structure on which it is important to improve the tests or to develop some other complementary tests [Abraham and Dérobert, 2003]. It is possible either to work point by point and to move the two transducers each time, or to move only one of the two transducers. A third possibility is to work with a series

Fig. 2.2 Ultrasonic
Transmission device
with plane coupling probes

Fig. 2.3 Ultrasonic
Transmission device
with plane coupling probes
(Pundit from CNSFarnell)

of transducers for the reception and / or for the emission. In each case, information got on each point is worked separately. It is also interesting to mix and to sum up all the information in order to get an image, for example to describe the structure. That is the ultrasonic tomography that is used to examine cracks, voids and other internal defects [Bond et al., 2000].

Today some new improvements are proposed in the modeling of the wave's propagation by the wave's homogenization, and in the signal analyses as well as in the surface wave applications (without contact and coupling).

1.3 Measuring Equipment and Handling

The typical industrial devices contain (Fig. 2.2 and 2.3):

- An electrical pulse generator (peak voltage from 150 V to 1000 V) and amplifier for the wave,
- an emitter transducer (mostly piezoelectric sometimes without contact). Sometimes the emitted wave is generated by an impact with a ball or a hammer,
- a receiver transducer (only one or several on a line to be precise on the distance value),

- sometimes, an automatic displacement device of ultrasonic displacement to obtain (A, B or C-scan),
- a calibration bar in metal or silica, to calibrate the measurement,
- an oscilloscope to see the signal and measure the time, or only a time calculator.

The transducers are generally plane with contact. To get a better transmission, the coupling is ensured by grease, paste or gel. Sometime the transducers can be bonded directly on the concrete surface. Some transducers include a cone for the tip to get a punctual contact that allows working, for the low frequencies, without coupling. Another specific air coupling transducers (piezo or capacitive) with specific amplifiers are developed to work without contact at a distance ranging from some millimeters to some centimeters between the transducer face and the concrete element. These transducers are new for NDT on concrete and they get rid of the sensitive problem of coupling. Then they allow working more easily on the attenuation properties. In some research works, the wave propagation can even be measured generated by laser interferometer without contact.

The equipment generally offers the direct digital read-out of transit time, the flaw detection, battery and A-C power, RS-232 output for computer uploading. The calibration can be done with the metallic bar to adjust the time measured or by an internal calibration.

The device can give the calculated P-wave or S-Wave velocity easily by direct reading. The elasticity dynamic modulus E_d or Poisson ratio ν are calculated under some conditions.

To estimate the material properties, the relationships between elastic constants and the velocity of respectively ultrasonic pressure wave V_L and shear wave V_L are derived from equations in an isotropic elastic medium of infinite dimensions:

$$V_L = \sqrt{\frac{E_d(1-\nu)}{\rho(1+\nu)(1-2\nu)}} \qquad V_T = \sqrt{\frac{E_d}{2\rho(1+\nu)}}$$

where:

E_d = the dynamic elastic modulus (MPa)
ν = the dynamic Poisson's ratio.
ρ = the density (kg/m^3).
V_L = the pressure (longitudinal) wave velocity (km/s).
V_T = the shear wave (transversal) velocity (km/s).

The relation with V_T is difficult to exploit because the shear wave velocity is not easy to determine owing to the multiple scattering in the concrete. For the wave length λ generally used (from 10 to 150 mm), the concrete is a very heterogeneous material that generates a lot of scattering of the ultrasonic waves and that perturbs the shear waves exploitation. So the first relation is generally used to calculate the dynamic modulus E_d. with a prior assumption on the Poisson ratio and the measurement of the density.

1.4   Guidelines, Recommendations

AIEA, Guidebook on non-destructive testing of concrete structures, Vienna 2002

ASTM C 1383 Test method for measuring the P-wave speed and the thickness of concrete plates using the impact echo method Annual Book of ASTM Standards Vol. 04.02, ASTM, West Conshohoken, PA, USA, 2000

ASTM C 597 – 83 (91) Standard test method for pulse velocity through concrete

BS 86 (British Standards) Recommendation for the measurement of velocity of ultrasonic pulses in concrete, Testing concrete, BS 1881 : Part 203, 1986

D6760-02 Standard Test Method for Integrity Testing of Concrete Deep Foundations by Ultrasonic Crosshole Testing

EN 12504-4, Testing concrete in structures – Part 4: Determination of ultrasonic pulse velocity, Norme Européenne

1.5   Common techniques and devices

The common devices are used for concrete quality control and for the evaluation of the dimensions of structures. Under some conditions, they can also correlate concrete strength to standard velocity measurement, using correlation laws that are not universal.

If their sizes are important enough, it is possible to identify honeycombs, voids, frozen concrete, cracks, delamination and other non-homogenous areas like those resulting from thermal, mechanical or chemical damages in concrete. In a recent French research program [Balayssac et al., 2008], the influence on the velocity and attenuation waves of the water saturation rate, porosity, carbonization, chloride content and damage were tested.

An important way to assess the concrete condition is to determine the material variations in space or over time (this is mainly used for young age cemetitious materials).

Ultrasonic testing can be applied to new and old structures, columns, walls, fire damaged areas, hydroelectric structures, bridge, piles, pipes, prefab and prestressed beams, cylinders and other concrete forms.

For transmission of P-waves, the emitter generates the signal and starts the time counting. The receiving transducer detects the arrival time of the leading vibration. For the low frequencies and if the length of the wave path is known, it is possible to measure the velocity in three directions depending on the accessibility of the structure faces [Farnell, 2008].

* between opposite faces (direct transmission), see Fig. 2.4
* between adjacent faces (semi direct transmission), see Fig. 2.5
* on a single face (indirect or surface transmission), see Fig. 2.6

The direct technique is the most accurate and must be chosen when possible. The difficulty is to access to the two sides. If the concrete is reinforced, the best solution is to locate first the rebar with an electromagnetic device and thus to test between them.

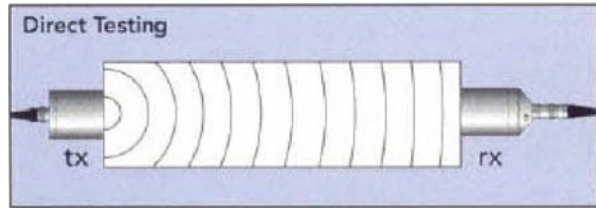**Fig. 2.4** Direct transmission ultrasonic testing

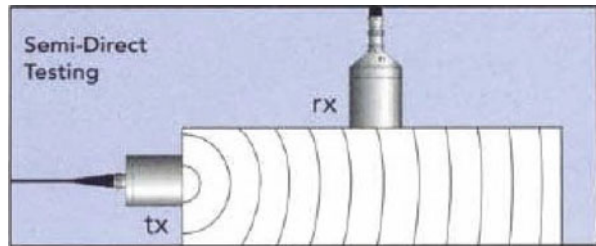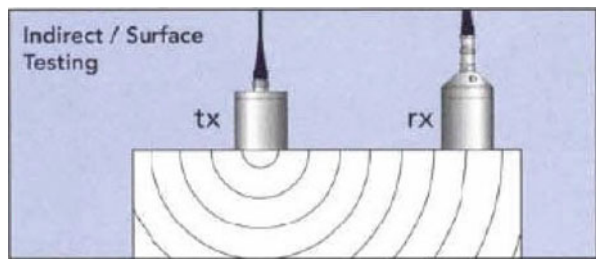**Fig. 2.5** Semi direct transmission ultrasonic testing

Fig. 2.6 Indirect transmission ultrasonic testing

The semi direct technique is easy to use but the distance between the two transducers is less well defined than the previous case. Its accuracy is generally below the first.

The indirect or surface technique is easily exploitable in situ with different configurations. The access to only one face is simpler.

The three types of control are commonly used on site today.

To detail the indirect method, it must be said that the emitter is fixed and the receiver is placed at different positions (x1 to x4 on Fig. 2.7) on a line and the signal is recorded for each of them. The minimum length x1 inspected has to be more than 5 times the mean aggregates dimension. The general value is 100 mm or 150 mm. The time is plotted versus the distance (Fig. 2.8). This distance between the emitter and the receiver is measured from centre to centre of the transducers. The slope of the straight line gives the wave velocity. The indirect wave velocity is lower than the direct one by about 5 % to 20 %, the difference depending on the concrete type. To increase the measure quality, it is possible to work with a series of fixed transducers instead of moving a unique transducer.

By indirect transmission, the slope analysis allows detecting the presence of voids or cracks as presented in Fig. 2.9. The P-wave follows the shortest path, it is
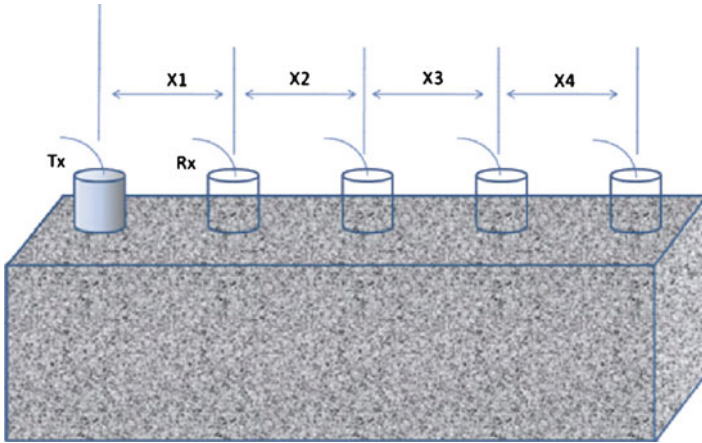
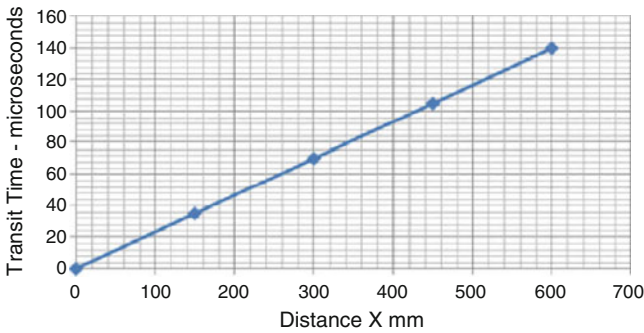**Fig. 2.7** Indirect method principle

Fig. 2.8 Time of flight versus distance

diffracted by the crack tip and transmitted to the receiver. A change of slope on the curve "time-distance" can give the position and the depth of the crack. However, in practice, the measurement is sometimes uneasy to work out because the partial closing or filling of the crack.

By indirect transmission, the slope analysis also allows to detect the presence of damaged layer as presented in Fig. 2.10. The variation of the slope can give the depth of the affected zone.

These evaluations can be perturbed by usual conditions on site:

* if the contact between the transducers and the concrete is irregular

* if the wave length is not adapted to problem: when the lengthwave is too high, small cracks cannot be detected; reversely, when the lengthwave is too small, an important attenuation increases the uncertainty

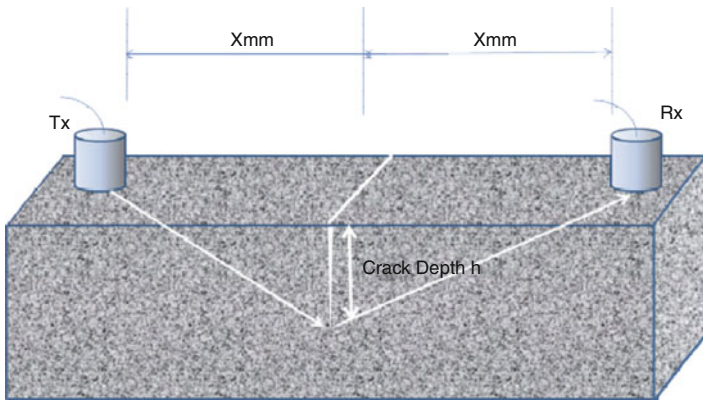* if some water and /or some particles fill up the cracks, the diffraction doesn't occur on the crack tip.
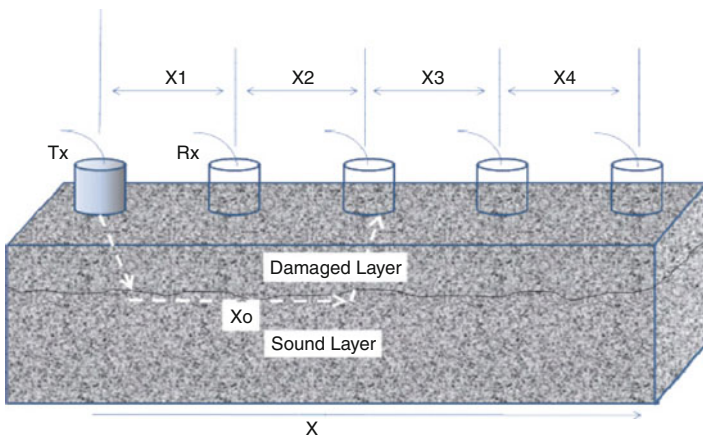
Fig. 2.9 Cracks detection principle

Fig. 2.10 Damage detection principle

1.6 Reliability and limitation of results

Many parameters influence the wave velocity. The effect of some of them is known and can be corrected in the best case, but in industrial conditions, the best way is often to work by comparisons between the different points of measurement or with cores extracted from the structure.

The standards give information on how to adjust the velocity value as a function of the lateral dimension of the concrete elements, of the rebar presence, of the moisture and temperature.

Many bias factors exist:

– The coupling conditions highly change the amplitude of the wave, they can disturb the attenuation evaluation and sometimes the velocity estimation.
– The lateral boundaries of the tested structure can generate a new type of waves that modifies the velocity of the apparent P-wave analyzed (reflected or Lamb waves).
– The presence of reinforcing steel bars can accelerate the wave if they are in the same direction as the waves. They can also scatter the waves and decrease their velocity when they are perpendicular.
– The moisture, the porosity and the temperature of the concrete modify the velocity up to 20 %.
– The choice of the transducers (mainly frequency and size) can modify the velocity by 15 or 20 %.
– The concrete nature (aggregate size, cement nature, porosity rate and density) modify the velocity from 5 to 20 %

In any case, the technician must be qualified.

To conclude, the ultrasonic inspection by transmission is a technique accessible that can provide information on the concrete condition. In the simple case, it enables comparisons between different types or zones of concrete in a structure. If care is devoted to control some experimental parameters on site, it is possible to optimize the experimental device and the procedure to get more information attached to the material properties.

1.7 Developments

Today a lot of developments and researches are developed in order to help the operator to extract better and more reliable information from the transmitted ultrasonic waves.

– The tomography that is used in situ improves the quantity of information concerning the defect detected or the zone tested. It allows confirmation and increases the capability of detection.
– The Spectral Analysis of surface Waves analyzes the propagation mode of the dispersive waves (Rayleigh and Lamb) that propagate just below the surface or in plates. Derived from this method, the Multichannel Analysis Surface Waves method allows the assessment of delaminations.
– The cover concrete is the first protection of the structure regarding all the aggressions from the environment. It can be assessed by analysing the Rayleigh waves with automatic devices.
– Modeling of the waves' propagation is developed by some laboratories that are working on the concrete homogenization. The objectives are to understand the propagation in such a heterogeneous material and to predict the velocity and attenuation of the waves. Some Finite Element Methods are also developed in this way.

References

Abraham O., Dérobert X. (2003) Non-destructive testing of fired tunnel walls: the Mont-Blanc tunnel case study, NDT&E Int., 36, 411–418.

Balayssac J.P., Arliguie G., Laurens S. (2008) Évaluation de l'état des ouvrages en béton par combinaison de techniques non destructives, Proc. COFREND days, Toulouse, May 2008.

Bond L.J., Kepler W.F., Frangopol D.M. (2000) Improved assessment of mass concrete dams using acoustic travel time tomography (Part I-Theory, Part II-Application), Constr. Build. Mat., 14, 133–156.

Evangelista A.C., Shehata A.I., Shehata L. (2003) Parameters That Influence The Results of Non-Destructive Test Methods for Concrete Strength, NDTCE Berlin, 2003.

Farnell (2008) Ultrasonic pulse velocity testing, Technical reference manual. CNS Farnell, August 2008.

Naik T.R., Malhotra V.M., Popovics J.S. (2004) CRC Handbook for NDT of Concrete, Second edition, Carino N.J. and Malhotra V.M., eds Boca Raton, Florida, CRC press 2004.

Popovics J.S. (2006) American Society for Nondestructive Testing, Analysis of the Concrete Strength versus Ultrasonic Pulse Velocity Relationship, 9 p.

2   Ultrasonic Echo

Martin Krause and Franck Mielentz

2.1   *Physical principles and theory*

Shortly described, the ultrasonic echo method (also named pulse echo method) measures the time of flight of elastic pulses, which are reflected at internal interfaces or are backscattered at internal objects, respectively. This method overcomes the drawback of ultrasounds through transmission that requires access to both surfaces. From the measured time of flight and the pulse velocity known from calibration measurements, the depth of the scatterers and interfaces can be deduced. Pressure waves (P-waves, longitudinal waves) as well as shear waves (S-waves, transverse waves) are used for NDT of concrete elements. For concrete, the typical frequency range is from 25 kHz to 300 kHz.

Generally the wave propagation velocity for a monochromatic wave (phase velocity) can be written as:

$$c = \lambda * f \tag{1}$$

where c is the wave velocity, λ is the wavelength and f is the frequency.

Pressure waves (P-waves) have a typical wave velocity of 4000 m/s in concrete, thus for a frequency of 100 kHz the wavelength is 40 mm.

The reflection R of P-waves at planar interfaces is defined by the difference of the acoustic impedance for two materials, whereas the acoustic impedance is

a material property defined as the density ρ multiplied by P-wave phase velocity:

$$R = \frac{z_2 - z_1}{z_2 + z_1} \tag{2}$$

where z is the acoustic impedance z in material 1 and 2, respectively, with:

$$z = \rho\, c \tag{3}$$

Since the acoustic impedance of air can be neglected compared to concrete, the reflectance at air interfaces is R = 1. When the impedance of material 2 is greater than for material 1, the sign of R is positive. When the acoustic impedance of the material 2 is smaller than for material 1, the sign of R is negative, that means that a phase jump of $\phi = 180°$ appears for the reflected wave pulse. This effect allows to distinguish between the reflection at the concrete/steel interface and reflection at the concrete/air interface.

Generally ultrasonic pulses are produced and measured with piezoelectric probes. Thus the measured AC voltage is proportional to the sound pressure P_s in the material, which is defined by:

$$\mathbf{P}_s = \rho\, c\, \varpi\, \zeta = z\, \varpi \zeta \tag{4}$$

where z is the acoustic impedance (see (3)), ϖ is the angular frequency (with $\varpi = 2\,\pi\, f$) and ζ is the amplitude of particle oscillation.

The base for ultrasonic echo applications for concrete are low frequency transducers (probes, centre frequency around 100 kHz), which must transmit broadband pulses. After basic research in the 1990's, transducers and equipment were developed, which allow measuring the thickness of concrete elements even in single point measurement, if the site conditions are not too difficult. This means for instance not too dense reinforcing layers or not too bad surface conditions.

In order to measure the dimension of a reflecting area, several points can be combined for providing an imaging result. This can be done by measuring lines manually or by an automated scanning.

The ultrasonic echo method has the potential to locate and identify discrete defects or objects if sufficient focusing is achieved by the transducers. Because the concrete contains aggregates and air pores, structural noise always appears, reducing significantly the signal to noise ratio. In order to overcome this problem, special transducers and imaging methods based on array techniques and synthetic aperture have been developed (and are continuously ameliorated) in research and development activities.

2.2   *Measuring equipment and handling*

For single point measuring, there are generally two types of equipment: transducers with planar contact on the measuring surface and dry contact transducers

Fig. 2.1 Array consisting
of 10 broadband planar
transducers for the frequency
range of 80 kHz to 200 kHz

(point contacts). An instrument or development equipment contains four general
features:

- A Electrical Pulse generation (AC Peak Voltage between 150 V and 1000 V)
- A piezoelectric Transducer
- A receiving unit and an amplifier
- Displacement device of ultrasonic measuring curve (amplitude vs. time; A-scan)
  and indication of time of flight or reflector depth.

Since the mid-1990s broadband transducers have been developed in the frequency
range of 20 kHz to 300 kHz, for P-waves as well as for shear waves. Fig. 2.1 shows
as an example ten pressure wave transducers arranged in a template to be applied as
an array. They have a planar surface, which means that coupling agent is necessary
(e.g. vaseline or glycerine) [Krause et al., 1997].

Low frequency shear wave transducers developed around 2000 have two main
advantages: firstly the shear wave is directly generated by a ceramic tip pressed to
the surface. There is no need for a delay wedge or coupling agent (dry contact).
Thus, secondly, the polarisation axis of the shear waves can directly be aligned
corresponding to the axes of symmetry [Kozlov et al., 2006].

Fig. 2.2 depicts some examples of dry contact transducers, which are available
as single transducers and transducer arrays in different arrangements. The fre-
quency ranges from 30 kHz to about 80 kHz (i.e. a wavelength range from about
100 mm to 33 mm for a typical wave velocity of C_s = 2700 m/s in concrete). For
manual measurements an electronic interface can be used. The probe has twelve
transmitting and twelve receiving transducers, which are working simultaneously.

For developing and optimizing low frequency ultrasonic techniques, often
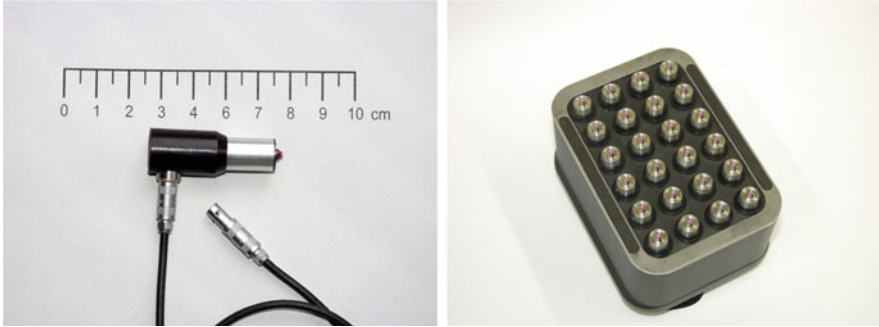arbitrary pulses are applied. A typical equipment is shown in Fig. 2.3.

Fig. 2.2 left: Point contact transducer, right: T/R probe with 12 transmitting and 12 receiving point contact transducers
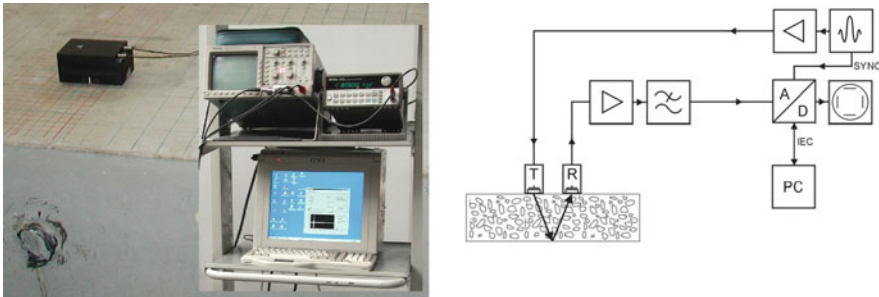

Fig. 2.3 left: Excitation of transmitting/receiving (T/R) transducer with arbitrary function generator, power amplifier (not imaged) and oscilloscope, right: Principle sketch for working with arbitrary pulses and data processing

Fig. 2.4 Ultrasonic Echo device with plane coupling probe (for thickness measurement of screed)

Two typical commercially available instruments are depicted in Figs. 2.4 and 2.5, left. Both permit point measurement with preferable separate transmitter and receiving transducers. For equipment 1, these are plane coupling transducers of the
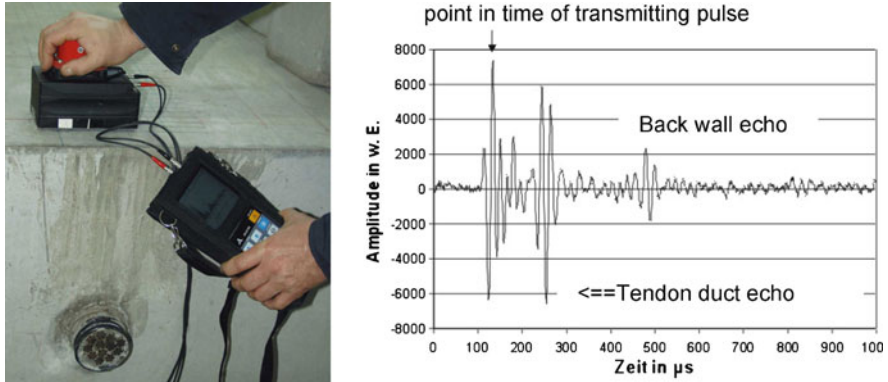
Fig. 2.5 left: Ultrasonic Echo Device with dry contact shear wave transducer and handheld electronic device, right: Ultrasonic time curve (Ultrasonic A-Scan)
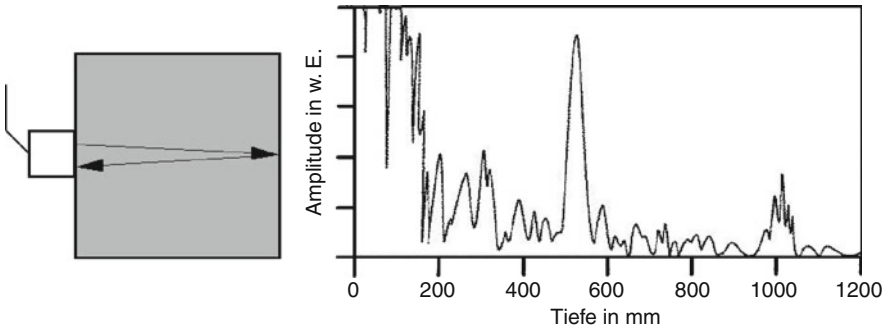

Fig. 2.6 Thickness measurement of concrete slab using a single probe in frequency range of 100 kHz

type explained above. Instrument 2 is constructed for point contact transducers, mainly for shear waves. Since the transducer tips are made of ceramic, they are simply pressed at the measuring surface without any need of coupling agent. The most frequent application for these transducers are shear waves (transverse waves) with a centre frequency of 55 kHz. The polarisation axis of these waves can be selected by the orientation of the device.

The handling of the electronic part of the device in Fig. 2.3 is similar to the frequently used commercial equipment, which is applied for ultrasonic testing steel in the frequency range between 1 MHz and 10 MHz. Fig. 2.5, right, shows as an example a typical ultrasonic time curve (*A-Scan*, see below) when the transducer is positioned above a tendon duct. The echo signals of the tendon duct and the back wall are visible. Around the origin of the time axis surface wave signals occur.

There are several systems working with the equipment explained in chapter 2. Typical testing tasks are e.g. measuring the thickness of concrete elements (Fig. 2.6)
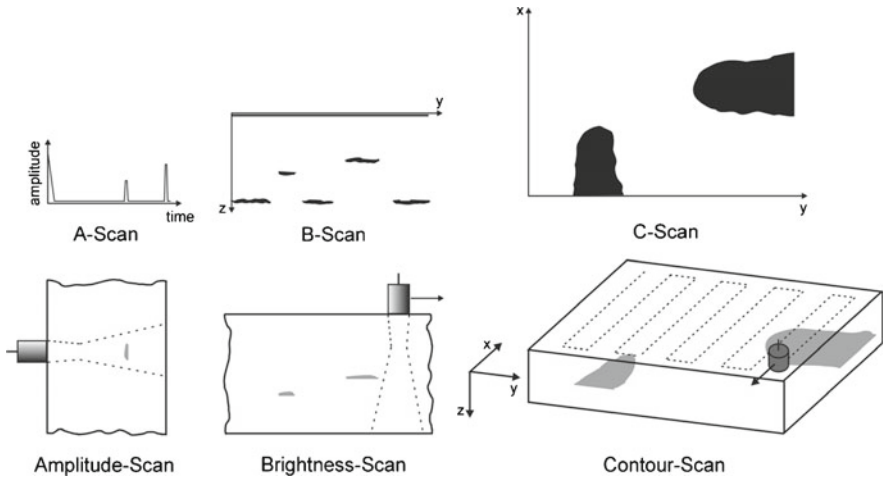
Fig. 2.7 Overview for general utilization of the terms A-scan, B-Scan, and C-Scan in ultrasonic echo measurement

or localizing structural details. In some systems several measuring points can be stored in lines or/and 2D-Datasets for displaying them B-scans or C-scans, respectively ([Kozlov et al., 2006],[Krause et al., 1997]).

2.3 Data processing: display and imaging techniques

Generally the visualisations of ultrasonic measurement results are named A-scan, B-scan and C-scan. To say with usual words, these are respectively: the ultrasonic point measurement in the time domain (A-scan), an ultrasonic cross- or longitudinal section (B-scan) or a depth section, parallel to the surface (C-scan). These three types of visualisation are demonstrated in Fig. 2.7.

Especially in low frequency ultrasonic technique, a more general application of the terms is used.

- **A-scan**: Amplitude of the measured signal vs. time (output voltage proportional to the sonic pressure) vs. time. Three types of A-scans are used: HF-signal (not rectified), rectified and calculated envelope function. Fig. 2.5 (right) shows the HF Signal of an echo measurement of a tendon duct in a concrete slab.
- **B-scan**: Amplitude of the time signal along the measuring (or a selected) axis showing the depth information of the reflection (alternatively named: longitudinal or cross section of ultrasonic amplitude. It consists of a line (x-axis) of several A-scans and corresponds to the Radargram for Radar or sonogram of geophysical experiments. It is usually shown in a false colour (or grey scale) representation. The y-axis is either the time of the receiver after pulse excitation or the depth after calibrating the sound velocity (Fig. 2.8b)
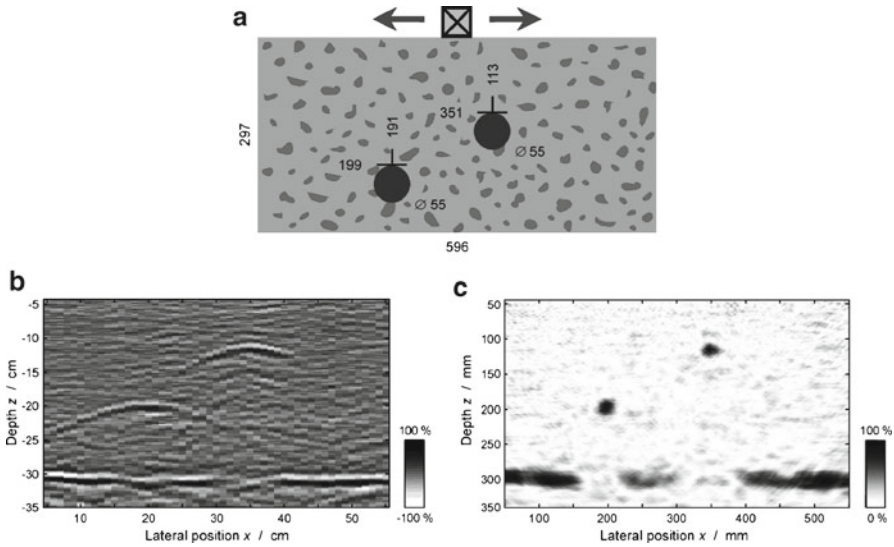
Fig. 2.8 B-scan of a measuring line above to bore holes in a concrete specimen. (**a**) plan speci-
men, (**b**) Ultrasonic B-scan of measuring line, axes in mm, (**c**) Reconstruction with SAFT (Linear
Synthetic Aperture Focusing Technique, here 2-dimensional)

(after [Schickert et al., 2003]).

- **C-scan**: Amplitude of the measured signal parallel to the surface at a specific
  depth (alternatively named: depth section of ultrasonic amplitude). It corresponds
  to the "time slices" in case of Radar results.

For physical reasons, transducers having a diameter in the order of the wave-
length or smaller produce a wave field with a large angle of aperture containing
pressure and shear waves. For this reason ultrasonic measuring and evaluation
methods known from material testing and medical diagnosis methods cannot simply
be transferred to concrete testing. Therefore scanning and imaging methods have a
special relevance in low frequency applications.

The measuring procedure depends on the testing task. For instance, for thickness
measurement of concrete elements which are not densely reinforced, simple point
measurements with handheld equipment can be applied. But in most cases the eval-
uation of data requires imaging methods, which means that the data are measured in
lines or 2-dimensional grids.

In civil engineering the direct representation of measuring data is mostly applied
for planar objects (e.g. layered structures) or wooden elements (timber). For more
sophisticated testing problems, where spatial resolution is of importance, the results
are calculated from linear ore planar measured data sets. For this, several approaches
of reconstruction calculation on the base of synthetic aperture exist (*SAFT: Synthetic
Aperture Focusing Technique*).

Synthetic aperture techniques offer a flexible way of focusing. A synthetic aper-
ture imitates a large transducer by sampling its area at many points. This can be done

either by an array of transducers measuring simultaneously, or by a single transducer approaching the aperture points in succession. Moved arrays, a combination of both, are also possible. Apertures considered here are linear or planar representing a large line or rectangular transducer, respectively [Schickert et al., 2003].

For focusing the pulse-echo measurements at the synthetic aperture, the received signals are processed using the SAFT-algorithm. The SAFT-algorithm focuses the received signals to any point of the reconstructed image by coherent superposition. In this way, a large virtual transducer with variable focus is synthesized. A high-resolution image results, which is two-dimensional (2D-SAFT) for the case of linear aperture, and three-dimensional (3D-SAFT) for the planar aperture. 2D-SAFT-images are B-scan cross sections, 3D-SAFT-images are often displayed as B-scan or C-scan sections through the three-dimensional data field.

In Fig. 2.8c) a simple example of 2D SAFT reconstruction is demonstrated for ultrasonic point measurements along a line of the specimen containing two drilled holes in concrete (already mentioned for the description of the B-scan (Fig. 2.8b). Fig. 2.8c) depicts the result of a time domain reconstruction calculation resulting in imaging the top side of the holes at correct location and depth (example from [Schickert et al., 2003]). Another kind of reconstruction calculation is based on inverse scattering theory applying Fourier-Transform-SAFT (FT-SAFT) and is better suited for three-dimensional imaging [Mayer et al., 1990].

Ultrasonic elastic wave propagation in inhomogeneous materials can also be modelled by *EFIT (Elastodynamic Finite Integration Technique)*. Here all elastic material properties as well as wave mode conversions are considered down to the mm scale [Mayer et al., 1990]. Comparing reconstruction results of synthetic data obtained from such elastic wave equations and real experimental data enables a much better understanding of the complex scattering processes in concrete. This may enhance the reliability of test results ([Mayer et al., 1990], [Krause et al., 2009]).

2.4   Guidelines, Recommendations

Merkblatt für Ultraschall-Impuls-Verfahren zur Zerstörungsfreien Prüfung miner-
    alischer Baustoffe und Bauteile (B4), Deutsche Gesellschaft für Zerstörungsfreie
    Prüfung e.V., Berlin (1999)

For pulse velocity (not echo)
ASTM C 597 – 83 (91) Standard test method for pulse velocity through concrete
DIN EN 13296 Determination of ultrasonic pulse velocity (2004)

2.5   Reliability and limitations

There are additional points to be taken into account, when applying the equipment described in §2.2.

The performance of ultrasonic echo measurement for concrete elements has been growing very much since the beginning of the century. The equipment is rather easy to handle and procedures without coupling agent facilitate the measuring process. Nevertheless during training (basic instructions) the basic knowledge about ultrasonic methods in the low frequency range should be communicated.

The physical parameter to be measured is the time of flight (transit time) of the exited ultrasonic pulse in the concrete. This parameter allows calculating the depth of the reflector. There are mainly three possibilities for measuring it:

1) Calibration at a point of known thickness of the building element,
2) Taking a core of sufficient diameter and measuring the wave velocity through transmission mode (the radius has to be significantly larger than λ),
3) Measuring the wave velocity of subsurface waves (longitudinal or shear waves corresponding to the applied wave mode). The homogeneity of ultrasonic wave velocity typically varies between about 2 % (for very homogeneous concrete) and 5 % (typical values, exceptions are possible).

Using the ultrasonic echo method one measures one or several reflectors/ scatterers inside the concrete element. If it is an air-filled layer it leads to a total reflection of the ultrasonic waves. Because of the concrete heterogeneity, it may be difficult to distinguish actual defects. Large aggregate have a significant scattering effect, preventing the use of a too high frequency. Because of time frequency dependent attenuation and structural noise the pulse form depends on the length of the ray path in concrete. For concrete, the measurement from the maximum of the transmitting pulse to the maximum of the echo pulse seems to be the most appropriate way. Measuring from slope of transmitting to echo pulse is only recommended in case of weak structural noise.

From all those influences on the depth value, the uncertainty of the result has to be estimated.

All low frequency transmitting transducers produce surface waves, which are captured by the receiver. These causes disturbing signals in the beginning of the measured time curve (compare Fig. 2.5, right, time range typically 50 µs to 100 µs after excitation). This is the reason, why the reliable measuring range of most equipment is limited. Another reason for that limitation is the wavelength in concrete, which is in the order of 30 mm to 60 mm for the most applications.

Especially when using dry contact transducers, users must be carefully with interpretations of single point results in case of bad surface conditions. At points with a rough surface, the transducers may oscillate in an undefined way, which will lead to misinterpretation in the time signal.

In the frequency range used for concrete the wavelength is mostly comparable to the transducer dimensions. The consequence is that not only the desired wave mode is transmitted in the concrete, but also shear waves and Rayleigh waves. The angle distribution of the applied transducers and the possible mode conversions in the concrete element should be taken into account for a proper interpretation of the results.
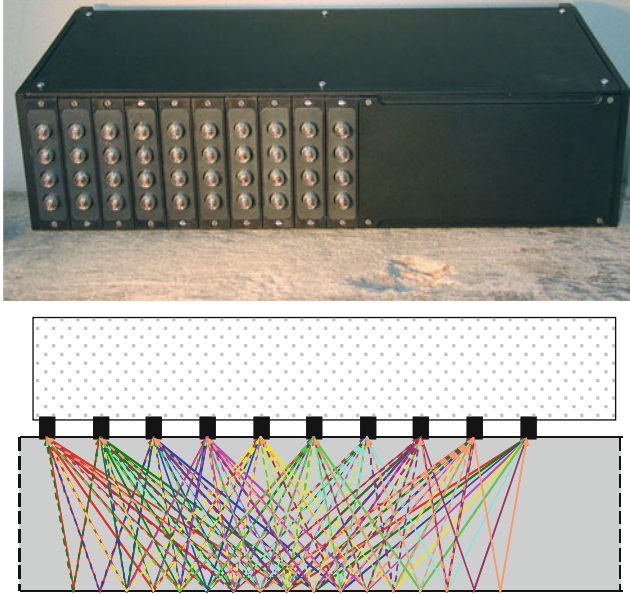
Fig. 2.9 Linear array with dry contact transducers (top), principle of data aquisition (bottom)

2.6   Developments

2.6.1   Linear Array

For automated measurement of larger surface areas linear arrays with multistatic triggering are available ([Kozlov et al., 2006], [Drinkwater and Wilcox, 2006]) (Fig. 2.9). Together with reconstruction calculation 3D imaging of section of building elements can be obtained very fast [Krause et al., 2008b].

Other approaches use differently controlled sensor systems [Schickert et Hillger, 2009].

An innovative device consists of 10 lines à 4 dry contact shear wave 50 kHz-transducers [Krause et al., 2008]. The distance of the lines is 35 mm in the current modification. The transducers and the electronics are mounted in a handheld box easily to be applied at concrete surfaces (Fig. 2.9 top). The ten lines are switched as a multistatic array, meaning that one line acts as transmitter, and all others as receiver, then the second as transmitter, and so forth as shown in Fig. 2.9 bottom. The data transfer is organized in the way that the whole data set is measured and stored in less than 1 second per location.

The data measured along a line can be combined to one data set and evaluated with fast FT-SAFT (Synthetic Aperture Focusing Technique) reconstruction calculation. Together with imaging technique, the scatterers and reflectors in the volume of interest can be analysed quickly on site with cross and longitudinal sections, as well
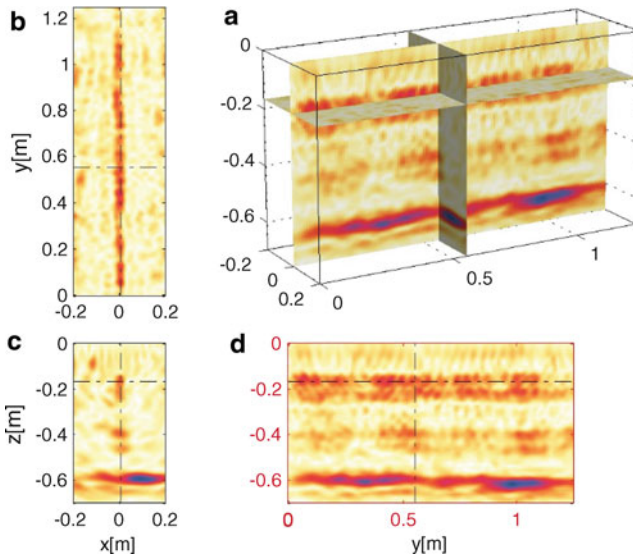
Fig. 2.10 Example of measurement with linear array and 3D imaging with FTSAFT (case of a cross girder bridge [Taffe et al., 2005]) (**a**) Cuboid of the reconstructed volume, with different sections: (**b**) Depth section (C-scan), (**c**) Cross section (B-scan parallel x), (**d**) Longitudinal section (B-scan parallel y)

as depth sections and phase evaluation. There are different SAFT approaches for evaluation (2- and 3-dimensional).

In Fig. 2.10 one practical application is presented as an example. The aim was to localise tendon ducts in a cross girder, which is 60 cm thick. The data were measured along a line (length 1.16 m) with a 2-cm step width (orientation of the array is perpendicular to the measuring line).

The result was obtained with a research version of 3D-FT-SAFT reconstruction and is depicted in Fig. 2.10 [Krause et al., 2008]. The cuboid at the right (a) represents the reconstructed volume (surface: 0.40 m x 1.26 m, depth: 0.70 m). The other parts of the graph represent the different sections, which can be interactively adjusted by three planes.

2.6.2   Special Techniques based on the Ultrasonic echo principle

The ultrasonic echo methods for application in civil engineering are continuously ameliorated by several research and development activities. In the following only few examples can be briefly mentioned. For some of the subjects more examples are described in the corresponding chapters. The main points are:

- Automated scanning of large surface areas (see Fig. 2.11 [Krause et al., 2006])
- 2D and 3 D imaging with reconstruction calculation (SAFT) ([Krause et al., 2006], [Krause et al., 2008a])

Fig. 2.11 2D scanner working with linear drives and a pneumatic system to press the point contact transducers without coupling agent (BAM) [Beutel et al., 2006]

- Interpretation of the phase of the receiving signal in order to characterize the type of a reflector (steel or air) => investigating of tendon ducts ([Krause et al., 2008a], Krause et al., 2009], see also this book, Chapter 6)
- Application of contactless sensors as Laser Interferometer, imaging of ultrasonic wave propagation [Algernon et al., 2008]
- Application of air coupled ultrasonic transducers [Krause et al., 2008b].

Several testing problems are now solvable with common techniques, others with help of synthetic aperture methods (reconstruction calculation, SAFT). Numerous testing tasks are in the intermediate state between research and systematic application. The uncertainty of the results depends on details of the construction work and the site condition. Several parameters influence the wave propagation in the concrete. These are: the type and density of reinforcing bars, the concrete composition (aggregates and pores), the mechanical properties and the surface conditions. Each investigation corresponds to a specific structure or building element and it is mandatory to calibrate the measurements for reliable results. Here it is useful to describe the capability of the methods using examples of successful NDT results, mainly at test sites.

References

Algernon D., Gräfe B., Mielentz F., Köhler B., Schubert F. (2008) Imaging of the Elastic Wave Propagation in Concrete Using Scanning Techniques: Application for Impact-Echo and Ultrasonic Echo Methods, J. Nondestructive Evaluation, 2, 1–3, pp. 83–97.

Beutel R., Reinhardt H.-W., Grosse Ch., Glaubitt A., Krause M., Maierhofer Ch., Algernon D., Wiggenhauser H., Schickert M. (2006) Performance Demonstration of Non-Destructive Testing Methods. In: Proc. 9th European Conf. on NDT, September 25–29, 2006, Berlin: DGZfP, BB 103-CD, Tu.3.2.2.

Drinkwater B.W., Wilcox P.D. (2006) Ultrasonic arrays for non-destructive evaluation:a review, NDT&E 39, 525–546, Elsevier.

Kozlov V.N., Samokrutov A.A., Shevaldykin V.G. (2006) Ultrasonic Equipment for Evaluation of Concrete Structures Based on Transducers with Dry Point Contact. In: Al-Quadi, I. and G. Washer (eds.); Proc. NDE Conf. on Civil Engineering, 14.-18. August 2006, St. Louis, MO, USA, pp. 496–498.

Krause M., Bärmann R., Frielinghaus R., Kretzschmar F., Kroggel O., Langenberg K., Maierhofer Ch., Müller W., Neisecke J., Schickert M., Schmitz V., Wiggenhauser H. Wollbold F. (1997) Comparison of pulse-echo methods for testing concrete. In: NDT&E International Sonderheft Vol. 30, 4, pp. 195–204.

Krause M., Gräfe B., Mielentz F., Milmann B., Friese M., Wiggenhauser H., Mayer K. (2008) Ultrasonic Imaging of Post-tensioned Concrete Elements: New Techniques for Reliable Localization of Grouting Defects, In: Alexander M. G., Beushausen H.-D., Dehn F. and Moyo P. (eds.); Proc. of the Concrete Repair, Rehabilitation and Retrofitting II, ICCRRR 2008, 24.-26.11.2008, Kapstadt, CD-ROM, pp. 521–527.

Krause M., Mayer K., Friese M., Milmann B., Mielentz F., Ballier G. (2009) Progress in ultrasonic tendon ducts imaging. In: Derobert, X. and Abraham 0. (eds.); 7th Int. Symp. NDT in Civil Engineering NDTCE 09, Nantes, F, 30.06.-03.07.2009, Proc. pp. 147–154 and CD ROM (77).

Krause M., Milmann B., Mielentz F., Streicher D., Redmer B., Mayer K., Langenberg K.-J. Schickert M. (2008) Ultrasonic Imaging Methods for Investigation of Post-Tensioned Concrete Structures: A Study of Interfaces at Artificial Grouting Faults and its Verification. J. Nondestructive Evaluation, 27, pp. 67–82.

Krause M., Milmann B., Schickert M., Mayer K. (2006) Investigation of Tendon Ducts by Means of Ultrasonic Echo Methods: A Comparative Study. In: Proc. 9th Eur. Conf. on NDT, September 25–29, 2006, Berlin: DGZfP, BB 103-CD, Tu.3.2.1.

Mayer K., Marklein R., Langenberg K.J., Kreutter T. (1990) Three-dimensional imaging system based on Fourier transform synthetic aperture focusing technique. Ultrasonics 28, 241–255.

Schickert M., Hillger W. (2009) Ein Ultraschall-Multikanal-Messsystem mit SAFT-Rekonstruktion für die Abbildung von Betonbauteilen, In: Berichtsband zur DGZfP-Jahrestagung 2009, 18.-20.05.2009, Münster, Beitrag auf BB 115-CD, Vortrag Mi.1.C.3, 10 Seiten.

Schickert M., Krause M., Müller W. (2003) Ultrasonic Imaging of Concrete Elements Using Reconstruction by Synthetic Aperture Focusing Technique. Journal of Materials in Civil Engineering (JMCE), ASCE Vol. 15, 3, pp. 235–246.

Taffe A., Krause M., Milmann B., Niederleithinger E. (2005) Assessment of foundation slabs with US-echo in the re-use process. In: Alexander M., Beushausen H.-D., Dehn F. and Moyo P. (eds); Proc. Int. Conf. Repair, Rehabilitation and Retrofitting (ICCRRR), 21.-23.11.05, Cape Town, South Africa, pp. 525–530, 2005.

3   Surface waves methods

John Popovics and Odile Abraham

3.1   *Physical principles and theory*

The non-destructive testing (NDT) methods that use ultrasound, acoustics, seismic wave and vibration are based on mechanical wave (also known as "stress wave") phenomena. Two types of mechanical waves can propagate within the body of a solid material: P-waves (also known as pressure waves or compressional waves) and S-waves (also known as shear waves). In addition, Rayleigh surface waves propagate along the free surface of a solid. P-waves travel with highest velocity and Rayleigh waves the lowest.

The characteristics of mechanical waves, such as propagating wave velocity or amount of wave energy reflected from an interface between two distinct media, are a function of the elastic properties and mass density of the solid materials. For example the velocity (speed) that these waves propagate through a material is controlled by the elastic moduli (Young's Modulus, Shear Modulus and Poisson's Ratio) and density of the material. Wave propagation characteristics are also influenced by the severity and location of internal defects such as cracking, honeycombing and delaminations. Thus mechanical wave measurements can be used to provide direct information about the condition of the material or structure under investigation.

Surface-guided waves propagate along the free surface of solid materials. In the case of a single thick layer comprised of homogeneous material, surface-guided P-wave, S-waves and Rayleigh surface waves propagate along the surface. Rayleigh surface waves are used most often for non-destructive evaluation. These waves are most efficiently generated by a dynamic point load, such as an impact event, acting on a free surface of a solid. Unlike P-waves and S-waves, most of the energy of Rayleigh surface waves is relegated to the near surface region, to a depth of approximately one wavelength away from the surface (ACI, 2005). This near-surface behavior can be used to characterize the thickness and stiffness of the individual components of layered structures such as tunnel liners. Surface guided wave propagation is more complicated In the case of solids that are comprised of multiple distinct layers. The wave energy is distributed among distinct propagating wave "modes," which have particular characteristics that depend on the structure and frequency of the wave energy. At limit cases (e.g. thick top layer and high frequency), the modes converge to the more simple behavior of the single half space.

3.2 Measurement equipment and procedure

The following equipment is needed to perform these tests: a wave source, wave detection sensors, and a data acquisition and analysis system, see Fig. 2.1. The wave source is typically provided by a local impact event, for example the impact of a steel sphere or a hammer on the surface of concrete.

The size of the impactor controls the frequency content: smaller size provides higher frequency contents, normally up to 15 kHz. The wave detectors are surface-mounted sensors, usually geophones or accelerometers. These sensors measure the surface motion that is caused by the wave propagation events. The sensors provide an analog voltage output, which is collected over some time period to give a time domain signal. The data acquisition system digitizes the analog signal data, performs the analysis in either the time and frequency domain, and where needed performs the inversion (where the unknown structure of the test material is predicted based on collected wave data) and matching process. These processes can be carried out on PC-based computer systems, using commercially available software platforms.

Fig. 2.1 Principle of Spectral Analysis of Surface Waves technique (after (Krstulovic-Opara et al., 1996)
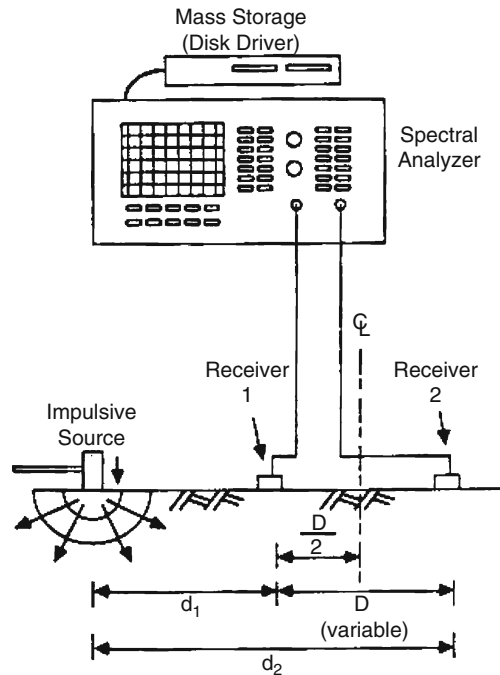
3.3   *Data analysis and interpretation*

Surface-guided waves can be analyzed and interpreted in the time domain or the frequency domain. Basic information about surface-guided wave arrival time and amplitude can be obtained from time domain signals, but this is only effective when the surface wave energy is principally relegated to the top surface, for example for high frequency waves or for a thick top layer. In these cases, the Rayleigh wave velocity of the top layer is obtained from determination for the group velocity arrival between two sensed locations on the surface. Group velocity is the measured wave velocity of an entire discrete packet or pulse of wave energy, as opposed to phase velocity, which is the measured velocity of a single phase value within the wave packet. For so-called "dispersive" materials both group and phase velocity vary with frequency.

Time domain analysis of surface-guided waves can also be carried out using multiple sensors to receive the wave data. This method, often called "seismic refraction", allows the arrival of the first propagating wave front (surface guided P-wave) to be discerned as a function of distance from the wave source. A plot of wave front arrival time vs. distance should have linear form for a homogeneous material. Slope modifications in this plot indicate the presence of a distinct subsurface layer beneath the surface layer (Abraham and Derobert, 2003). When the wavelength of propagating
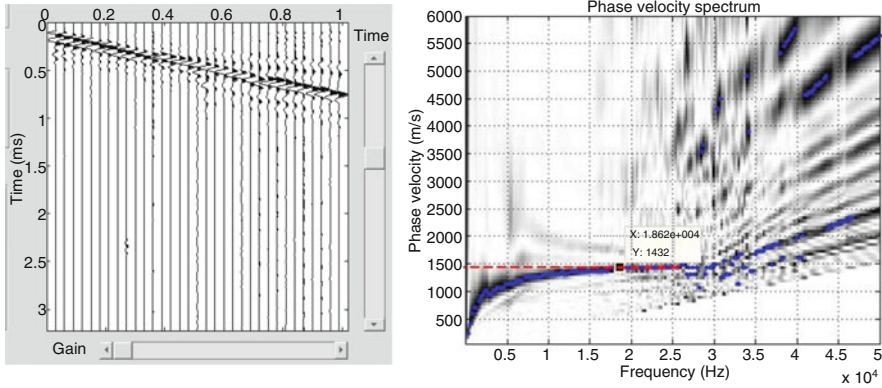
Fig. 2.2 Illustration of multi-channel surface seismic data collected from a concrete slab: time domain signals (left) and constructed phase velocity spectrum using the MASW method (courtesy of Dr. Nils Ryden)

waves is of the order of the layer thicknesses, then frequency domain analysis methods are more appropriate. Two commonly applied frequency domain methods are the spectral analysis of surfaces method (SASW) and the multi-channel analysis of surface waves method (MASW) (Ryden, 2004). One main difference between these two analysis methods is the number of data points (collected wave signals) needed to carry out the analysis. SASW requires only two data points, whereas MASW requires more, on the order of tens of points, depending on the required depth of analysis and resolution. Another important difference is the number of wave modes that are assumed in the analysis. In the case of SASW, only one dominant wave mode is assumed to exist. In the SASW method, the surface wave dispersion curve is computed across a range of frequencies and, if needed, sensor spacing. The dispersion curve is a plot of surface wave phase velocity as a function of frequency. The dispersion curve is obtained from relative phase values, as a function of frequency, of the two measured signals. The obtained experimental dispersion curve is then matched to that computed for a specific layered structure of known thickness and mechanical properties. The computed curve is iteratively adjusted until a best match is obtained between experimental results and that of the model. In the MASW method, the surface/plate wave dispersion curves of all the excited wave modes are computed across a range of frequencies. The dispersion curves are computed by processing of the multi-channel signals that are collected from sensors placed along a line. The presence of multiple wave propagation modes is observed, providing plots of phase velocity dispersion curves for the excited modes. The obtained experimental dispersion phase velocity curves are then matched to those (called pseudo-Rayleigh wave curves) computed for a specific layered structure of known thickness and mechanical properties. The computed pseudo-Rayleigh wave curves are iteratively adjusted until a best match is obtained between experimental results and that of the model (Ryden, 2004). Figure 2.2 illustrates the MASW process in the case of a concrete plate above a subgrade for which a pseudo-Rayleigh wave mode dominates.

3.4 Reliability and limitation of results

Surface wave methods have been applied to obtain estimates of layer thickness and stiffness in a multi-layered system such as pavements and tunnel liners. For example the velocity of measured Rayleigh wave and refracted P-wave modes can be used to evaluate substrata conditions: low velocity values can indicate weak surface conditions due to scaling, spalling or minor cracking. The method can also be applied to detect the extent of a damaged zone near the surface of the tunnel liner, for example that caused by internal fire to a concrete (Abraham and Derobert, 2003).

These methods have the advantage that access to only one surface is needed. When applied properly, the methods provide an estimate of layer thicknesses and mechanical properties, although the accuracy of the thickness estimate is not as reliable as provided by other methods.

The analysis and inversion methods can be numerically intensive, and it may not always approach the correct solution; this is especially true for the SASW method. As a result, a considerable amount of user expertise may be needed to apply the SASW method. Because the sensors require physical contact with the surface of the tested specimen, the methods (using current, standard technology) are not readily applied for rapid scanning. Also, the surface conditions may adversely affect the results, and in some cases of extremely rough surface or limited access cannot be applied. However, recent developments in technology such as wheeled sensor systems and contactless air-coupled sensors may provide some solutions for the contact problem (Zhu and Popovics, 2005). Results collected from tunnels with cast iron liners may not accurately characterize the properties of the substrata.

References

Abraham O., Dérobert X. (2003) Non-destructive testing of fired tunnel walls: the Mont-Blanc tunnel case study, NDT&E International, Volume 36, pp. 411–418.

ACI Committee 228 (2005) Non-destructive test methods for concrete, Committee Document 228.2R, American Concrete Institute, Farmington Hills, MI.

Krstulovic-Opara N., Woods R.D., Al-Shayea N. (1996) Nondestructive Testing of Concrete Structures Using the Rayleigh Wave Dispersion Method, ACI Materials Journal, V. 93, No. 1, Jan-Feb 1996, pp. 75–85.

Ryden N. (2004) Surface Wave Testing of Pavements, Ph.D. dissertation. Lund Institute of Technology.

Zhu J., Popovics J.S. (2005) Non-contact imaging for surface-opening cracks in concrete with air-coupled sensors, RILEM Concrete Science and Engineering/Materials and Structures, Volume 38, pp. 801–806.

4   Impact echo

Andrzej Moczko

4.1   Physical principles and theory

Impact-Echo is based on the use of transient stress waves. The principle of measurement is described at Fig. 2.1. A short-duration stress pulse is introduced into the member by mechanical impact. This impact generated three types of stress waves that propagate away from the impact point. A surface wave (Rayleigh wave or R-wave) travels along the top surface, and a P-wave and an S-wave travel into the member.

In Impact-Echo testing, P-wave is of primary importance because the displacement caused by P-waves are much larger than those caused by S-waves at points located close to impact point. When the P-wave reaches the back side of the member, it is reflected and travels back to the surface where the impact was generated. A sensitive displacement transducer next to the impact point picks up the disturbance due to the arrival of the P-wave. The P-wave is then reflected back into the member and the cycle begins again. Thus the P-wave undergoes multiple reflections between the two surfaces. The recorded waveform of surface displacement has a periodicity related to the thickness (T) of the member and the wave speed (C_p).

The frequency of P-wave arrivals at the transducer (f) is determined by transforming the recorded time-domain signal into the frequency domain using the fast Fourier transform technique (FFT). The frequencies associated with the peaks in the resulting amplitude spectrum represent the dominant frequencies in the waveform. These frequencies can be used to determine the distance to the reflecting interface. As a result the thickness of the member could be defined by simple equation:
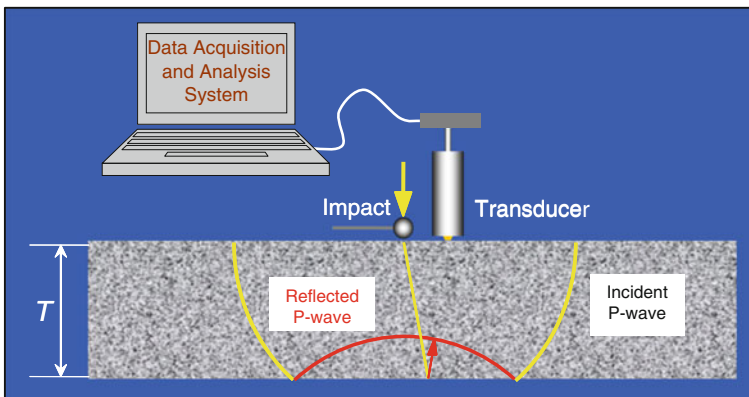
$$T = \frac{C_p}{2f}$$

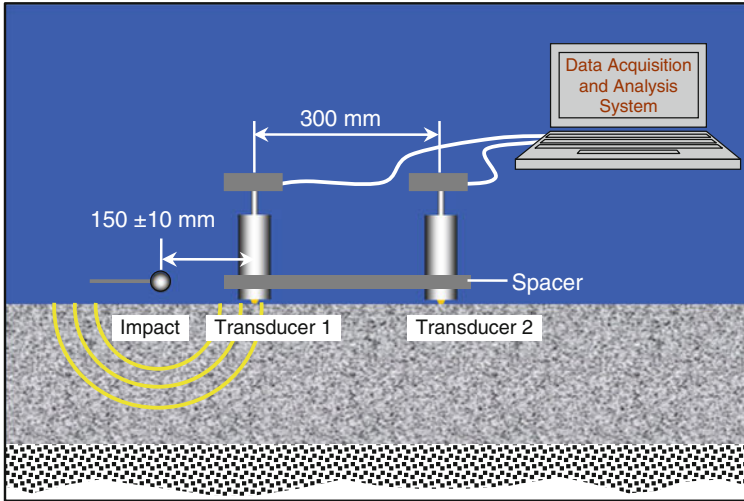**Fig. 2.1** Principle of impact echo measurement

Fig. 2.2 Calibration principle for the P-wave speed determination

Naturally, to determine the thickness of concrete element the P-wave speed should be known. For determining the P-wave speed two methods are permitted. One method is by determining the thickness frequency and then measuring the actual plate thickness at that point.

Alternatively, C_p may be determined by measuring the time for the P-wave to travel between two transducers with a known separation (Fig. 2.2). The transducers are placed 300 mm apart and the impactor is about 150 mm from one of the transducers one the line passing through the transducers. The distance L (300 mm) between the transducers, is divided by time difference Δt between arrival of the P-wave at the second and first transducers. When the wave speed is determined by the surface measurement method, the resulting value has to be multiplied by 0.96 prior to using it to calculate thickness. Thus the correct equation for thickness calculation in such case is:

$$T = \frac{0.96C_p}{2f}$$

The same principle applies to reflection from an internal defect (delamination or void). Thus, the impact-echo method is able to determine the location of internal defects as well as measure the thickness of a solid member.

The P-wave generated by impact will reflect at interfaces within the concrete where there is a change in acoustic impedance, which is defined by the density and wave speed of a material. At a concrete-air interface, there is complete reflection of the P-wave, and this permits the detection internal defects such as delaminations, cavities, and honeycombed concrete.

Fig. 2.3 (**a**) Impactors and transducer (**b**) Acquisition system
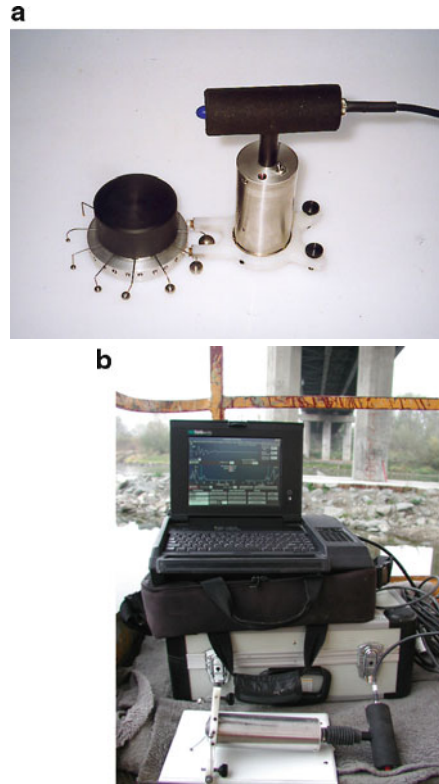
4.2 Measurement equipment and handling

Up to now the number of commercially available Impact-Echo devices is limited. The data acquisition and analysis capabilities of these systems are quite similar. In general Impact-Echo test system consists of three components (Fig. 2.3a and 2.3b): impactors, a receiving transducer and a portable computer with a data-acquisition card. The impactors are hardened steel spheres attached to spring steel rods to be operated by hand.

Typical diameters of impactors are 5, 8 and 12.5 mm. Testing are usually manual, performed from point to point. To do the measurement a spring is lifted with two fingers to a selected height and released for impact. There are also possibilities to perform impacts automatically for increasing the speed of testing what is especially suited when large areas need to be tested with close spacing between test points.

The receiving transducer is a broadband displacement transducer. A thin sheet (cap) of lead is used between the conical piezoelectric element and the concrete
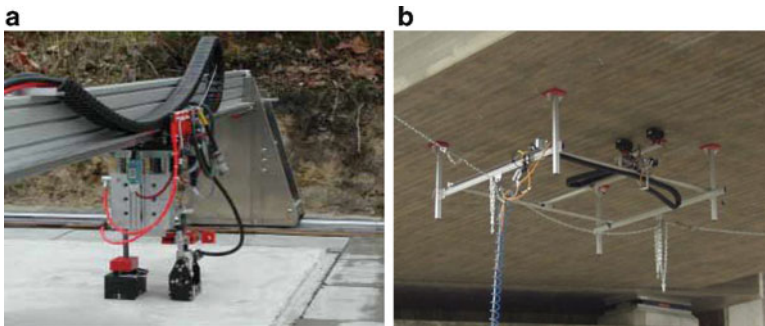
Fig. 2.4a-b Examples of automatic scanning devices

surface. Always the test area has to be smooth to achieve good contact between the transducer element and concrete. A portable, computer-based, data acquisition system is used to capture the output of the transducer, store the digitized waveforms and perform signal processing and analysis.

It is particularly important that cap's intent has to rest against the surface when the handle is depressed. In general, it is recommended to start out testing with as big size of impactor as possible that can detect the solid frequency of interest.

Should the measured frequency change compared to this frequency, a smaller impactor is chosen subsequently, in attempt to detect the depth of the defect causing the change of the solid frequency.

The surface at the transducer point has to be smooth. If not, it is necessary to grind a spot. It is imperative that there is electrical contact between the transducer tip/cap and concrete surface.

Point method of measurements has been improved by BAM (Federal Institute for Materials Research and Testing – Germany) into a scanning test method to visualize test results as an Impact-Echogram, similar to B-scan in ultrasonic pulse echo (see §2.3. in Ultrasonic echo) or a GPR radargram. A self driven scanner for horizontal surfaces was developed for both, Impact-Echo and ultrasonic sensors (Fig. 2.4a-b).

4.3   Guidelines, references and standards

- ASTM C1383-98 – Standard Test Method for Measuring the P-Wave Speed and the Thickness of Concrete Plates Using the Impact-Echo Method.
- Advice Notes NDT Highway Structures, UK, August 2006, Ed. Forde M., BA 86/06, Part 7, A.N. 3.1.
- Recommendation of Polish Highway and Road Directory concerning NDT "in-situ" quality control of concrete bridge structures during constructing process. Wrocław, 1998.
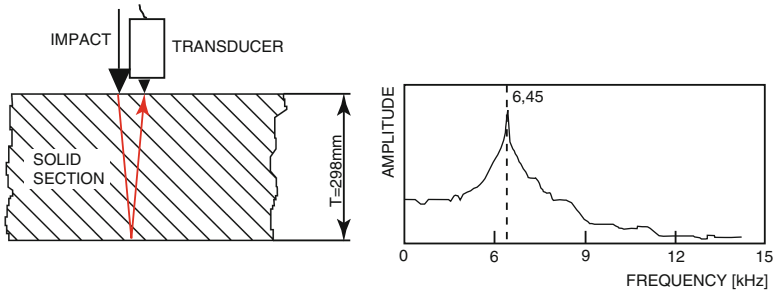
Fig. 2.5 Principle of impact-echo for thickness measurement

- Recommendation of Polish Highway and Road Directory concerning NDT "in-situ" examination of existing concrete bridge structures. Wrocław, 1998.
- An Impact-Echo Guideline of DGZfD (German Society of Non Destructive Testing) – Working title: Application of Impact-Echo for NDT of construction elements (in preparation).

4.4   Calibration and interpretation of results

The Impact-Echo method is based on monitoring the arrival of reflected stress waves and is thus able to obtain information on the depth of the internal reflecting interface. The main application which was stimulating development of this technique was a need to identify the presence and depth of anomalies in concrete structures which are accessible only from one side. In particular, the possibility of thickness measurement of the solid plates, like pavements, asphalt overlays, slabs-on-ground and walls is worth of interest. In such case the spectrum of solid part of testing plate is dominated by a single large-amplitude peak – the plate thickness frequency (see Fig. 2.5).

However Impact-Echo can be also used for several other practical applications, as an example:

- detecting the presence and depth of voids and honeycombing,
- localization of delaminated surveys of bridge decks, piers, tunnel lining elements, cooling towers and chimneystacks,
- detecting voids below slabs-on-ground,
- detecting debonding areas between reinforcement and concrete, caused for example by corrosion,
- evaluation of the quality of grout injection in post-tensioning cable ducts,
- integrity testing of a membrane below an asphalt overlay protecting structural concrete.

In the case of a defect which is large enough to be detectable, the amplitude spectrum will show two peaks (Fig. 2.6): one corresponds to reflection from the
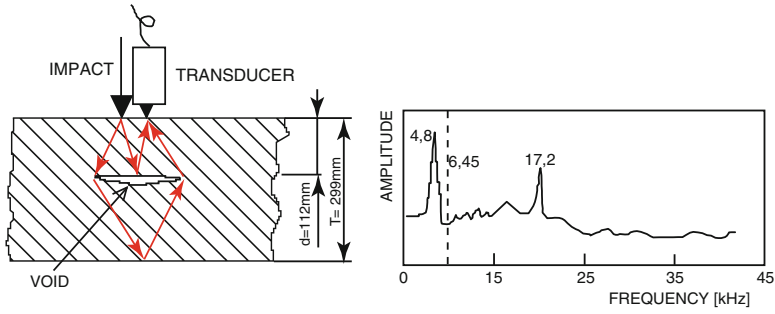
Fig. 2.6 Amplitude spectrum with two peaks, giving defect depth and total thickness
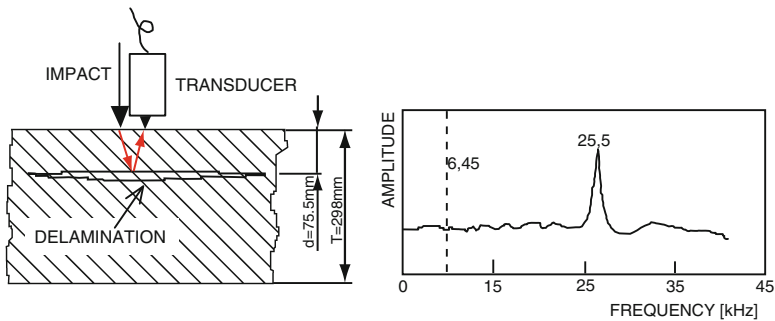

Fig. 2.7 Amplitude spectrum with screening effect of a large defect

interface and the other corresponds to the portion of the P-wave that travels around the defect and reflects from the opposite surface of the plate. The frequency associated with the portion of the P-wave that travels around the defect will be shifted to a lower value than the solid plate thickness frequency because the wave travels a longer distance than the thickness, and this provides further evidence that a defect is present.

If the plan area of the reflecting interface is larger (e.g. when the concrete section is delaminated), the generated stress wave does not propagate to the bottom of the testing plate. In such case all energy is reflected by the defect, which screens the bottom part of the concrete plate. The impact-echo response is shifted to a higher value and the plate thickness frequency) is not observed at all (fig. 2.7).

As it has been shown above localization of different types of defects has been widely applied by identifying peak frequencies in the frequency spectrum. Nevertheless, the frequency spectrum can not be always interpreted successfully, because the peak frequencies in the frequency spectra can consists of reflections from the boundary surfaces of the structure and those of from the defects. To improve Impact-Echo measurements a rather new method for identification of the defects in concrete structures has been developed, applying a scanning procedure. Thus, stack imaging of spectral amplitudes based on impact-echo (SIBIE) was developed.

Among other things it has been proven that SIBIE procedure could be successfully applied for detection ungrouted tendon ducts of prestressed concrete elements, like an example bridge girders.

4.5   Reliability and limitation of results

It is essential to ensure that the impact frequency, determined by the size of the ball bearing, is sufficiently high to identify existing defects. The interaction of stress waves with internal discontinuities depends critically upon the relationship between wavelength and the dimension and depth of the discontinuity. In general stress waves of wave length "λ" will be reflected by defects having dimensions approximately equal to or greater than "λ", but will not see those that are smaller. The minimum depth at which discontinuity can be detected is assumed to be equal to half the minimum input wavelength.

Care should be also taken to ensure that the concrete surface does not crumble on ball bearing, otherwise the longer contact time will result in a lower frequency input signal with longer wavelength.

For P-wave speed determined by calibration with a known thickness, the error in thickness measured by the commercially available Impact-Echo systems is estimated to be within $\pm$ 2 %. This assumes that the same P-wave speed is applicable at all test points. In the case of thickness measurement based on measuring the P-wave speed from surface measurements, the error in thickness dues to systematic errors associated with the digital nature of the measurements is about $\pm$ 3 %. This assumes that the P-wave speed is uniform with depth.

References

Abraham O., Leonard C., Cote P., Piwakowski B. (2000) Time frequency analysis of impact-echo signals: numerical modelling and experimental validation., ACI Mat. J., 97, 6, 645–657.

Ata N., Mihara S., Ohtsu M. (2007) Imaging of ungrouted tendon ducts in prestressed concrete by improved SIBIE. NDT&E Int., 40, No 3: 258–264.

Carino N.J., Sansalone M.J. (1992) Void detection in grouted ducts using the Impact-Echo method. ACI Materials Journal., 89, 3, 296–303.

Colla C., Schneider G., Wostmann J., Wiggenhauser H. (1999) Automated Impact-Echo: 2 and 3-D imaging of concrete elements, NDT, 4, 2.

Gipson A., Popovics J. (2005) Lamb wave basis for impact-echo method analysis, J. Eng. Mech., ASCE, 5, 438–443.

Jaeger B.J., Sansalone M.J. (1996) Detecting voids in grouted tendon ducts of post-tensioned concrete structures using the impact-echo method. ACI Structural J., 93, 4, 462–472.

Ohtsu M., Watanabe T. (2002) Stack imaging of spectral amplitude based on impact-echo for flaw detection. NDT & E Int., 35, 189–96.

Sansalone M.J., Impact-Echo (1997) The complete story. ACI Structural Journal, 94, 6, 778–786.

Sansalone M.J., Streett W.B. (1997) Impact-Echo – Nondestructive Evaluation of Concrete and Mansory. Bullbrier Press.

5   Impulse response

Andrzej Moczko and Claus Germann Petersen

5.1   Physical principles and theory

The Impulse-Response technique was developed by Davis in the end of twentieth century. He adapted the Pile Integrity Testing procedure (cf Chapter 4, § 2.4.1.) for evaluating the integrity of concrete plate-like structures. A low-strain impact, produced by an instrumented rubber tipped hammer is used for sending stress waves through the tested element. The impact causes the element to vibrate and a velocity transducer (geophone), placed near the impact point, measures the amplitude of the response. The technique is based on the analysis of structural mode shapes. The hammer load cell and the velocity transducer are linked to a portable field computer with impulse-response software for data acquisition, signal processing and storage (Fig. 2.1). The time histories of the hammer force and the measured response velocity are transformed into the frequency domain using the fast Fourier transform (FFT) algorithm. The resultant velocity spectrum is divided by the force spectrum, to obtain the "mobility" as a function of frequency. The graph of the mobility plotted against frequency contains information on the condition and integrity of the structure.
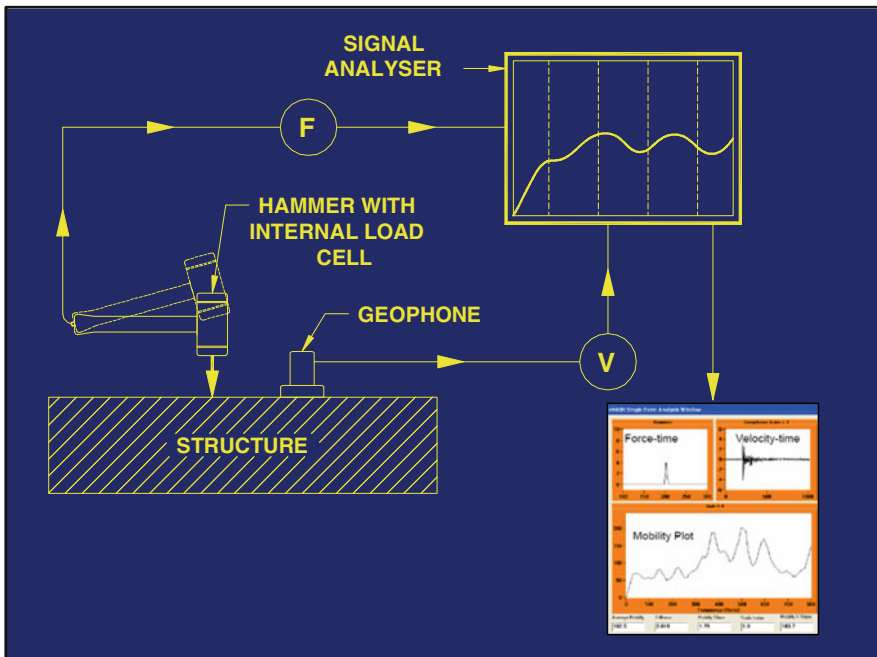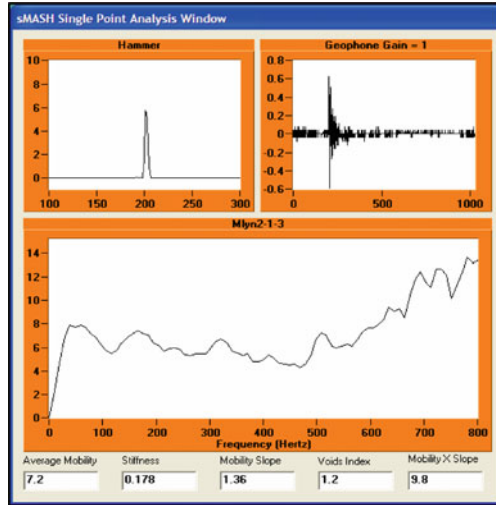

Fig. 2.1 Principle of the Impulse Response measurements

Fig. 2.2 Building the mobility curve

An example of typical test results is given at Fig. 2.2. The top left window is the force-time curve obtained from the impact of the instrumented hammer. The top right window shows the velocity-time curve obtained from the geophone in contact with the concrete surface. The lower window shows the mobility plot obtained from the two previous wave forms. At the bottom part of the screen shot the various parameters calculated from the mobility plot are displayed. Mobility is expressed in units of velocity per unit force, such as (m/s)/N. In general, the integrity of the concrete element under test is evaluated using parameters obtained from the mobility plot-frequency plot over the 0-800 Hz range.

Impulse-Response testing method is mainly used for fast screening of large areas of concrete structures with the purpose to control their structural integrity and to determine local areas with possible flaws for subsequent detailed analysis, e.g. by the impact-echo test, ultrasound shear waves or by invasive inspection with drilled cores. In particular Impulse-Response inspection may be conducted for:

- locating delaminations and honeycombing in bridge decks, slabs, walls and large structures such as dams, chimney stacks and silos,
- detecting the curling of slabs,
- detecting voids beneath concrete slabs in highways, spillways and floors,
- detecting debonding of asphalt and concrete overlays and repair patches from concrete substrates,
- evaluating anchoring systems of wall panels.

5.2 Measurement equipment and handling

Up to now the number of commercially available Impulse-Response devices is limited. The data acquisition and analysis capabilities of these systems are quite

Fig. 2.3 Typical equipment

Fig. 2.4 Measurement process

similar. In general Impulse-Response test system consists of three main components (see Fig. 2.3 and 2.4): instrumented rubber tipped hammer equipped with a load cell, broadband velocity transducer (geophone) which must have constant sensitivity over the range 15-1000 Hz and a portable field computer with proper software for data acquisition, signal processing and storage. Manual testing is usually performed across a grid of points marked on the surface of the structure. Grid node spacing normally ranges between 450 mm and 900 mm; however, grid spacing can be selected as a function of the size and shape of the element to be tested.

The velocity transducer has to be placed at a distance of between 75mm and 150mm from the point of impact. The test surface can be dry, moist or wet, but not inundated. It is necessary to remove any debris from the immediate vicinity of each test point. If the test surface is too rough, it can prevent to achieve good contact between the transducer and the concrete. In such a case, the surface should be ground so that good contact is achieved and loose material removed prior to placing the transducer on the surface.

The hammer-time graph must display a single positive voltage peak with a constant base voltage, not necessarily triangular like on Fig. 2.2. The velocity time curve must oscillate around zero, indicating that the transducer is stable during data acquisition.
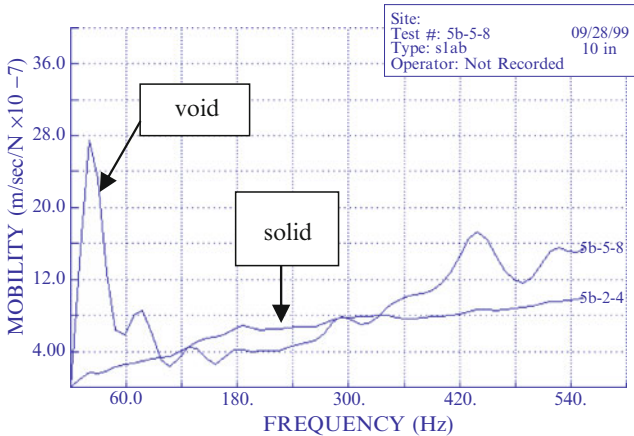
Fig. 2.5 Typical mobility curves in the case of a continuous material, and in the case of a void

5.3 Guidelines, references and standards

ASTM is preparing a proposal (not yet approved): ASTM C09.64 – Standard Practice for Measuring the Integrity of Concrete Plates Using the Impulse Response Method.

5.4 Calibration and interpretation of results

The main evaluation criterion for concrete structure integrity assessment is mobility plot obtained directly from the measurements. The test graph of mobility plotted against frequency from 0 to 800 Hz contains information on the relative quality of the concrete in the tested element (Fig. 2.5). In the case of the defect which is large enough to be detectable, a high mobility is measured at low frequencies (below 100 Hz). If there are not any significant delaminations or voids, mobility plot is rather stable over the frequency range.

For a more detailed **evaluation of Impulse-Response data, the following parameters are usually used:**

– Stiffness: the initial slope of the mobility frequency curve below 100 Hz defines the dynamic compliance or flexibility of the area around the test point for a nor-malized force input (Fig. 2.6). The inverse of this slope is the dynamic stiffness of the structural element at the test point. It is a function of concrete quality, ele-ment thickness and element support conditions.
– Average Mobility: the mean of the mobility measured at the point, calculated from the mobility curve between 100 and 800 Hz is related to the density and the thickness of a plate element (Fig. 2.6). A reduction in plate thickness corresponds
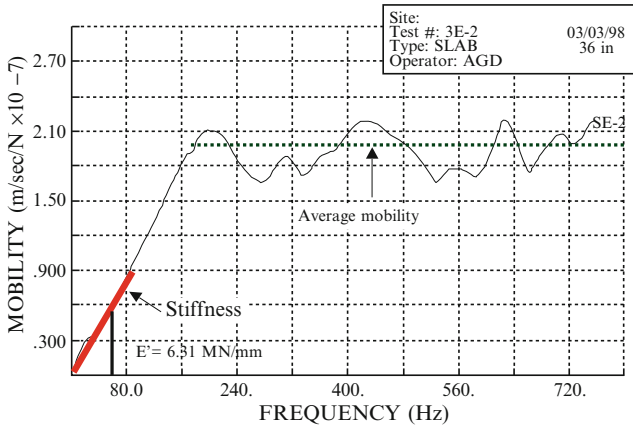
Fig. 2.6 Stiffness and average mobility determination on a mobility curve
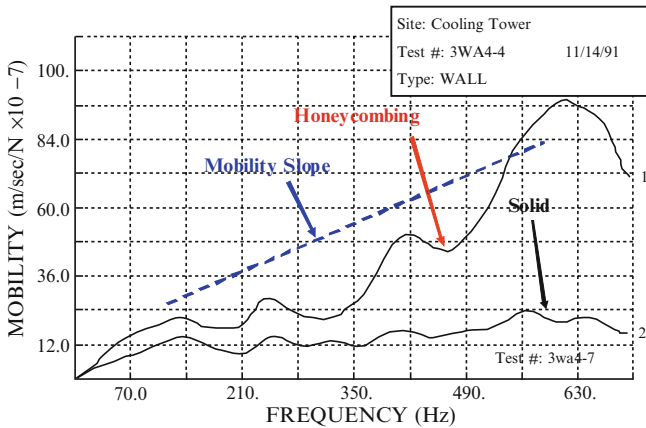

Fig. 2.7 Stiffness and average mobility determination on a mobility curve

to an increase in average mobility, even if these two parameters are not formally related to each other.

– Mobility Slope: this parameter is defined by calculating the linear best fit of the frequency spectrum between 100 and 800 Hz, then dividing the 800-Hz mobility by the 100-Hz mobility values on this linear best fit (Fig. 2.7). This parameter is considered as a function of concrete consolidation. When mobility slope values significantly increase, poor consolidation and honeycombing can be expected.

– Void Index: the ratio of the peak mobility value between 0 and 100 Hz and the average mobility between 100 and 800 Hz (Fig. 2.5). Void Index it is an indicator of the presence and degree of either severe debonding within the element or voiding. When debonding or delamination are present within a structural element, or when there is loss of support beneath a concrete slab on grade, the peak mobility below 100 Hz becomes appreciably higher than the average mobility between 100 and 800 Hz.
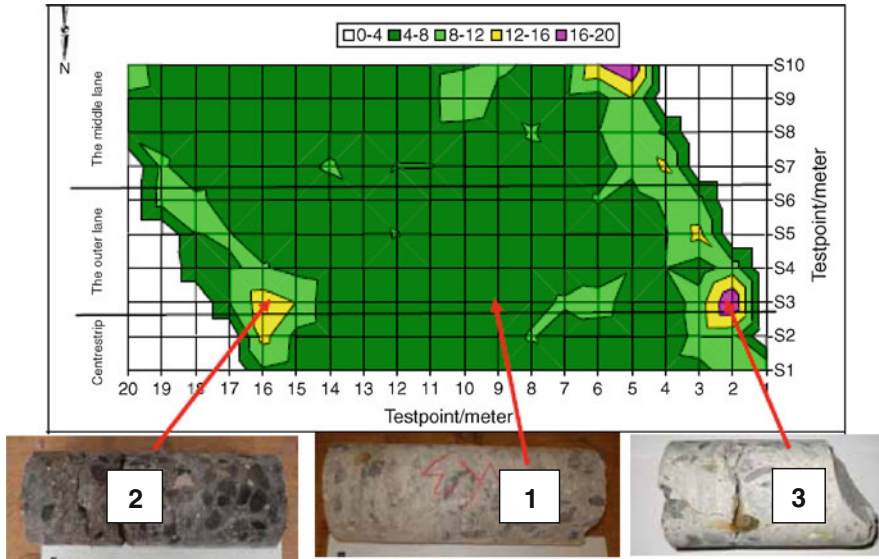
Fig. 2.8 Average mobility mapping on a bridge deck for detecting delamination

Results can be also presented as colour pictures showing the distribution of particular evaluation parameters on the surface of the tested element. As an example, a contour graph of the Average Mobility obtained by from measurements performed on the soffit of a bridge slab that was suspected of containing delaminations are shown at Fig. 2.8. Tests were performed on a 1 x 1 m grid. After testing, three locations were selected for drilling cores for experimental verification of the results obtained: (1) region of low value of average mobility, (2) region of intermediate mobility and (3) region of high mobility. Visual inspection of the cores confirmed that low mobility corresponds to a solid section of the concrete slab and higher values of average mobility correspond to the presence of delaminations.

5.5 Reliability and limitation of results

The main advantages of Impulse Response method are: access to only one face is needed, equipment is commercially available, the method does not require coupling materials and large areas can be tested in a relatively short amount of time. However, an experienced operator is required.

As any NDT method it is not recommended to use Impulse Response to evaluate concrete structures. The method is primarily considered as a relative method used for screening of large surfaces. The measurements should always be supplemented and verified with other more direct examinations. These verifications can be done

by means of drilling cores, breaking up concrete or the use a borescope. Screening with the impulse-response gives the possibility to identify potentially damaged areas. Because the physical properties of concrete can vary from point-to-point in the structure due to differences in concrete age or batch-to-batch variability, the measured mobility and dynamic stiffness can vary from point to point in a plate element of uniform thickness.

The impulse-response technique does not give any depth indications for the flaws. Only relative values of the various parameters can be evaluated for the structure in question, which give an indication of "good" and "bad" areas. Other tests or invasive verification are needed to confirm the interpretation from the measured mobility plots.

Any test results from within 300 mm of the edge of a plate-like structure should be disregarded, because of the edge effect of the plate on the test result. The effective radius of influence of the hammer blow limits the maximum concrete element depth or thickness that can be tested. This maximum depth can exceed 1000 mm; however, the apparatus shall not be used beyond these limits.

Impulse Response testing procedures are not influenced by traffic noise or low frequency structural vibrations set up by normal movement of traffic across a structure. They are also applicable in the presence of mechanical noise created by equipment (jack hammers, sounding with a hammer, mechanical sweepers, and the like) impacting on the structure. Nevertheless, Impulse Response technique is not applicable in the presence of high amplitude electrical noise, such as may be produced by a generator or some other sources, which can be transmitted to the data-acquisition system.

References

ASTM D 5882-00: Standard Test Method for Low Strain Integrity Testing of Piles. American Society for Testing and Materials, Philadelphia, PA. 19103, USA.

Clausen J.S., Knudsen A. (2009) Nondestructive Testing of Bridges Decks and Tunnel Linings Using Impulse-Response, Proceedings of Tenth ACI Int. Conf. on Recent Advances in Concrete Technology and Sustainability Issues, Seville, Spain, October 2009, SP-261-19, pp. 263-275.

Davis A.G. (2003) The Non-Destructive Impulse Response Test in North America: 1985-2001, NDT & E International, 36, pp. 185-193, Elsevier Science Ltd.

Davis A.G., Hertlein B.H. (1987) Nondestructive Testing of Concrete Pavement Slabs and Floors with the Transient Dynamic Response Method, Proceedings International Conference on Structural Faults and Repair, London, July 1987, Vol. 2, pp. 429-433.

Davis A.G., Hertlein B.H. (1995) Nondestructive Testing of Concrete Chimneys and Other Structures, Conference Nondestructive Evaluation of Aging Structures and Dams, Proc. SPIE 2457, pp. 129-136, Oakland CA, June 1995.

Moczko A., Rybak J. (2010) Impulse Response – Modern NDT Technique for Concrete Structures Integrity Testing, Budownictwo Technologie Architektura, No 1, pp. 46-50.

Ottosen N.S., Ristinmaa M., Davis, A.G. (2004) Theoretical Interpretation of Impulse Response Test of Embedded Concrete Structures, ASCE Journal of Engineering Mechanics, Vol. 130, No. 9. Sept. 2004, pp. 1062-1071.

6   Acoustic emission

Jean-Paul Balayssac and Masayasu Ohtsu

6.1   *Physical principles and theory*

Acoustic emission (AE) is a stress wave emission technique used to monitor defect formation and failures in structural materials. What is the basic concept of AE? When an acoustic emission occurs at a source within a material due to inelastic deformation or to cracking it generates an elastic wave which can be detected by an adapted receiver (Fig. 2.1). The signal recorded by the receiver can be affected by the nature of the source, the geometry of the tested specimen and the characteristics of the receiver.

Acoustic emission testing is a "passive" monitoring method in which the detection system waits for the occurrence and capture of stress wave emissions associated with cracking, corrosion, or wire breaks. By contrast, classical flaw detection methods, such as those discussed in the previous sections (impact echo, surface waves…), are considered "active" because a stress wave is sent into the test object to identify the presence of defects. Moreover AE will be very sensitive to defect activity when a structure is loaded beyond its service activity in a proof test.

AE is used successfully in a wide range of applications including: detection and locating defects in pressure vessels or leakage in storage tanks and pipes, corrosion processes, removal of protective coatings… Concerning the application of acoustic emission for concrete assessment, three famous papers were historically
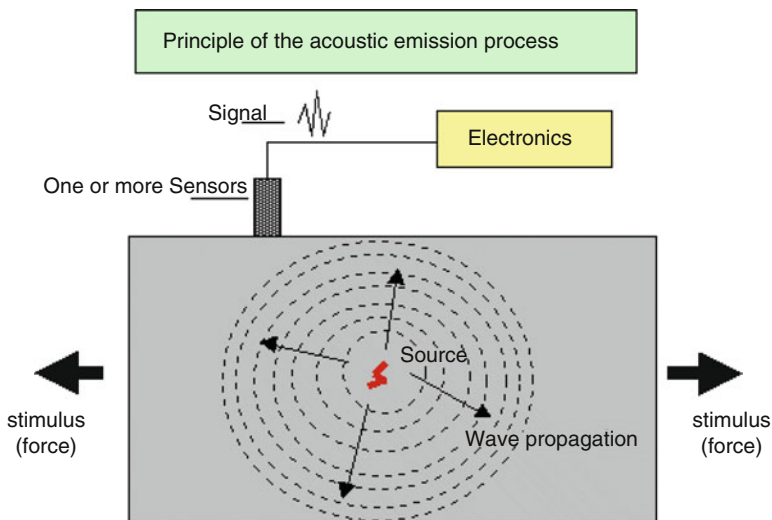

Fig. 2.1 Principle of acoustic emission

known, tracing back to 1960's. In 1959, H. Rusch studied the noise emitted during application of a compressive load in concrete. This is known as one of the first studies of the Kaiser effect in concrete. He found that AE events were recorded above 75% load level of failure load, and reported that generating behaviour of AE was closely related with the volumetric change and the absorption on ultrasonic waves. Applied researches are still in progress for instance for the detection of concrete reinforcement corrosion.

Even if AE is very reliable for the detection of the defects, it cannot provide quantitative information related to the extension of the damage. So other methods are still needed to provide such information. Moreover service environment is generally very noisy and the AE signals are usually very weak. Thus signal discrimination and noise reduction are not easy but extremely important for successful AE applications.

6.2   *Measurement equipment and handling*

The most widely used sensors are resonant piezo-electric accelerometers which convert the surface displacement into an electric signal. Resonant sensors are only very sensitive to a certain frequency but some wide band, high sensitivity sensors are now available. For civil engineering applications the sensor frequency is quite low (from 20 to 150 kHz). If several sensors are used and are located around the source, the mechanical wave will be successively received by each of these sensors, and so it will be possible to locate this source. The system consists on sensors, conditioners and a computer. The signal is amplified, conditioned and stored by a computer (Fig. 2.2). The conditioner can also provide solutions for the monitoring of additional parametric inputs.

Mainly due to practical reasons the implementation of the AE technique on site can be difficult. One of the difficulties is linked to the necessity of using a couplant between the sensor and the surface to ensure a good quality of the measurement and a good reproducibility. Like the test has to be performed during a long time the couplant qualities have to be preserved.

The number and the type of sensors (broad-band, resonant, bandwidth) must be defined in relation with the application. If the location is necessary, the definition of the sensor repartition grid is important. In this grid the distance between the sensors must be defined in relation with the attenuation of the waves.

The calibration of the acquisition system is very important. The quality of the sensor coupling and the accuracy of the source location must be assessed by mean of an artificial AE source (HSU Nielsen, also named pencil lead break).

AE waves are detected by AE sensor, which converts dynamic motions at the surface of a material into electric signals. Because AE signals are weak, they are normally amplified by two amplifiers (a pre-amplifier and a main amplifier). The signal-to-noise ratio of equipments used to be low, the amplifiers often provided more than 1000 times gain. Lately, it is normally 100 times or so.
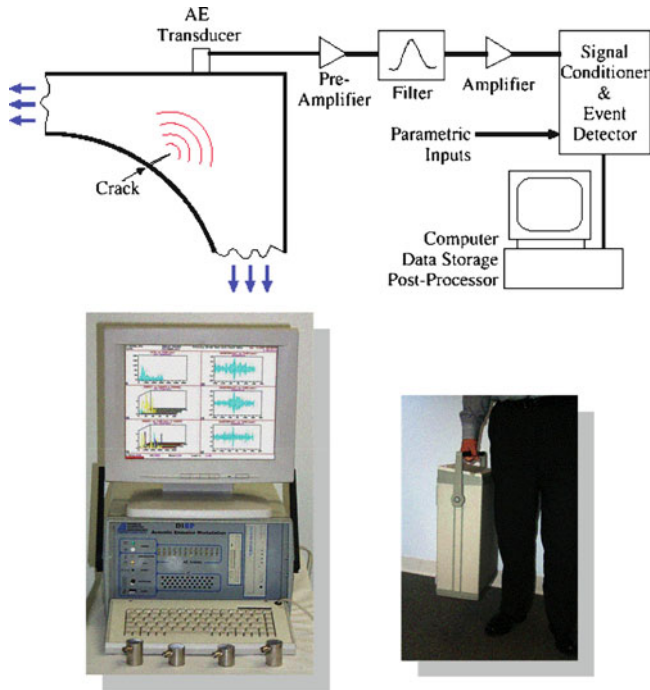
Fig. 2.2 Typical AE system

The band-pass filter is employed to eliminate the noises. In civil engineering materials, the band width from several kHz to several 100 kHz is recommended in the measurement.

Physically, AE waves are elastic waves due to dislocation motions (discontinuity of displacements as cracking) in a solid. As a result, they consist of P-wave (pressure wave, longitudinal wave or volumetric), S-wave (transverse wave or shear), and such other waves as surface waves (Rayleigh wave and Love wave), reflected waves, diffracted waves and interface wave (Lamb wave and other plate waves). The latter portion of AE waveform, in addition, is often associated with resonance vibration of AE sensor, which turns wave motions into electrical signals.

6.3 Guidelines, references and standards

The following standards concern terminology used for AE examinations, general principles and equipment characterisation. Regarding specific applications, standards are mainly focused on the examination of storage tanks or pressure vessels and from the point of view of materials, fiber-reinforced polymer-matrix composites, metals and ceramics. Regarding specific examinations of concrete structures

Fig. 2.3 Typical burst and usual parameters
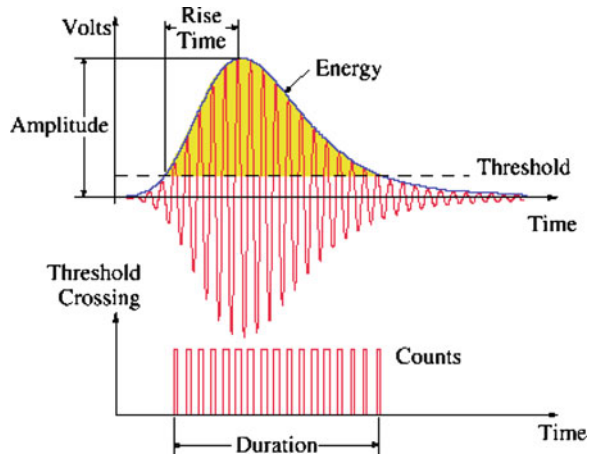
Japanese Standard and Recommendation are available. Some committees in RILEM (TC 212-ACD) have recently issued recommendations.

– ASTM E1316-07C – Standard Terminology for Non Destructive Examinations
– ASTM C1175-99A – Standard Guide to Test Methods and Standards for Non Destructive Testing of Advanced Ceramics
– EN 13554 – Non Destructive Testing – Acoustic Emission – General Principles
– EN 13477 – Non Destructive Testing – Acoustic Emission – Equipment Characterisation Part 1 & 2
– EN 1330-9 – Non-destructive testing – Terminology – Part 9: terms used in acoustic emission testing
– NDIS 2421, Recommended Practice for In-Situ Monitoring of Concrete Structures by AE, Japanese Society for Nondestructive Inspection, JNSDI, Tokyo, 2000
– JCMS-III B5706, Monitoring method for active cracks in concrete by acoustic emission, Federation of Construction Materials Industries, Japan, 2003.

6.4 Calibration and interpretation of results

The amount of charges measured by the sensor is translated in a transient signal in volts (V) or dB$_{AE}$ versus time. The Fig. 2.3 shows an example of a received signal, the burst. A detected burst signal can also be named hit. After applying a threshold, the following AE parameters can be extracted from the burst:

– the maximum of amplitude: the amplitude of the maximum peak of the burst
– the number of counts: number of detected burst signals over the detection threshold
– the rise time: time interval between the first signal over the threshold and the maximum peak amplitude

– the duration: time interval between the first and the last time the detection threshold is exceeded by a burst
– the energy: relative energy of the acoustic emission burst. The measurement of the energy is depending on the acoustic emission equipment
– the number of counts up to the peak.

Up to now only the features previously listed were analyzed because of the limitations of the sensors as well as the data storage and the processing capabilities. In the recent years, wide band, high sensitivity sensors have been developed to capture the whole waveform. In the same time, the storage and the processing of these waveforms became possible with the advancement of computer technology. So it is now possible to characterize the nature of the AE sources from the waveform analysis.

When an array of sensors is used, by extracting the arrival times of the bursts received by each of them it is also possible to locate the source. Once a source is located it is usual to talk about acoustic events for the hits linked to this source. The location can be done in real-time (during the sounding) and the results can be displayed immediately. The location is achieved by means of specific algorithms and several approaches can be used. Linear location, i.e. one dimensional requiring two or more channels, planar location i.e. two dimensional requiring three or more channels and finally volume location i.e. three dimensional requiring five or more channels. Linear and planar locations are most widely used.

However, an important problem is how to differentiate the events of interest, for instance those due to crack growth or corrosion, from different noises in a large dataset. Often, the real AE events are measured in the presence of noise due to vibration, fretting and electromagnetic interference and so, an automatic procedure for noise rejection is required before correlating AE activities with crack initiations or progressive failures. In many cases, traditional signal processing techniques such as filtering, energy analysis and spectrum analysis are insufficient to achieve this separation. One possible approach is to use statistic tools like artificial neural networks (ANN) or wavelet analysis that are able to separate and cluster the different events. The classification and the clustering can be done with or without supervision. Generally a main components analysis is used before the implementation of the artificial neural network in order to reduce the number of events. Commercial softwares are available for this kind of application.

In the case of crack detection it is possible to distinguish different modes of cracking by the moment tensor analysis.

6.5   Reliability and limitation of results

If the attenuation is too high during the propagation towards the surrounding medium up to the sensor the event cannot be detected.

If the environment is very noisy the extraction of relevant information is difficult.

Like it is a passive technique it is necessary to make a monitoring and to wait for the occurring of damage.

The structure must be under loading to stimulate the evolution of the defect.

The choice of the sensors is a condition for obtaining reliable results.

The grid repartition of the sensors is important if the location of the events is required.

Up to now it is difficult to give accurate quantitative information on the defect range.

Up to now it remains difficult to cluster different events from a large dataset.

References

Breysse D., Abraham 0. (2005) Méthodologie d'évaluation non destructive de l'état d'altération des ouvrages en béton, D. Presses de l'Ecole Nationale des Ponts et Chaussées, ISBN 2-85978-405–5.

De Oliveira R., Marques A.T. (2008) Health monitoring of FRP using acoustic emission and artificial neural networks, Computers & Structures, 86, n. 3-5, p. 367–373.

Grösse C.U, Ohtsu M. (2008) Acoustic Emission Testing, Springer Editions, 408 pp.

Grösse C.U., Finck F., Kurz J.H., Reinhardt H.W. (2004) Improvements of AE technique using wavelet algorithms, coherence functions and automatic data analysis, Construction and Building Materials, Vol. 18, 203–213.

Rusch H. (1959) Physical Problems in the Testing of Concrete. Zement Kalk-Gips 12, 1, 1–9.

Shigeishi M., Ohtsu M. (2001) Acoustic emission moment tensor analysis: development for crack identification in concrete materials, Construction and Building Materials, Vol. 15, 311–319.

7 Ground Penetrating Radar

Johannes Hugenschmidt and Jean-Paul Balayssac

Ground-Penetrating-Radar (GPR) is an electromagnetic investigation method. It is also known as Surface Penetrating Radar, Electromagnetic Reflection Method or Radar. Main advantages of the method are that is non-destructive and fast (hundreds of measurements per second) and that it can be used in non-contact mode.

7.1 Physical principles and theory

Radar (**Ra**dio **D**etection **a**nd **R**anging) and Ground-Penetrating-Radar are electromagnetical methods. In principle GPR can be used in reflection or transmission mode. As reflection methods are by far the widely used, the following description will focus on this mode. The basic principle is presented in Fig. 2.1, where an electromagnetic pulse is emitted via a transmitter antenna, reflected at the surface and interior layer boundaries of an object and recorded via the receiver antenna.

Fig. 2.1 GPR principle

Transmitter Receiver **Monitor**

Central unit

Object

Amplitude

Time

Time

Emitted signal

a

b

c

Recorded signal

a – Surface reflection
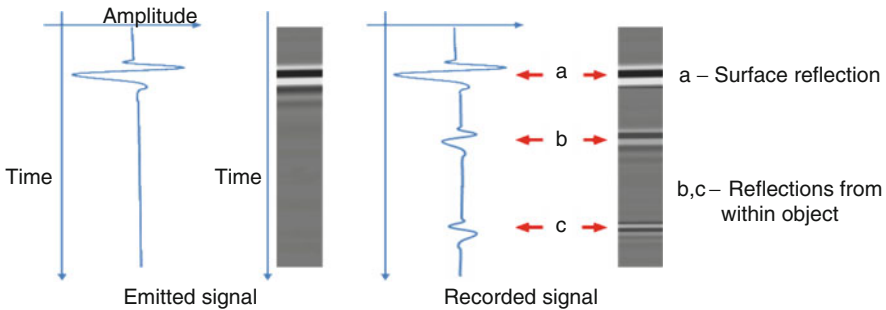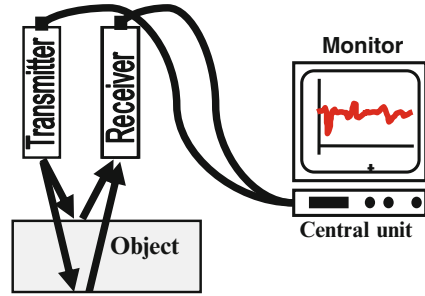
b,c – Reflections from within object

Fig. 2.2 Emitted and recorded signals

A sketch of the emitted and recorded signal is presented in Fig. 2.2 where the vertical axis is a time axis.

The following description will focus on Ground-Penetrating-Radar working in the time-domain. Systems working in the frequency-domain (stepped frequency systems) are also available but their dissemination is rather limited.

An electromagnetic impulse is emitted via an antenna. It propagates with the propagation velocity

$$v = \lambda * f \qquad \qquad \text{Eq. 1.}$$

with v = propagation velocity, λ = wavelength, f = frequency.

In order to obtain an impulse of finite length, a range of frequencies is used. The larger the bandwidth of this range, the shorter is the emitted impulse. GPR antennas are therefore usually denoted by their centre-frequency. Typically antennas with a higher centre-frequency also have greater bandwidth and shorter pulse length.

The propagation of electromagnetic waves in materials is characterized by the dielectric permittivity ε ($\varepsilon = \varepsilon_r \varepsilon_0$), conductivity σ and magnetic susceptibility μ ($\mu = \mu_r \mu_0$). ε_0 and μ_0 are constants with $\varepsilon_0 = 8.85 \ 10^{-12} \ A^2 \ s^2/ \ Nm^2$ and $\mu_0 = 4 \ \pi \ 10^{-7}$ N/ A^2. From Maxwell's equations it can be derived that:

$$v = 1/\sqrt{(\varepsilon_r \varepsilon_0 \mu_r \mu_0)} \qquad \qquad \text{Eq. 2.}$$

In vacuum ($\varepsilon_r = \mu_r = 1$) this leads to

$$v = 1 / \sqrt{(\varepsilon_0\, \mu_0)} = 2.998 \cdot 10^8 \ m\,/\,s = \text{speed of light c} \qquad \text{Eq. 3.}$$

For all non-ferromagnetic materials (ferromagnetic materials are not inspected with GPR due to their high conductivity) μ_r can be approximated as 1 leading to $\mu = \mu_0$. Thus, the signal velocity for such materials can be described as

$$v = c / \sqrt{\varepsilon_r} \qquad \text{Eq. 4.}$$

which means that for practical purposes the signal velocity within a material depends on ε_r only. If an electromagnetic wave hits an interface, part of the energy will be transmitted and part will be reflected. For a plain electromagnetic wave in a low loss material hitting at vertical incidence an interface between two materials with ε_1 and ε_2, the reflected wave can be described as

$$\text{Reflected Wave} = R * \text{Incident Wave}$$

with

$$R = (\sqrt{\varepsilon_1} - \sqrt{\varepsilon_2}) / (\sqrt{\varepsilon_1} + \sqrt{\varepsilon_2}) = \text{reflection coefficient} \qquad \text{Eq. 5.}$$

This means that there is no reflection if $\varepsilon_1 = \varepsilon_2$ (materials with identical properties) and the reflection amplitude becomes negative (phase shift by 180 degrees) if $\varepsilon_2 > \varepsilon_1$.

The time a GPR signal requires to travel through a material layer, get reflected and travel back through the layer is

$$\text{Two-way-traveltime} = \text{twt} = 2\,D\,/\,v \qquad \text{Eq. 6.}$$

with D being the thickness of the layer. If this thickness has to be computed from twt this equation can be rearranged to

$$D = \text{twt}\ v\,/\,2 \qquad \text{Eq. 7.}$$

This corresponds to the usual case where the thickness is computed with a known twt derived from the GPR data. The velocity v, necessary to compute depths or thicknesses from twt is a priori unknown. It can be estimated using experience or velocity tables, calibrated by comparison of twt with known thicknesses or by special setups during GPR data acquisition. Equation 0 is valid only if the distance between transmitter and receiver is zero or small enough to be neglected.

The ability of the method separating single objects (lateral resolution) is limited by the size of the Fresnel region which characterizes the area where reflected waves

add together constructively. Single points within this area cannot be distinguished by the GPR signal. The radius of the Fresnel region is described as

$$r = \sqrt{(D\,v\,/\,2\,f)} \qquad\qquad \text{Eq. 8.}$$

Thus lateral resolution increases with frequency f and decreases with the depth (distance) D of the target.

7.2   Equipment and handling

Today a wide range of GPR-equipment from different manufacturers is available. A GPR system consists of one or several antennas, a central unit usually including a monitor for real time data display and accessories such as cables and energy supply.

Antennas

The frequency content of the emitted and recorded GPR signal is mainly defined by the antenna. As a general rule of thumb it can be said that the higher the centre frequency of the antenna, the better the resolution but the lower the depth of penetration of the GPR signal and thus the possible depth of investigation. This means that the choice of the appropriate antenna(s) is crucial for the success of GPR investigations. Today antennas with centre frequencies between some MHz (low resolution, high depth of penetration, for geological applications) and some GHz (high resolution, low depth of penetration, used for non-destructive –testing) are available. Antennas can be monostatic (transmitter and receiver at fixed distance in the same box) or bistatic (transmitter and receiver as separate units. Depending on the antenna type and characteristics antennas are coupled to the object or used in non-contact mode (e.g. horn antennas).

Central unit

Central units have one or several channels for using one or several antennas at the same time. The possible data acquisition rate (number of measurements per second) depends mainly on the central unit and can reach up to several hundred of measurements per second. Data storage and real time display are other tasks performed by the central unit. Often data can be processed in real time for an enhanced display of the data.

Accessories

As GPR is a fast and non-contact method, it can be used for the inspection of large structures such as roads or bridges. In this context the knowledge of the position of each measurement is essential. Modern surveying equipment such as GPS or automated theodolites can provide a means for an efficient position control.

Acquisition of GPR data is only one step of a GPR survey which is followed by data processing and interpretation. The availability of appropriate software is essential for performing those steps satisfactorily.

Fig. 2.3 Mobile GPR-system
(courtesy EMPA)
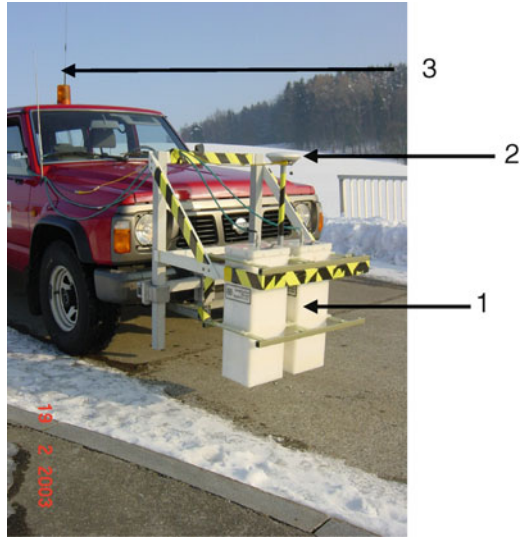
Example

In Fig. 2.3 a mobile acquisition system is shown which is used for the inspection of roads and bridges. The two horn antennas (arrow 1, transmitter and receiver) are mounted in a height of about 0.25m above the ground. This facilitates data acquisition while the vehicle is moving. The GPS-antenna (arrow 2) is sitting on top of the GPR antennas for position control. A radio antenna (arrow 3) enables the communication of the on–board GPS-system with the GPS base-station thus ensuring an accuracy of the position control of some millimetres.

7.3   Guidelines and standards

There is a range of standards and guidelines available describing the application of the GPR method to concrete and related problems. A selection is listed below.

– ASTM D4748-06 Standard Test Method for Determining the Thickness of Bound Pavement Layers Using Short-Pulse Radar
– ASTM D6087-07 Standard Test Method for Evaluating Asphalt-Covered Concrete Bridge Decks Using Ground Penetrating Radar
– ASTM D6429-99(2006) Standard Guide for Selecting Surface Geophysical Methods
– ASTM D6432-99 Standard Guide for using the Surface Ground Penetrating Radar Method for Subsurface Investigation
– DGZfP, Merkblatt über das Radarverfahren zur Zerstörungsfreien Prüfung im Bauwesen (B10), Deutsche Gesellschaft für Zerstörungsfreie Prüfung e.V., Berlin (2001) (Technical guideline, in German)
– The Concrete Society, Technical Report 48, Guidance on Radar Testing of Concrete Structures
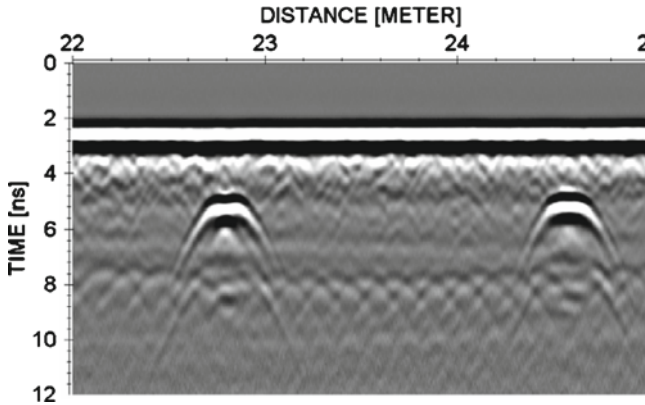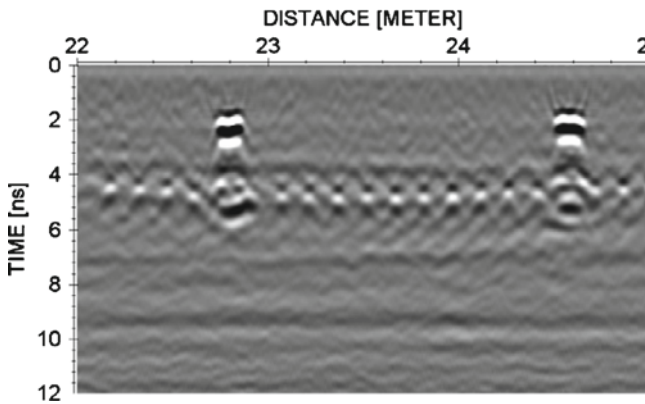
Fig. 2.4 Raw data

Fig. 2.5 Processed data

7.4 Data processing, calibration and interpretation

Data processing is an essential step within a GPR survey. The optimal processing sequence depends on the GPR data, the object under inspection and the problem to be solved by the GPR survey. Some common aims of data processing are:

– Improvement of signal/noise ratio
– Correction of surface reflection to time/depth zero
– Migration (correction of the position of reflection energy that has been reflected sideways)
– Gain correction (amplification of signals depending on twt)

An example of a simple processing sequence applied to data acquired on an industrial railway track embedded in concrete is presented in Fig. 2.4 (raw data) and Fig. 2.5 (processed data). The length of the section shown is 3.0 metres, the vertical
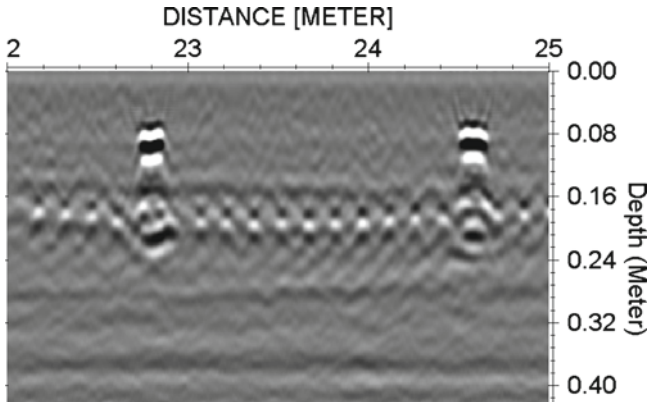
Fig. 2.6   Data with interpretation

time scale is 12 nanoseconds. The processing sequence included a bandpass filter (improvement of signal/noise ratio), the correction of the reflection at the concrete surface (black band in Fig. 2.4) to time 0, migration (focussing of energy that has not been reflected vertically but sideways) and gain correction (amplification with respect to twt).

In Fig. 2.6 the original time scale has been replaced by a depth scale. In order to do this the signal velocity within the material has to be calibrated with a core, obtained from the GPR data or estimated. In this example an estimated signal velocity within concrete of 0.08 m/ns was used for time-depth conversion.

Interpretation is the final step of a GPR inspection during which reflections are related to physical structures within the object. The many reflections distributed on the whole profile at 0.2 m in Fig. 2.6 have been interpreted as single bars of a layer of rebar, while the two reflections at 22.8 m and 24.6 m have been interpreted as sleepers embedded in concrete.

7.5   Applications, reliability of results and limitations

The GPR method can be applied to a wide range of problems, such as:

–   Determination of layer thicknesses: concrete cover of rebar, asphalt pavement, concrete tunnel walls, subbase and geological layers
–   Locating of structures: rebar, tendons or tendon ducts, anchors, dowels, cavities…
–   Identification of material properties: humidity, chloride content, voids, air content. In general, it can be stated that the investigation of material properties is more demanding than the investigation of structural elements and in many cases still under development. In this case, other characteristics of the the GPR signal can be analyzed, like the direct wave propagation and its attenuation (Sbartai et al., 2007).

(Daniels, 2004) gives a detailed description of GPR and its applications.

Several studies have investigated the accuracy of GPR results [(Hugenschmidt and Mastrangelo, 2006), (Maser et al., 1994), (Maser (1996), (FDoT, 2000), (Willet and Rister, 2002), (Al Qadi et al., 2003)]. There are several limitations restricting the use of GPR and the accuracy of results. We have seen (equation 0) that a sufficient contrast in material properties is required if the interface between two materials has to be investigated. Without such contrast the boundary will not appear in the GPR data. If the thickness of a certain layer has to be investigated, the signal velocity within this layer has to be known (equation 0). If the velocity is calibrated with a single core and used for the time to depth conversion, this implies the assumption of constant velocity within the layer. This assumption is used successfully in many cases. However, it should be kept in mind that existing velocity variations will lead to errors in the result for the layer thickness.

The attenuation of the GPR signal within materials is caused by many factors, the electrical conductivity being an important factor for practical purposes. GPR waves in conducting materials lead to stray currents reducing the depth of penetration of GPR signals. Within certain limits this can be avoided using low frequency antennas (in most materials lower frequency waves experience less damping) but this will lead to a reduced resolution (equation 0) and may therefore not be feasible.

As described above interpretation links reflections in GPR data to physical structures within the object under inspection. In many cases an unambiguous relation between reflections and physical structures is not straightforward. In such cases it is a necessity to have additional information such as cores or plans available to support the interpretation, in all other cases the availability of such additional information is still desirable.

References

Al Qadi I., Lahouar S., Loulizi A. (2003) GPR, From State of the art to the State of the art of practice, Proc. NDT-CE 2003, Berlin, Germany.

ASTM (2005) Standard Guide for using the Surface Ground Penetrating Radar Method for Subsurface Investigation, Book of Standards 04.09, D6432–99.

ASTM (2006) Standard Guide for selecting Surface Geophysical Methods, Book of Standards 04.09, D6429–99.

ASTM (2006) Standard Test Method for Determining the Thickness of Bound Pavement Layers using Short-Pulse Radar, Book of Standards 04.03, D4748–06.

ASTM (2008) Standard Test Method for Evaluating Asphalt-Covered Concrete Bridge Decks using Ground Penetrating Radar, Book of Standards 04.03, D6087–08.

Bungey J.H. (2004) Sub-surface radar testing of concrete: a review, Constr. Build. Mat., 18, 1, pp. 1–8.

Daniels D. (2004) Ground Penetrating Radar, 2nd edition, The Institution of Electrical Engineers.

Deutsche Gesellschaft für zerstörungsfreie Prüfung (2008) Merkblatt über das Radarverfahren zur zertörungsfreien Prüfung im Bauwesen, Merkblatt B10.

FDoT (2000) Florida Department of Transportation Research Center, Research Today, Fall 2000, Tallahassee, USA.

Hugenschmidt and Mastrangelo (2006) GPR inspection of concrete bridges, Cement & Concrete Composites, 28, pp. 384–392.

Maser K. (1996) Evaluation of pavements and bridge decks at highway speed using ground penetrating radar, ASCE Str. Congress XIV, Chicago, USA.

Maser K., Scullion T., Roddis W.M., Fernando E. (1994) Radar for pavement thickness evaluation, Non-destructive testing of pavements and backcalculation of moduli, ASTM STP 1198, Philadelphia, USA.

Sbartai Z.M., Laurens S., Rhazi J., Balayssac J.P., Arliguie G. (2007) Using radar direct wave for concrete condition assessment: correlation with electrical resistivity, J. Appl. Geophysics, Vol. 62, pp. 361–374.

The Concrete Society (1997) Technical Report 48, Guidance on Radar Testing of Concrete Structures.

Willet D.A., Rister B. (2002) Ground penetratin radar « pavement thickness evaluation », Res. Rep. KTC-02-29/FR101-00-1F, Kentucky Transp. Center, Univ. Kentucky, Lexington, USA.

8 Capacitive technique

Xavier Dérobert

8.1 Physical principles and theory

The principle consists in placing two electrodes (or more) on the outer surface of a medium, and applying an electric current between them through a resonant circuit. The combination electrodes/medium forms a capacitor, and changes in capacitance are indicative of internal constituents of the medium (like the nature of its components or the moisture content).

Indeed, the configuration of a conventional parallel plate capacitor would require a contact with the material under study from two opposite sides (Fig. 2.1).
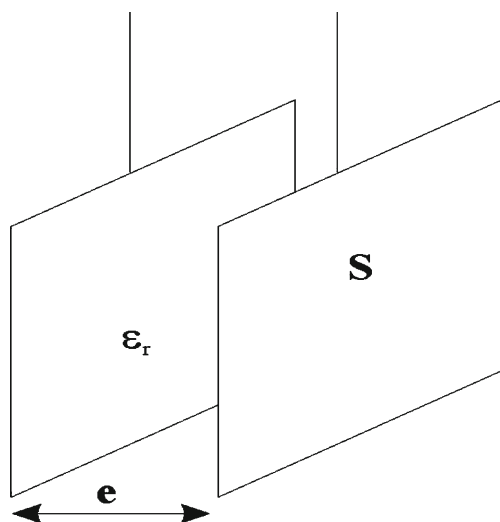

Fig. 2.1 The simplest type of capacitive probe is based on the so-called parallel plate capacitor
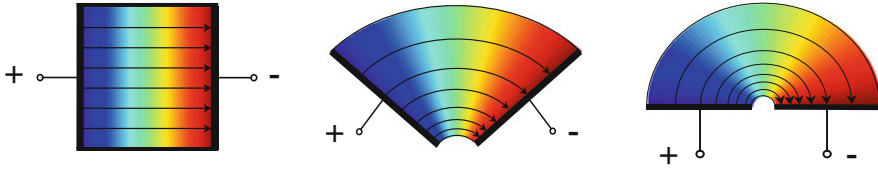
Fig. 2.2 Configuration of a capacitive sensor designed for cover concrete

As a first approximation (the result is only valid when the spacing between the plates is much smaller than their dimensions), the value of the capacitance C (in Farad) is obtained from the following formula:

$$C = \varepsilon_o \, \varepsilon_r \, S / e \qquad\qquad \text{Eq. 1.}$$

where S [m^2] is area of the electrodes, e [m] the distance between them, ε_o [~ 8.854 10^{-12} F.m^{-1}] the permittivity of vacuum, and ε_r the dielectric constant which determines some kind of ability to store electric charge.

For the application related to measurements of the moisture content of cover concrete, the difference is that the electrodes of the sensor are placed next to one another (Fig. 2.2), in order to provide a sufficient penetration depth of the electric field between sensing and driven devices on one side of the material under study. Then, this configuration can be seen as the result of gradually opening the angle between two electrodes of a parallel plate capacitor (Fig. 2.2, from left to right).

However, for measurements carried out from the surface, neither the volume of investigation, nor the penetration depth are precisely defined (which can vary from few millimeters to several centimeters depending to the geometry of the electrodes). Actually, the situation is complex, because the system appears as a heterogeneous mixing of dielectric materials and conductors. As a consequence, there is no analytical formulation (like for the parallel plate capacitor) giving the value of the capacitance as a function of the characteristics of the investigated media, and one has to calibrate the measurements on known homogeneous materials.

Spaces on both sides of the electrodes intervene, and the resulting layout doesn't constitute a single capacitor but a set of two capacitors in parallel. The first one (Ci) incorporates the medium under survey and the second one (Ce) the surrounding environment (principally air and Plexiglas making up the probe), so that the total capacitance is the sum.

The capacitance is determined by means of a (high frequency) resonant circuit delivering an alternative voltage. The resonant frequency shift is then obtained by a mere frequency analyzer. The relationship between the capacitance and the resonant frequency shift can be obtained, knowing the inductance of the circuit. For practical reasons, since we are interested in the changes (whereas Ce is a constant, provided that some precautions are taken to prevent "hands effect" and interference of external electrical field by adding a screen), we can deal with Ci, the capacitance of the inside volume.
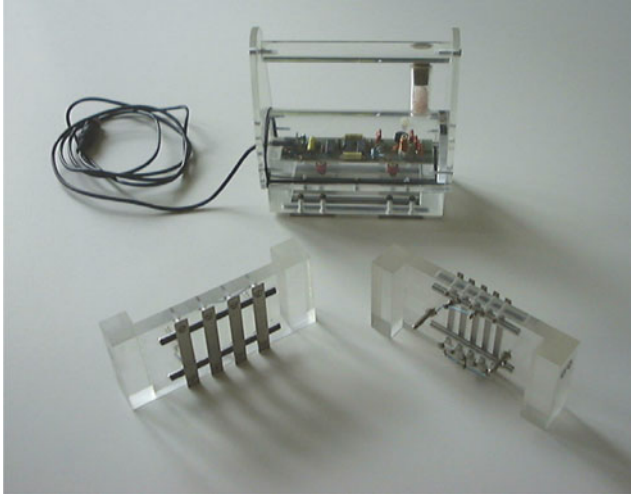
Fig. 2.3 Prototype of a capacitance probe for measuring the water content of flat concrete structures, with its sets of electrodes

8.2   *Measuring equipment and handling*

Applications of capacitive techniques have been various in the civil engineering field, from the estimation of water content of soils (Eller and Denoth, 1996; Johnson et al. 2004), including the ice-water phase transition (Fen-Chong et al., 2006), and the snow (Louge et al., 1998) study, to the dielectric characterization of concrete mixing (Al-Qadi et al., 1995; Diefenderfer et al., 1998).

This technique has already been studied over few decades in the French network of Public Works Laboratories, initially for the measurement of water content in soils (Baron and Tran, 1977; Blaszczyk et al., 1993), and afterwards on reinforced concrete before being adapted to post-tensioned structures (Dupas et al., 2001; Iaquinta, 2004). Lately, capacitive measurements were performed on concrete slabs, stored in homogeneous known water content (Derobert et al., 2008).

In order to minimize the influences of temperature and ionic conduction, the oscillator of the resonant circuit operates at 65 MHz. Practical reasons (related to the transmission of information over long distances) require the implementation of a frequency divisor to decrease the signal towards lower frequencies in the range of 5 000 Hz.

The current system can have the possibility of employing different configurations of electrodes in order to reach various depths of penetration, as illustrated on the Fig. 2.3: large plates (70*40 mm, 40 mm spacing), average size plates (70*10 mm, 10 mm spacing) and small plates (70*5 mm, 5 mm spacing).
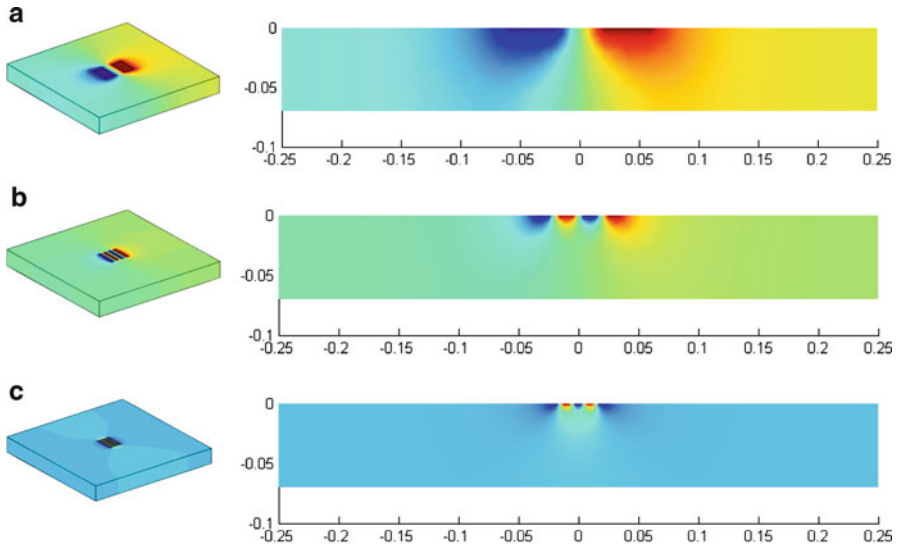
Fig. 2.4 Comparison of electric potential calculations for a 70 mm-thick slab of 500x500 mm. On the left side, equipotential surfaces for: large, average size and small plates. On the right side are shown the corresponding vertical cross section plots in the center of the concrete slab

8.3 Data processing, calibration and interpretation

The main purpose, when employing electrodes of varied dimensions and spacing, is to reach different penetration depths in order to acquire an information about the gradient of moisture inside the cover concrete. Unfortunately, because of a strong dependency on the intrinsic material characteristics, it is rather difficult to delimit the investigation.

However, we can have an indication of the inspected volume by considering the three arrangements of electrodes placed in the center of the upper face of a concrete slab (homogeneous), as displayed on the Fig. 2.4a-c. These numerical simulations were conducted with the commercial finite elements software package FEMLAB 2.3 [FEM 03].

Basically, we handled a three-dimensional electrostatics model of the system with linear homogeneous isotropic materials. Modeling the electric field is carried out using the electric potential V, calculated from the Laplace equation (eq. 2). Regarding the boundary conditions, the electrodes are equipotential surfaces, and the remainder is considered as insulated electrically

$$\Delta V = 0 \qquad\qquad \text{Eq. 2.}$$

From a qualitative point of view, the intensity of the electric field is extremely variable according to the configuration, in particular along the depth in the sample.

Fig. 2.5 Normalized
capacitance values as a
function of the thickness
of a concrete sample for the
different probes geometry
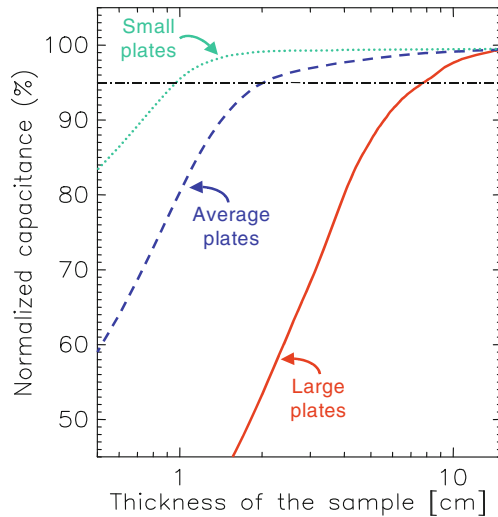
Furthermore, the influence of the probe ranges from several centimeters (for that
equipped with the larger set of electrodes), to a few millimeters (when the device
is mounted with the smaller plates). Figure 2.5 presents the normalized capaci-
tance values as a function of the concrete thickness coupled with the three sets of
electrodes.

These values should be regarded as an order of magnitude (it may depend on the
moisture content), but it can be taken as a good indicator of the penetration depth of
the sensors (the effective penetration depth being identified at 5% reduction of from
the maximum capacitance – arbitrary choice). Then we can estimate to 5-7 mm, 2-3
cm and 7-8 cm the depth penetration of the small, the average and the large size
electrodes respectively.

Calibration can be done on homogeneous materials, which dielectric constants
are known and non frequency dependent. For that, measurements were done with
the panel of electrodes on PTFE, PVC, granite, marble and limestone respectively,
thus corresponding to increasing dielectric constant. Results are presented in
Fig. 2.6, and show linear relations between the measured frequency and the electro-
magnetic property of homogeneous media. The measurements are subtracted to a
reference done in the air in order to remove the effect of the environment, including
the sensor itself and the hand of the operator. The slopes of each calibration curve
express the capacitance or the sensitivity of each electrode to the dielectric constant
of the surveyed medium.

The various slopes showing the sensitivity of the electrodes are due to their
dimension – and then their capacitance values – associated to the chosen frequency
band in the resonant circuit of the sensor.

Then, capacitive measurements done on concretes, and transformed in dielectric
constant values due to the calibration curves from Fig. 2.6, can provide information
on the moisture of the mixing, the dielectric constant being related to the volumic
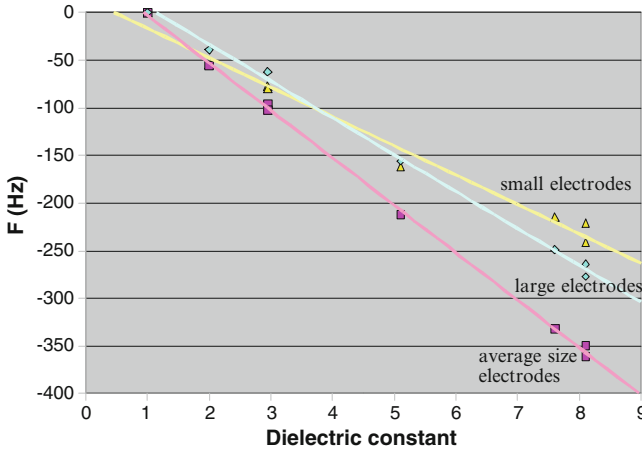
Fig. 2.6 Capacitive calibration of the set of electrodes on homogeneous media

water content of such material. Moreover, the variation of depth penetration of the set of electrodes can give an indication of the hydric gradient with depth.

8.4   Limitations and reliability

The most important limitations of the technique are related to the flatness of the concrete surface, the absence of knowledge of the location of the reinforcement and the need of calibration on the concrete material itself in order to obtain water content values.

Concerning the flatness of the surface, all the effects due to the building of the concrete structure, such as border of successive formworks presenting steps, or important spherical voids due to air bubbles, can lead to important errors.

For accurate measurements, we have to get the information of the location of the rebar in order to do punctual measurements in the center of the reinforcement mesh. Indeed, the presence of rebar in the coupling volume under the electrodes induces a slight decrease of the measurement values, which could be interpreted as a dryer material than the reality.

Then, the knowledge of an equivalence of dielectric constant remains insufficient to get water-content accurate values. Knowing the strength of concrete (C25, C40,…) can give a good indication of the relation between the capacitive measurements and the water content, but keeping in mind that the nature of the aggregates themselves biases the relation.

For the second aspect more related to the reliability, the relative measurements induce a strong limitation of the temperature influence and prevent any "hand effect". Moreover, the average of elementary measurements (~5) a few centimeters around the

measurement location decreases the noise in the value and strongly diminishes the influence of the size of aggregates in the mixing considered as homogeneous material.

At last, this technique is limited to the water content estimation of homogeneous concrete which thickness should remain above 10 cm.

References

Al-Qadi I.L., Hazim O.A., Su W., Riad S.M. (1995) Dielectric properties of Portland cement concrete at low radio frequencies. Journ. Mat. Civil Eng., 7, 192–198.

Baron J.P., Tran N.L. (1977) Méthodes de mesure et de contrôle des teneurs en eau de matériaux dans les LPC. Bull. Lab. Ponts Chauss., 87, 85–96.

Blaszczyk F., Blaszczyk R., Trochet B., Bigorre M., Dupas A. (1993) Mesure de la teneur en eau en continu d'un matériau granulaire : TRITON II. Mesure à la jetée d'un transporteur. Bull. Lab. Ponts Chauss., 186, 85–87.

Dérobert X., Iaquinta J., Klysz G., Balayssac J.P. (2008) Use of capacitive and GPR techniques for non-destructive evaluation of cover concrete. NDT&E Int., 41, 44–52.

Diefenderfer B.K., Al-Qadi I.L., Yoho J.J., Riad S.M., Loulizi A. (1998) Development of a capacitor probe to detect subsurface deterioration in concrete. Mat. Res. Soc. Symp. Proc., 503, 231–236.

Dupas A., Sudret J.P., Chabert A. (2001) Méthode de diagnostic de câbles de précontrainte externe contenus dans des gaines. French Patent n° 0107719, INPI, Paris.

Eller H., Denoth A. (1996) A capacitive soil moisture sensor. Journ. Hydro., 185, 137–146.

FEMLAB (2003) Reference manual - Version 2.3. COMSOL, http://www.comsol.com

Fen-Chong T., Fabbri A., Azouni A. (2006) Transient freezing-thawing phenomena in water-filled cohesive porous materials. Cold Reg. Sci. Techn., 46, 12–26.

Iaquinta J. (2004) Contribution of capacitance probes for the inspection of external prestressing ducts. World Conf. NDT Proc., Montréal.

Johnson R.H., Poeter E.P. (2005) Iterative use of the Bruggeman-Hanai-Sen mixing model to determine water saturations in sand. Geophys., 70, K33–K38.

Louge M.Y., Foster R.L., Jensen N., Patterson R. (1998) A portable capacitance snow souding instrument. Cold Reg. Sci. Techn., 28, 73–81.

9   Electrical resistivity measurement

Jean-François Lataste

9.1   Physical principle and theory

Electrical resistivity measurements on reinforced concrete are used to assess probability of corrosion. They are sensible to factors influencing rebar corrosion (salt and moisture) and allow a more accurate interpretation of electrochemical measurement results (polarization resistance or half cell potential measurement).

Due to their sensitivity to on site concrete parameters, research is now oriented to the use of electrical resistivity to assess concrete conditions directly.

Electrical conduction in porous materials is described by the empirical Archie's law (Archie, 1942):

$$\rho_r = a\,\phi^{-m}\,s^{-n} \qquad\qquad \text{Eq.1}$$

Table 2.1 parameters of Archie's law, after (Naar, 2006)

Parameter	a	m	n
	Depend on lithology	Depend on cementation	
Value for rocks	0.6 to 2 (increases with porosity)	1.3 to 2.2 (increases with cementation)	About 2
Value for concretes	0.1 to 0.8	4.6	2.43

where ρ_r is the resistivity of rock, φ the porosity, ρ_w the resistivity of the fluid in the rock, s the saturation degree, a, m and n are three constants linked to the studied material.

This empirical relation has been established for rocks, but works show it is possible to use for concrete. Parameters have then to be determined (Table 2.1).

The measured resistivity is linked to nature and volume of fluids in concrete (parameters ρ_w, and s of Archie's law), but also to microstructural parameters of concrete (porosity, interconnectivity of pores, tortuosity (Andrade et al., 2000)). Thus, electrical resistivity is considered as an indicator of concrete transfer properties. Recent works suggest using it as an indicator of durability to characterize concretes (Baroghel Bouny et al., 2004).

Any significant change in porosity (between different types or because of an alteration) influence electrical resistivity properties of concrete. Any interface either electrically insulator or conductive can also have consequences for resistivity measurements.

9.2 Measurement techniques and handling

9.2.1 Laboratory

The laboratory measurement of the resistivity of concrete can be done using two probes or four probe equipment. In a two probe arrangement the sample (poured in mould, or from coring) is saturated by water and put between two metallic probes (equipped with moistened sponges to improve electrical contact – see Fig. 2.1). An electrical current (I in amperes) is injected between the probes and the potential difference (ΔU in volts) is measured. The electrical resistance (R in Ohm) is calculated by Ohm's law:

$$R = \Delta U / l \qquad \text{Eq. 2.}$$

The pressure on probes is constant and fixed by the constant mass. A calibration of sponge resistivity is done (a measure with the two sponges and without any sample), to extract the exact resistance of sample:

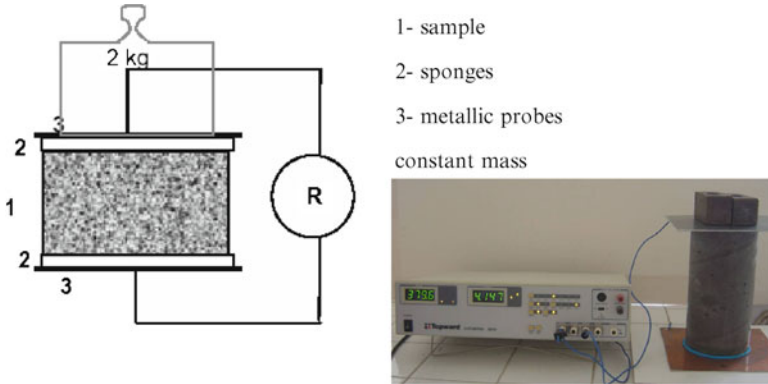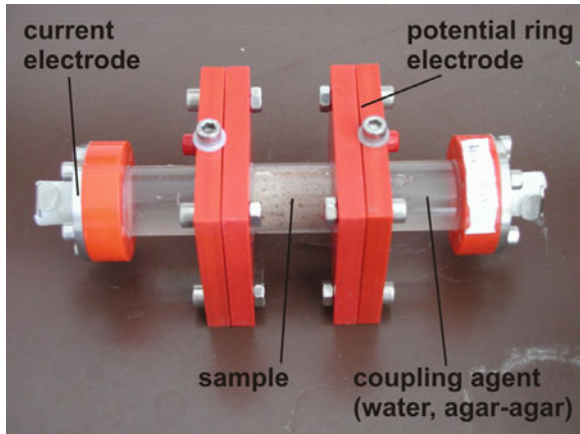$$R_{sample} = R - R_{sponges} \qquad \text{Eq. 3.}$$

Fig. 2.1 Two probe laboratory electrical resistivity measurement device

Fig. 2.2 Four-probe
laboratory electrical
resistivity measurement
device

Measurement can also be done with a four probe arrangement. Only the device change, the principle is the same. The potential measurement is done at separate electrodes (Fig. 2.2.). Main advantage is the independence from any contact resistances ($R_{Sponges}$ in the formulation above). The measurement cell is somewhat more complicated, but accuracy is significantly higher. For impedance measurements (see §9.2.4) in the low frequency range the use of four electrode arrangements is a requirement.

Finally, the resistivity (ρ in Ohm.m) of material is deduced integrating geometrical factors (or cell factor): height (l in m), and section (S in m²):

$$\rho = R_{sample} \, S / l \qquad\qquad \text{Eq. 4.}$$

Resistivity is independent of geometry and size of sample. The technique allows characterisation of concrete under controlled conditions. This resistivity is

Fig. 2.3 Electrical resistivity
measurement device for cover
concrete characterization
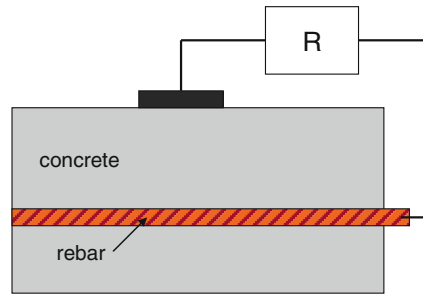
representative of average properties of material at the scale of sample. A resistivity
variation in the sample cannot be characterised.

This method is proposed to assess properties of initial concrete as a conformity
test for new concrete, as for example today compressive strength test.

9.2.2 On site measurement of cover concrete resistivity

Electrochemical measurements to detect corrosion activity in reinforced concrete
are strongly influenced by the concrete's resistivity. Simple two probe measure-
ments are providing the required information. Resistance (R in Ohm) between a
probe at the concrete surface (generally a little disc with D its diameter in m) and
the reinforcement is measured (Fig. 2.3). The resistance (R in Ohm) is calculated
from the potential drop measured by an electrical current impulse (Feliu et al.,
1990). The resistivity (ρ in Ohm.m) is given as:

$$\rho = 2\,R\,D \qquad\qquad \text{Eq. 5.}$$
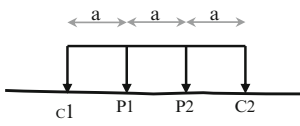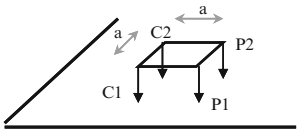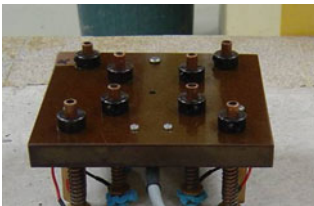
This approach is generally used simultaneously to electrochemical measure-
ments because it needs to connect probe to reinforcement. The measure has to
be done right to the rebar. It complete electrochemical measurement (corrosion
rate).

9.2.3 On site measurement with four probe devices

General on site resistivity measurement have to be done with four probe devices.
This approach is used to detect factors conditioning reinforcement corrosion
(moisture, salts, etc.) and probability of corrosion (Polder et al., 2000). Some others
applications have been developed independently of the rebar corrosion study (Sirieix
et al., 2007), (Klysz et al. 2006).

An electrical current is between two probes (I in A). The potential difference
(ΔU in volts) is measured between two separate ones. By using Ohm's law R = ΔU
/ l, the measured resistance (R in Ohm) is calculated. The size and geometry of the

Table 2.2 devices for on-site measurements of electrical resistivity

Device		Geometrical factor
Wenner configuration		$k = 2 \cdot \pi \cdot a$
Square configuration		$k = \dfrac{2 \cdot \pi \cdot a}{2 - \sqrt{2}}$

electrode arrangement are taking into account to calculate the apparent resistivity (ρ_a in Ohm.m), by the geometrical factor k (in m):

$$\rho_a = k\,R \qquad\qquad \text{Eq. 6.}$$

In homogeneous material the apparent resistivity equals true electrical resistivity. In structures with layers, inclusions or property variations, a mixed ("apparent") resistivity is measured. True values can be approximately calculated from sets of measurements with different spatial sensitivity and mathematical inversion: this is called electrical resistivity tomography, still in development on concrete.

Two different electrode configurations are generally used (Table 2.2). The electrode distance a (m) influences the depth of investigation. Many devices are using a = 0,05 m. By this way, concrete is characterised on the first few centimetres.

9.2.4   Frequency Domain Methods

Electrical resistivity measurements are normally done using direct current, in most cases alternating direction to avoid electrode polarisation. Using alternating currents at various frequencies additional parameters can be derived. Most of them are related to solid/liquid interfaces, thus providing information about the microstructure of concrete.

High frequency methods (several kHz – several MHz, Electrical Impedance Spectroscopy, EIS) can be used to assess the dielectric constant ε (Ping Gu *et al.*, 1993). The technique consists in the measure of electrical responses (not only resistivity) of concrete for several signal frequencies. This technique is currently focused on the study of concrete hardening (Ping Xie et al., 1993), or on the system

Table 2.3 Corrosion speed probability from resistivity measurements

Electrical resistivity (Ohm.m)	Probability of corrosion speed
> 1000 – 2000	Negligible (concrete is too dry)
500 – 1000	Weak
100 – 500	Moderate to high (when steel is active)
< 100	Resistivity is not the driving factor of corrosion

rebar-concrete in the aim of rebar corrosion study (Koleva et al., 2008). The method is not well adapted to on site investigations, even some results are on monitoring of concrete structures (Ozyurt et al., 2006).

Low frequency applications (several mHz – several kHz, Spectral Induced Polarisation, SIP) are currently under research. Results from other material as masonry indicate, that SIP might be able to provide information about porosity and geometry related parameters as permeability or formation factors ($F = a\,\varphi^{-m}$ in eq.1) as well as a method to distinguish between saturation and salt contamination effects (Kruschwitz, 2008).

9.3 Calibration, data processing, interpretation of results

As many factors are influencing the electrical resistivity the interpretation is mainly based relative variations. For characterisation of probability of corrosion by electrical resistivity, threshold values are proposed for on site assessment. The method measures only the presence of factors influencing rebar corrosion, which have both similar effects on resistivity: moisture and salts. Both decrease electrical resistivity (Table 2.3). But many cases prove the limitation of interpretation based on these thresholds. So today, engineers prefer to adapt the treshold values in each case by a visual inspection of rebars (opening a window in concrete).

9.4 Reliability and limitation of results

Resistivity of concrete is influenced by many parameters, linked with the material properties, with the structure or with the environment:

– Parameters depending on the concrete composition: cement type (Hammond and Robson, 1955), water/cement ratio (Hammond and Robson, 1955), (Whittington et al., 1981), aggregate (nature, quantity, etc.) (Millard, 1991),(Morris et al., 1996)
– Environmental factors: temperature (Spencer, 1937), moisture (Wolf and Lauer, 1980), salt ingress (Saleem et al., 1996)
– Geometrical effects: influence of rebar and edges (Millard, 1991), (Lataste et al., 2003b).

Table 2.4 Some electrical resistivity ranges for concrete

Influence of concrete		Electrical resistivity (Ohm.m)
Ordinary Portland Cement (35MPa)		500 – 1400
Self compacting concrete (35MPa)		300 – 1000
High Performance concrete (65MPa)*		850 – 1500
Fibre Reinforced Concrete		80 – 400
Influence of conditions	Electrical resistivity (Ohm.m)	
Environment	Ordinnary Portland Cement	Other concrete
Very wet, spayed atmosphere	50 – 200	300 – 1000
Natural atmosphere	100 – 400	500 – 2000
External atmosphere (she ltered concrete, 20°C/80%HR)	200 – 500	1000 – 4000
Carbonated concrete	1000 and more	2000 and more
Internal atmosphere (20°C, 50%RH)	3000 and more	4000 and more

* Containing slag (>65%), or fly ashes (>25%), or silica fume (>5%)

The variation ranges for the resistivity depending on the value taken by some of these parameters are provided at Table 2.4. These multiple influences restrict the interpretation to the delineation of relative variations of resistivity. An isolated value of resistivity cannot be interpreted. However variations in time or geometry (lateral variations or in depth) make it possible to assess material or structure characteristics.

9.5   Guidelines for use, references, standards

Currently there are nor guidelines, references or standards available. Recommendations can be found. They give some elements allowing reliability of resistivity measurements (Polder *et al.*, 2000) (Chlortest, 2006)

9.6   On-going developments: problems under research, new questions, specific developments

Electrical resistivity is sensitive to many factors which are important for the assessment of concrete structures. Porosity, humidity and salt (e.g. chlorides) are three main parameters leading the electrical behaviour of material. So, resistivity has the potential to be used as an indicator for durability and to characterise the material. There for this this measure might be considered as laboratory conformity test in the future.

Main problem for interpretation of on site measurements in terms of the damage detection and assessment is to separate quantitatively the various factor influencing

the measurement. This point was studied in the frame of the French ANR-SENSO project, where two possibilities were identified:

– better definition of parameters a, m, and n for concrete in the Archie law (for inverse analysis of measurements);
– using resistivity in combination with other techniques to assess values of porosity or saturation rate of concrete.

Others topics in progress are: on site crack investigation (Lataste et al., 2003a), characterisation of steel fibers in FRC (Lataste et al., 2008) (Ozyurt et al., 2006), electrical resistivity tomography (Chouteau et al., 2002), EIS for rebar corrosion assessment (Koleva et al., 2008), application of SIP techniques (Kruschwitz, 2008).

References

Andrade C., Alonso C., Arteaga A., Tanner P. (2000) Methodology based on the electrical resistivity for calculation of reinforcement service life. Fifth CANMET/ACI International Conference, 899–915.

Archie G. (1942) The electrical resistivity log as an aid in determining some reservoir characteristics, Transaction of the American Institute of Mining and Metallurgical Engineers, vol. 146, pp. 54–62

Baroghel-Bouny V. (2004) Conception des bétons pour une durée de vie donnée des ouvrages – maîtrise de la durabilité vis-à-vis de la corrosion des armatures et de l'alcali réaction, documents scientifiques et techniques de l'AFGC, 252p.

CHLORTEST – Resistance of concrete to chloride ingress – From laboratory tests to in-field performance – Testing Resistance of Concrete to Chloride Ingress: – A proposal to CEN for consideration as EN standard (2006) 22 p.

Chouteau M., Beaulieu S., Fréchette V., Toe E. (2002) Application de la tomographie de résistivité électrique aux infrastructures routières en béton, INFRA, Montréal, Québec.

Feliu S., Andrade C., Gonzalez J.A., Alonso C. (1996) A new method for in situ measurement of electrical resistivity of reinforced concrete, Material and Structures, vol. 29, pp. 362–365.

Hammond E., Robson T. (1955) Comparaison of electrical properties of various cement and concrete, The Engineer, vol. 199, pp. 78–80 and pp. 114–115.

Klysz G., Lataste JF., Fnine A., Dérobert X., Piwakowski B., Buyle-Bodin F. (2006) Auscultation non destructive du chevêtre du pont de la Marque (59), Revue Européenne de Génie Civil, 10(1), pp., 1–24

Koleva D.A., Van Breugel K., De Wit J.H.W., Van Westing E., Copuroglu O., Veleva L., Fraaij A.L.A. (2008) Correlation of microstructure, lectrical properties and electrochemical phenomena in reinforced mortar. Breakdown to multi-phase interface structures. Part I: Microstructural observations and electrical properties, Materials Characterization, vol. 59, pp. 290–300.

Kruschwitz, S. (2008) Assessment of the complex resistivity behaviour of salt affected building materials. Ph.D. thesis, BAM/ TU Berlin.http://www.bam.de/de/service/publikationen/publikationen_medien/dissertationen/diss_30_vt.pdf

Lataste JF., Behloul M., Breysse D. (2008) Characterisation of fibres distribution in a Steel Fibre Reinforced Concrete with electrical resistivity measurements, NDT&E international, 41(8), pp. 638–647.

Lataste JF., Sirieix C., Breysse D., Frappa M. (2003a) Electrical resistivity measurement applied to cracking assessment on reinforced concrete structures in civil engineering, Non Destructive Testing and Evaluation International, vol. 36 n°6, pp. 383–394.

Lataste JF., Sirieix C., Breysse D., Frappa M. (2003b) Improvement of electrical resistivity measurement for non destructive evaluation of concrete structures, 2nd International RILEM

workshop on life and aging management on concrete structures, Paris (F), May 5-6 2003, pp. 93–102 (ISBN 2-912143-36-5).

Millard S.G. (1991) Reinforced concrete resistivity measurements techniques, Proceedings of the Institution of Civil Engineers, Part 2, vol. 91, pp. 71–88.

Morris W, Moreno E.I., Sagues A.A. (1996) Practical evaluation of resistivity of concrete in test cylinder using wenner array probe, Cement and Concrete research, Vol. 26, n 12, pp. 1779–1787.

Naar S. (2006) Evaluation non destructive du béton par mesures de résistivité électrique et thermography infra rouge passive, Thèse de l'université Bordeaux 1, 248p.

Ozyurt N., Mason T.O., Shah S.P. (2006) Non destructive monitoring of fiber orientation using AC-IS : An industrial-scale application, Cement and Concrete Research, Vol. 36, pp. 1653–1660.

Ping Gu, Zhongzi Xu, Ping Xie, Beaudoin JJ. (1993) Application of A.C. Impedance techniques in studies of porous cementitious materials, (I) Influence of solid phase and pore solution on high frequency resistance, Cement and Concrete Research, vol. 23, pp. 531–540.

Ping Xie, Ping Gu, Zhongzi Xu, Beaudoin J.J. (1993) A rationalized AC impedance model for microstructural characterization of hydrating cement systems, Cement and Concrete Research, vol. 23, n°2, pp.359–367.

Polder R., Andrade C., Elsenser B., Vennesland O., Gulikers J., Weidert R., Raupach M. (2000) Rilem TC154-EMC: electrochemical techniques for measuring metallic corrosion, Materials and structures, vol. 33, pp. 603–611.

Saleem M., Shameem M., Hussain S.E., Maslehuddin M. (1996) Effect of moisture, chloride and sulphate contamination on the electrical resistivity of Portland cement concrete, Construction and Building Materials, Vol. 10, n°3, pp. 209–214.

Sirieix C., Lataste JF., Breysse D., Naar S., Dérobert X. (2007) Comparison of non destructive testing : infrared thermography, electrical resistivity and capacity methods in a reinforced concrete structures Tarbes' precast duct, Journal of Building Appraisal, Vol. 3, n°1, pp.77–88

Spencer R.W. (1937) Measurement of the moisture content of concrete, Journal of the American Concrete Institute, Vol. 9, n°1, pp. 45–61

Whittington H.W., Mc Carter J., Forde M.C. (1981) The conduction of electricity through concrete, Magazine of Concrete Research, Vol. 33, n° 144, pp. 48–60.

Woelfl G.A., Lauer K. (1980) The electrical resistivity of concrete with emphasis on the use of electrical resistance for measuring moisture content, Cement Concrete and Aggregates, Vol. 1, n°2, pp. 64–67.

10   Infrared thermography

Didier Defer and Christiane Maierhofer

10.1   Physical principles and theory

Infrared radiation covers the spectral range from 0.78 to 1,000 μm. For standard application in infrared thermography, a range from 1.5 to 14 μm is used. This type of radiation is mainly emitted by the object itself. Spectral range and intensity of the emitted radiation depend on the temperature, which describe the molecular movement, and the emissivity. For a black body, the spectrum of thermal radiation can be described by Planck's law (Eq. 1):

$$L_\lambda^{black\_body}(T) = \frac{C_1 . \lambda^{-5} .}{\pi . \left[\exp\left(\frac{C_2}{\lambda.T}\right) - 1 \right]} \qquad \text{Eq. 1.}$$
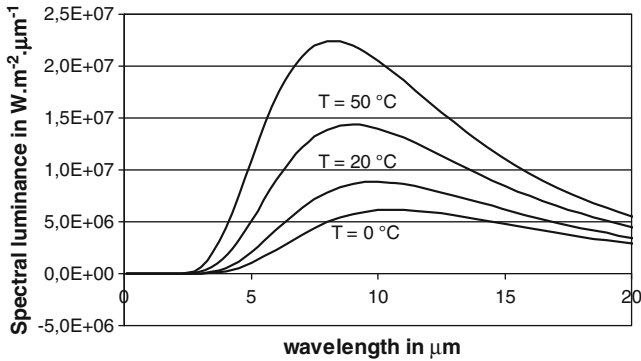
Fig. 2.1 Spectra of blackbody radiation vs wavelength for different temperatures

Table 2.1 Normal total emissivity at 20° C for classical building materials

Materials	Rough concrete	Asphalt	Red brick	Plaster	Dry soil Wet soil
ε	0.92	0.93	0.93	0.91	0.9 0.95

where $L_{\lambda}^{black-body}(T)$ is the spectral brightness (W.m^{-2}.µm^{-1}.sr^{-1}) emitted by the black body, λ is the wavelength (m) and C1 and C2 are two constants of radiation.

Fig. 2.1 shows the appearance of spectra of radiation of black bodies for various temperatures.

The emissivity ε is the ratio between the radiated power emitted by a general structure in relation to the power emitted by an ideal radiator (black body). For a black body, the radiated power is independent of material properties and depends only on its temperature. Therefore, the emissivity of a blackbody is always 1. The emissivity of real structures varies between 0 and 1 ($0 < \varepsilon < 1$) and depends more or less on the temperature, the wavelength, the polarisation and the angle to the normal. This dependency is influenced by the surface properties like roughness and contamination. For each body, the directed spectral emissivity is equal to the directed spectral absorptivity (Kirchhoff's law). Table 2.1 shows typical values of emissivity for some building materials.

At ambient temperatures, a large part of this radiation is situated in the spectral range between 1.5 and 20 µm where the human eye is insensitive. To detect this radiation, infrared cameras are used which include one detector or a detector array (focal plane array, FPA) to convert this radiation into an electric signal. Two atmospheric transmission windows are used (3 to 5 µm or 8 to 12 µm). For FPAs, each detector receives radiation from a small solid angle (instantaneous field of view, IFOV).

The radiometric equation (Eq. 2) describes the calculation of temperature from the measured radiation intensity. A camera which observes an object (Fig. 2.2) receives radiation that is made up of three parts: the radiation emitted by the object at a constant temperature T_0, the radiation of the environment at the temperature T_e

Fig. 2.2 Composition
of the radiation received
by the camera
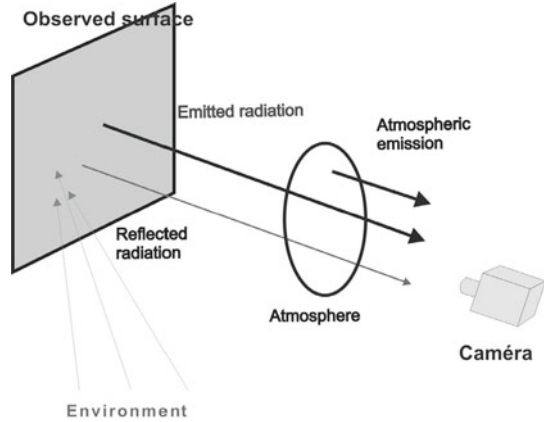
reflected by the object (if the emissivity is < 1) and the radiation emitted by the atmosphere between the object and the detector.

$$I' = \tau_{atm}[\varepsilon_0 I_0 + (1-\varepsilon_0)I_e] + (1-\tau_{atm})I_{atm} \qquad \text{Eq. 2.}$$

where the three parts $\varepsilon_0 I_0$, $(1 - \varepsilon_0) I_e$ and $+ (1 - \tau_{atm}) I_{atm}$ respectively correspond to the surface emission, the reflected variation and the atmospheric emission, with:

I' = radiation detected by the camera [W.m^{-2}.sr^{-1}]
I_0 = radiation of the object itself [W.m^{-2}.sr^{-1}]
I_e = radiation of the environment [W.m^{-2}.sr^{-1}]
I_{atm} = radiation of the atmosphere [W.m^{-2}.sr^{-1}]
ε_0 = emissivity of the object
τ_{atm} = coefficient of transmission of the atmosphere

The atmospheric transmission τ_{atm} is a function of the distance between the surface under test and the camera and the atmospheric properties. For short distances, it can be approximated by 1. Beyond several metres the absorption and emission of the atmosphere itself can no longer be neglected. The humidity affects transmission in a great deal.

When the parameters of the radiometric equation are estimated, the average temperature of the surface may be deduced. The quality of the estimation of temperature values is directly linked to the validity of the hypotheses and the accuracy with which the various parameters are determined.

The methods of auscultation by infrared thermography may be classified in two categories:

• Passive methods, for which no additional source of heat is used specifically to carry out the auscultation.
• Active methods, for which the diffusion of heat is provoked by artificial means, set up to carry out the auscultation.

The characteristics of these two categories will be discussed in the following.

10.2   Measuring equipment and handling: the infrared camera

In the 1990s, focal plane arrays (FPA) were developed and the increase of array size, thermal resolution and image repetition frequency during the last ten years has accelerated the applications in several areas. Adjusted to the area of application and to the environmental conditions, different IR cameras can be used which are mainly distinguished by the detector types. Among others, these detectors are characterized by their spectral range, spatial resolution, noise equivalent temperature difference (NETD, thermal resolution), integration time and long term stability. With these detectors, commercial IR cameras with a full frame rate of up to 1 kHz for a FPA size of 256 x 256 were achieved. For lower frame rates, larger arrays (1024 x 1024) can be used. The maximum thermal resolution (NETD) is less than 15 mK.

For a thermographic study, the choice of camera's position results of a compromise between spatial resolution and size of observed area. Numbers of detectors (pixels) and optic system of the camera are parameters of the choice. The required objective has to be selected (wide angle, normal, tele). For example, with an objective of 24°x18° (horizontal field of view x vertical field of view) and a matrix of 320x240 detectors, the IFOV is 1.3 mrad. If the camera has a distance of one meter from the surface, the observed area is a 40 x 30 cm² rectangle. Each pixel corresponds to a 1.3 x 1.3 mm² rectangle.

If possible, the camera should be positionned following the surface normal. Before starting data acquisition, the camera should be switched on for at least 30 min.

10.3   Data processing, calibration and interpretation

Infrared thermography allows observing a field of temperature on a surface. The information is extracted from gradients observed at the surface at one time. Information may also be deduced from evolutions of the temperature field with time. Temperature gradients or variations can only be observed if the system is submitted to heat transfer.

When considering the investigation of civil engineering structures by infrared thermography, we are faced with difficulties which make the exploitation of numerical values of temperature difficult. The temperature of the environment is an ideal that is hard to establish. The emissivity of the material is not known with great accuracy and it might vary along the surface and with the angle of observation. However surfaces of non-metallic elements in civil engineering have high emissivities and low reflection coefficients. Strong reflections due to direct sunlight for example must be avoided. Most of the applications developed up to now for testing of structural elements or buildings involve qualitative exploitation. They aim to interpret temperature differences. In a quantitative procedure, the analysis of absolute temperatures is envisaged.

In case of on-site applications, the influence of rain, fog and wind has to be considered.
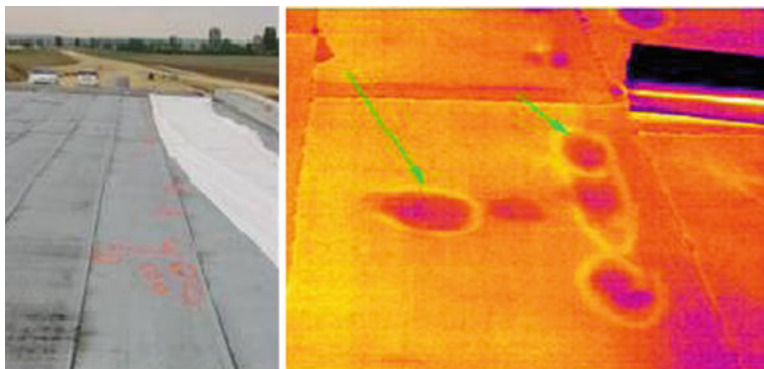
Fig. 2.3 Study of waterproof covering: visible image (left) and infrared image (right)

10.4   Passive thermography applied to the investigation of discontinuities

10.4.1   Principles

Temperature gradients at the surface may denote the presence of an anomaly under the surface of the material when the surface is exposed to the environment (sunshine, variation of the daily ambient temperature, etc.). If the surface is submitted to a thermal variation, the heat diffuses inside the material. The presence of a discontinuity such as a delamination, cavity or crack introduces a change of thermal properties which alters heat transfer. For instance, a hotter zone might appear at the surface depending on the thermal properties. Conversely, if there is heat loss (cooling), the signature will be a cold layer. Heat diffusion may also be modified by contrasting thermo-physical properties within the material.

The following example concerns the investigation of a waterproof covering on a bridge. The defects of adhesion of the covering are easily detected by using infrared thermography. The parts that have come unstuck appear warmer at the surface (see Fig. 2.3-right). Natural environmental effects are sufficient to generate a serious temperature contrast. Figure 2.4 shows the case of a concrete structure reinforced by composite plates. Preliminary thermography studies can be used to control the quality of reinforcement.

10.4.2   Limits and reliability

For detecting inhomogeneities, the following conditions must be satisfied:

First, the thermo-physical properties of the defect and the material must be contrasted enough.
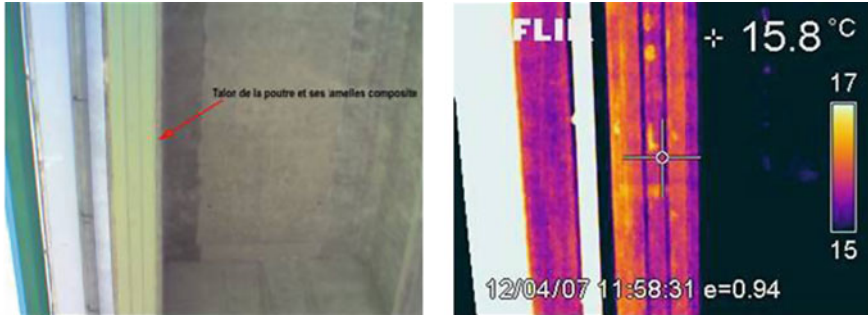
Fig. 2.4 Study of the quality of interface between concrete and composite reinforcing plates: visible image (left) and infrared image (right)

For estimating the detectability of defects and inhomogeneities in structures, the heat transfer can be described by the thermal wave propagation (harmonic heating process with wavelike temperature field) (Maldague and Moore, 2001). In this model, the reflectivity of thermal waves at interfaces is determined by the differences between the effusivities of the contiguous materials. For the one-dimensional case, the reflection coefficient R of a plane thermal wave for transmission from medium 1 to medium 2 is equal to:

$$R_{12} = \frac{e_1 - e_2}{e_1 + e_2} = \frac{\sqrt{\rho_1 c_1 \lambda_1} - \sqrt{\rho_2 c_2 \lambda_2}}{\sqrt{\rho_1 c_1 \lambda_1} + \sqrt{\rho_2 c_2 \lambda_2}}$$

Thus, for a successful detection of inhomogeneities, there must be a sufficient difference between the thermal properties of medium 1 and 2. The larger the difference between the effusivities of the two media, the higher the thermal signature of the inhomogeneities is. For instance, the reflection coefficient at a concrete/air interface is about 100%, while the reflection coefficient of a concrete/steel interface is about -24%.

The second condition is on size: at a given depth, defects can be detected only when they are large enough. Typically, the size must be at least equal to the depth.

The third condition for detectability is linked to the heat wave penetration depth. The study of the heat wave propagation shows that a sinusoidal variation at the surface is propagated in the material with amplitude which decreases exponentially with the depth. The depth at which the amplitude is decreased to e^{-1} is the penetration depth p:

$$p = \sqrt{(a / \pi\, f)}$$

where p is the depth of penetration (m), a is the thermal diffusivity ($m^2.s^{-1}$), f is the thermal excitation frequency (Hz).

At the surface, the response to thermal excitation is not sensitive to the presence of a discontinuity if its depth exceeds three times the penetration depth.

Fig. 2.5 Temperature variations on the surface for a plain slab and a slab with delamination
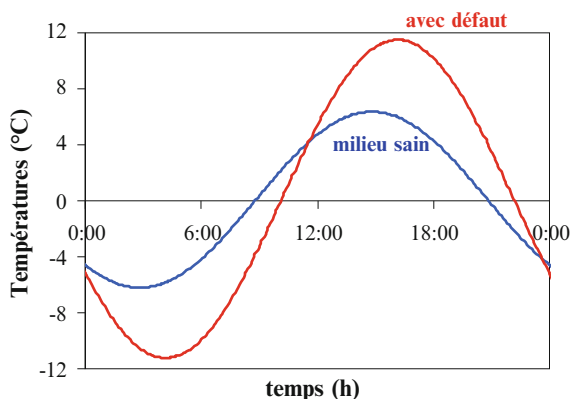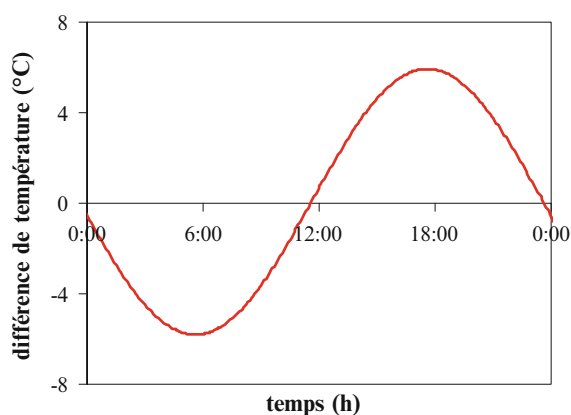

Fig. 2.6 Temperature difference between a point above the defect and a zone with defect

For example, a day-night cycle can be assimilated as a first approximation to a sinusoidal variation of 1.16×10^{-5} Hz. For concrete, the depth of penetration corresponding to this frequency is of the order of 10 cm. This means that defects deeper than 30 cm cannot be easily detected. Thus lower frequencies are required. For example, the response to the annual seasonal cycle can highlight anomalies situated at a few metres in depth. Day/night variations are often used for the detection of defects located near the surface.

Results of a simulation is presented there. A concrete slab in which a void is present at depth e is submitted to a 24h-harmonic thermal excitation. The imposed heat flux on the upper surface follows a sinusoidal variation. Fig. 2.5 show surface temperatures evolutions. In this case, a 1-cm thick air gap is situated 5 cm from the surface and above sound material.

The temperature time variations appear to be more contrasted above the delaminated zone, which are warmer during the day and colder during the night. The simulations show that the morning (6h) and the late afternoon (18h) are the most interesting times of the day, since they enable the highest temperature differences between the zones with and without a defect to be observed (see Fig. 2.6).
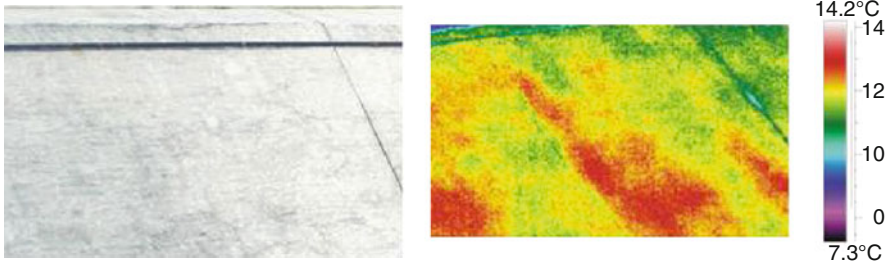
Fig. 2.7 Study of a concrete siding: visible image (left) and infrared image (right)

The fourth condition is to have a thermal excitation whose amplitude is sufficient. The thermal contrast may be reduced if the convection at the surface that is too strong (e.g. due to wind).

Figure 2.7 illustrates the investigation of a concrete facing installed on the edge of a lock. Delaminations are detected by a thermogram recorded at the end of the day.

10.5 Investigations with active thermography

10.5.1 Principles

Active infrared thermography methods are based on the active heating or cooling of the structures under test to provide an unsteady temperature gradient (Maldague and Moore, 2001). In civil engineering, two of these active methods, impulse-thermography (IT) and pulse phase thermography (PPT), have been proven to be very useful for the investigation of structures close to the surface.

Experimental set-up and data acquisition are identical for IT and PPT: the surface of the structure to be investigated is heated by using a radiation source (also other energy sources are applicable depending on the testing problem) as visualised in Fig. 2.8. After switching off the heating source, the cooling down behaviour is recorded in real time with an infrared camera. The propagation of the heat depends on the material properties like thermal conductivity, heat capacity and density. If there is an inhomogeneity in the near surface region of the object with different thermal properties, the heat flow will slow down or accelerate in these local areas. While observing the temporal changes of the surface temperature distribution with the infrared camera, near surface inhomogeneities will be detected if they cause measurable temperature differences on the surface.

The main approach of IT in analysing the thermal data was to interpret the function of surface temperature versus cooling time (see Fig. 2.9) for selected areas with and without inhomogeneities. These selected transient curves were compared and difference curves (difference between transient above a void and transient above a
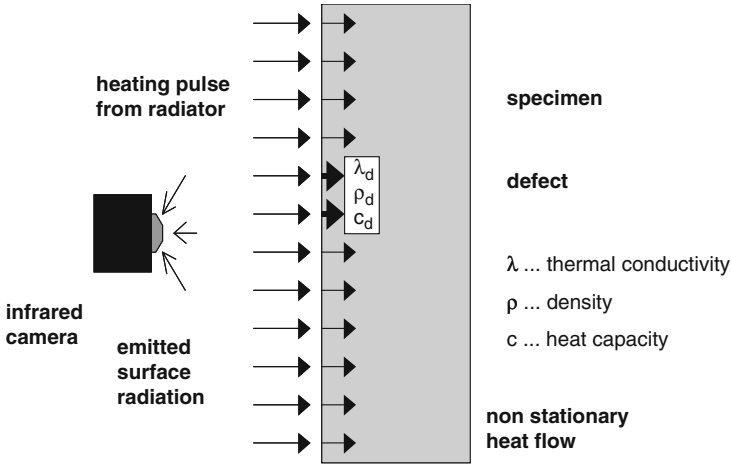
Fig. 2.8 Principle of impulse-thermography and pulse-phase-thermography. The surface is heated up with a heating impulse and the cooling down behaviour is observed with an infrared camera
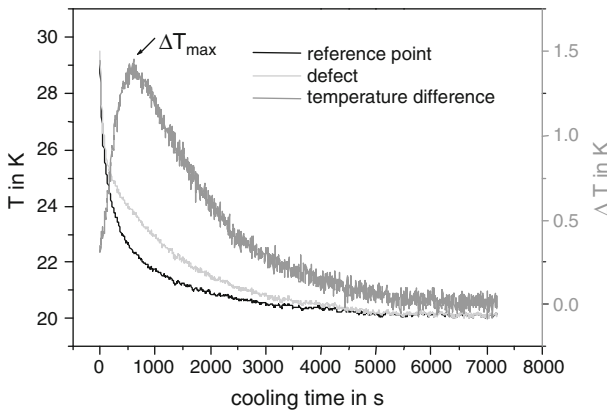
Fig. 2.9 Transient curves above a reference point and above a defect and the respective difference curve with a maximum temperature ΔT_{max} at a distinct time t_{max}

sound area) were calculated as shown in Fig. 2.9. The difference curves usually have a maximum of the temperature difference ΔT_{max} at a distinct time t_{max}, which depends mainly on the difference of the thermal properties, the depth of the void and the heating time. For solving the Inverse Problem, i. e. to get information about the thermal and geometrical properties of the detected defect from the difference curves, numerical simulations are performed (Maldague and Moore, 2001).

PPT is based on the application of the Fast Fourier Transformation (FFT) to all transient curves of each pixel. Thus, one obtains amplitude and phase images for all

frequencies. Amplitude images show the internal structure of a specimen up to a maximum available depth depending on the frequency (low pass filter behaviour). Phase images show the internal structure within a certain depth range depending on the frequency (band pass filter behaviour) [(Maldague and Moore, 2001), (Maldague, 2001), (Wedler et al., 2003), (Maldague, 1993)].

10.5.2 Measurement equipment and handling (general)

The experimental set-up consists of a thermal heating unit, an infrared camera and a computer system, which enables digital data recording in real time.

For the civil engineering applications, the heating pulse is realised as a square pulse, which can be described as a superposition of different frequencies with varying amplitudes.

In most cases, infrared radiators have be proven to be the most suitable sources, being fast and efficient and generating a homogeneous temperature increase. For this, the heating procedure is usually done dynamically by moving the radiators (computer-controlled) at an appropriate distance from the surface and by using an automatic scanner system to obtain the best possible homogeneous heating. The heating time varies from several seconds up to 60 min. It must be considered that the surface temperature should not rise higher than 50°C to avoid any damage. This temperature has to be even less for sensitive surfaces. The cooling down process of the surface is observed with an infrared camera. This camera and the related software for data acquisition and analysis should at least fulfil the following conditions:

– availability of recording of sequences of thermal images with a minimum frame rate of 1 to 10 Hz to record fast cooling down processes;
– known file format of thermal sequences for further data analysis;
– extraction of transient curves (temperature as a function of time for one pixel) must be possible;
– for on-site measurements, the heating source has to be placed close to the surface under investigation (distance 10 to 20 cm) and should be moveable to obtain a homogeneous heating. A respective power supply must be available.

An operational test should be performed measuring the surface temperature of a known object (reference object). A first thermogram of the surface to be investigated should be recorded to have a reference image in more or less thermal equilibrium. During the whole time range of data recording, it should be ensured that nothing and nobody is crossing in the area between camera and observed surface.

10.5.3 Data Processing related to impulse-thermography (IT)

Data processing related to IT is performed if qualitative and quantitative information is needed about inhomogeneities and defects near below the surface.

As raw data, temporal sequences of thermograms are available containing information about environmental and measurement parameters in the header. The single steps of IT data processing are the following:

– Correction of temperature data related to surface emissivity and environmental parameters, if this has not been already performed on-site;
– enhancement of the signal to noise ratio, e. g. by averaging of thermograms or spatial or temporal filtering;
– location of defect areas by visual examination of the thermograms. Contrast areas can be accentuated by edge filtering or through further steps of image processing;
– transformation of geometrical parameters (size and position of measurement area, planar size and position of inhomogeneities or defects);
– selection of transient curves (temperature of a pixel as a function of time during cooling down) of pixels above sound and defect area, calculation of the difference curve;
– calculation of maximum thermal contrast ΔT_{max} and the respective time t_{max} after the switching off of the heating source by analyzing the temporal variation of contrast, as on Fig. 2.9;
– from calibration curves and/or numerical simulations, the Inverse Problem can be solved, e. g. quantitative information can be obtained about the depth (concrete cover). But this is only possible if a lot of prior knowledge is available, e. g. the thermal properties of sound and defect material must be known.

10.5.4   Data processing related to Pulse-phase thermography

Data processing related to PPT is also performed if qualitative and quantitative information are needed about inhomogeneities and defects near the surface. In PPT, non unique emissivity at the surface and indirect reflection have a reduced influence on the results. The sensitivity to deeper defects is thus enhanced.

As raw data, temporal sequences of thermograms are available containing information about environmental and measurement parameters in the header similar to IT. The single steps of PPT data processing are the following:

– Correction of temperature data related to surface emissivity and environmental parameters, if this has not been already performed on-site;
– enhancement of the signal to noise ratio, e. g. by averaging of thermograms or spatial or temporal filtering;
– calculation of Fast Fourier Transformation (FFT) of each transient curve resulting in amplitude and phase spectra. For enhancing the frequency resolution, zero padding of the transient curves can be performed (enhancing the transient curves in total time range with room or offset temperature). Since most of the information in the spectra is included in the very low frequencies, zero padding is essential;
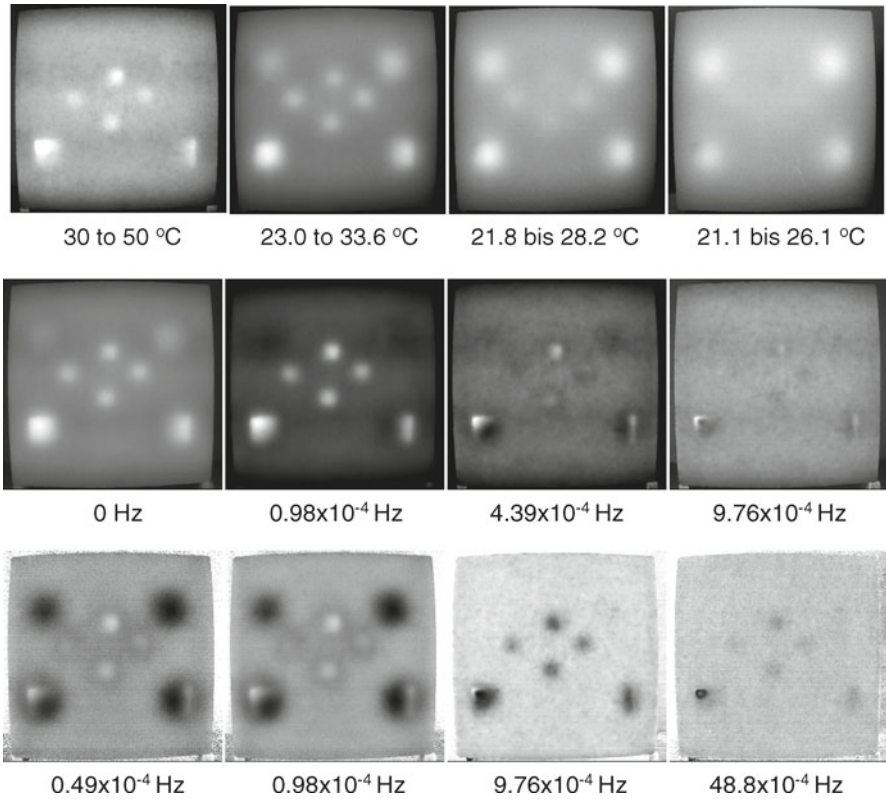
30 to 50 °C	23.0 to 33.6 °C	21.8 bis 28.2 °C	21.1 bis 26.1 °C

0 Hz	0.98x10⁻⁴ Hz	4.39x10⁻⁴ Hz	9.76x10⁻⁴ Hz

0 Hz 0.98×10^{-4} Hz 4.39×10^{-4} Hz 9.76×10^{-4} Hz

0.49×10^{-4} Hz 0.98×10^{-4} Hz 9.76×10^{-4} Hz 48.8×10^{-4} Hz

Fig. 2.10 Images built at respective times (0, 34.5, 68.5 and 102.8 min after 30 min heating time): thermograms (top), amplitude images (middle) and phase images (bottom). The concrete specimen contains voids at varying depth from 2 to 8 cm

– for each frequency, amplitude and phase can be presented for each pixel resulting in amplitude and phase images. Thus also in amplitude and phase images can be presented in sequences (as a function of frequency).

As an example, selected thermograms, amplitude and phase images of the concrete test specimen with voids at different depths are shown in Fig. 2.10. In the phase image at the lowest frequency in Fig. 2.10, all defects can be clearly seen with better contrast as in the time sequences. With increasing frequency, the deeper defects disappear in the amplitude as well as in the phase images, but earlier in the amplitude images.

The data processing described above might lead to identify inhomogeneities inducing after thermal activation a lower or a higher surface temperature than in the sound area. As mentioned above, the thermal properties and the depth of these inhomogeneities can only be determined if comprehensive prior-knowledge is available.

In most cases, further quantitative results will be available only on the depth of inhomogeneities or defects, which will have more or less large relative errors.

10.6   Guidelines and Standards

For the applications of active thermography for concrete testing, at time there are no standards. Guidelines for the investigation of historic masonry structures have been developed during the EC funded project ONSITEFORMASONRY and will be enhanced by the RILEM TC SAM.

In the following, related standards concerning passive and active thermography are listed:

ASTM C 1046, Standard practice for in-situ measurement of heat flux and temperature on building envelop components, 1995

ASTM C 1060, Standard practice for thermographic inspection of insulation installations in enbvelope cavities of frame buildings, 1990

ASTM C 1153, Standard practice for location of wet insolation in roofing systems using infrared imaging, 2003.

ASTM D 4788, Standard test method for detecting delaminations in bridge decks using infrared thermography, 2003

DGZfP-B, Guideline for thermographic investigations at building elements and building structures, Edition 1993-10 (in german)

DGZfP-TH 1, Characterization of thermography systems, Edition 1999-03 (in german)

DIN 54162, Non-destructive testing – Qualification and certification of personnel for thermographic testing – General and special principles for level 1, 2 and 3, Edition 2006-09

DIN 54190-1, Non-destructive testing – Thermographic testing – Part 1: General principles, Edition 2004-08

DIN 54190-2, Non-destructive testing – Thermographic testing – Part 2: Equipment, Edition 2005-08

DIN 54190-3, Non-destructive testing – Thermographic testing – Part 3: Terms and definitions, Edition 2006-02

DIN EN 13187 Thermal performance of buildings – Qualitative detection of thermalnirregularities in building envelopes – Infrared method, Edition 1999-05

References

Busse G., Wu D., Karpen W. (1992) Thermal wave imaging with phase sensitive modulated thermography, J. Appl. Phys., 71, 3962.

Maldague X. P. (1993) Nondestructive Evaluation of Materials by Infrared Thermography, Springer-Verlag.

Maldague X.P., Couturier J.P. (1997) Review of pulsed phase thermography, Atti della Fondazi one G. Ronchi, Carloma G.M. and Corsi C. (eds), pp. 271–286.

Maldague, X. P. (2001a) Theory and Practice of Infrared Technology for Nondestructive Testing, Wiley.

Maldague, X. P., Moore P. (2001) Nondestructive testing handbook, Infrared and thermal testing, ASNT.

Vavilov V., Marinetti S. (1999) Thermal Methods Pulsed Phase Thermography and Fourier-Analysis Thermal Tomography, Russian Journal of Nondestructive Testing, 35, 134-145.

Wedler G., Brink A., Röllig M., Weritz F., Maierhofer C. (2003) Active Infrared Thermography in Civil Engineering - Quantitative Analysis by Numerical Simulation, Int. Symposium NDT-CE, Berlin.

11   Radiography

Jean-Paul Balayssac

11.1   Physical principles and theory

Radiography in civil engineering can concern a lot of structures. Theoretically the limitations are only related to the penetration depth of the rays and to the exposure rate of the emitter. It can be used on concrete, reinforced or prestressed concrete, stone, mortar and steel.

Like it is a transmission technique, it needs to access to the two opposite faces of the structure. One face is highlighted by the source and the sensitive film is placed on the other one. In radiography, the radiation is either X-ray or gamma-ray. Gamma rays are emitted by an artificial source (Cobalt 60 or Iridium 192). In the case of X-rays, accelerators are used to obtain higher energy. For usual applications, the radiation attenuation through the material is measured with a sensitive film located on the opposite face (Fig. 2.1).

Field applications of radiography include the detection of reinforcement location, voids, cracks, the quality of grouted post-tensionned tendons and the failure of cables. As well, radioscopy is a different form of radiography in which the transmitted radiation is converted into a visible light and recorded by a video camera. Radioscopy has been used in France for the detection of grouting defects.

Classically, industrial radiography is able to observe:

– the presence of cavities inside the concrete
– the presence of grout inside the prestressing ducts and also its defects
– the localization of tendons
– the localization of the reinforcement and the diameter of the rebars
– the discontinuities of the ducts
– the broken wires or cables in some cases.

11.2   Measurement equipment and handling

The source is chosen in relation with the scope of the investigation (size of the target, thickness of the concrete element, implementation conditions and radioprotection). The weight of the source is linked to its power of penetration through the material. Table 2.1 gives examples of source characteristics. The picture of Fig. 2.2 illustrates an example of a source of Iridium 192.

The choice of the source depends on the exposure time, the thickness of the element and the required resolution.

For the receptors, the use of photographic films (emulsion) is very usual and the different categories of films are defined by standards. The film is always associated to a filter and a reinforcing screen. The choice of the film is done regarding the thickness
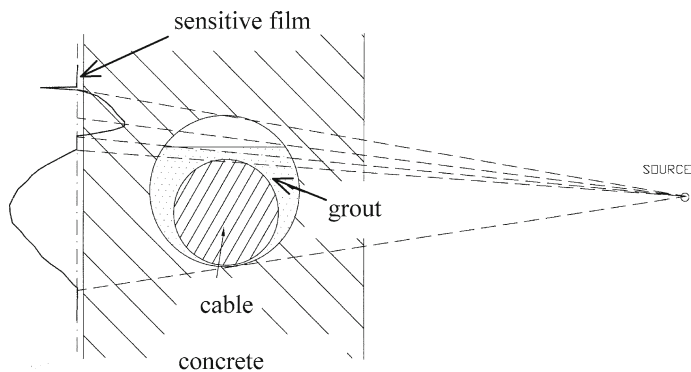
sensitive film

SOURCE

grout

cable

concrete

Fig. 2.1 Principle of radiography

Table 2.1 Source characteristics

Source	Radioactive half-life	Weight of the source (kg)	Maximal thickness (cm)
Iridium 192	74 days	25	30
Cobalt 60	5.3 years	120	40
Cobalt 60	5.3 years	350	65
X-rays		45 to 120	130

Fig. 2.2 Source of Iridium 192

of the element, the required sensitivity and also the exposure time. The image quality depends on the emitter, the distance between the source and the film, the incidence of the rays, the choice of the film, the reinforcing screen and the filter. The distance between the source and the film depends on the thickness of the element.
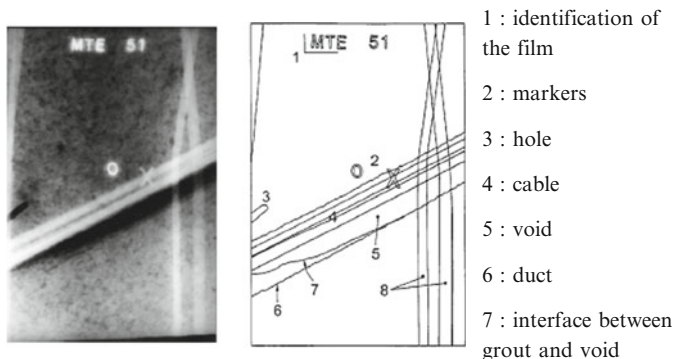
1 : identification of the film

2 : markers

3 : hole

4 : cable

5 : void

6 : duct

7 : interface between grout and void

Fig. 2.3 An example of radiogram and interpretation – sounding of an internal tendon [NF A 09-202]

The use of radioactive sources being very hazardous, specifically trained and accredited persons for implementing the technique and for protection aspects are required. A protection area must be defined around the sounded structure and it is necessary to move away all the persons from it, during the entire test. It can be disturbing for the users, particularly if the structure is a flat building.

11.3 Guidelines, references and standards

NF A 09-202 : principes généraux de l'examen radiographique, à l'aide de rayons X et gamma, des matériaux béton, béton armé et béton précontraint

NF EN 1330-3 : Essais nos destructifs – Terminologie – Partie 3 : Termes pour le contrôle radiographique industrielle (indice de classement : A09-020-3)

BS 1881: Part 205, Recommendations for radiography of concrete, British Standards Institute, London, 1986.

11.4 Calibration and interpretation of results

The optical density related to the grey levels of the sensitive film is analysed. The quality of the images is generally good because the attenuating characteristics of steel, concrete, and air differ greatly (Fig.2.3).

The radiographic techniques can provide very useful information because of their ability to observe cross-sectional images of the object. They are applicable for every kind of concrete structures. However, these methods currently pose the problem of safety and other limitations. With further advancements in portable radiography equipment for field applications, such devices could have widespread use. In particular, safety increasing, and imaging speed advances to permit practical scanning rates should greatly improve the technique.

11.5   Reliability and limitation of results

Despite its high interest of providing an image of the internal structure of concrete, radiography has several limitations:

– Being a technique by transmission, two faces of the structure must be accessible
– Depth limitation: 60 cm for penetration of gamma rays is a limit, but 120 cm can be reached with X-rays
– Only small surfaces can be sounded due to the limited size of sensitive film
– The time of exposure is rather long (especially for gamma-rays)
– Steel bars (cables or reinforcement bars) can mask the target
– Important weight of the usual radiation sources can prevent the investigation of some parts of a structure
– The use of radioactive source being hazardous, a safety area is required around the structure. It is sometimes impossible to restrain the access of the surroundings
– The implementation of the technique is expensive if very large areas need to be sounded (especially with X-rays). For this reason, radiography is sometimes relegated for use in specific conditions only
– The image does not provide any information about the depth of the defect.

References

Mitchell T.M. (1991) Radioactive/Nuclear Methods, in *CRC Handbook on Non Destructive Testing of Concrete*, Malhotra and Carino Editors, CRC Press, 1991, p 235.
Roenelle P. (2005) Méthodes radiographiques d'évaluation non destructive, Chapter B7, in Méthodologie d'évaluation non destructive de l'état d'altération des ouvrages en béton armé, Ed. D. Breysse et O. Abraham, Presses de l'Ecole Nationale des Ponts et Chaussées, pp. 305–328.

12   Rebound hammer

Markus Fischli and Andrzej Moczko

The Rebound Hammer was developed in 1948 and patented in 1950 by Ernst Schmidt, a Swiss engineer. The device is based on the rebound principle, which is an indicator of the hardness of concrete. In the rebound hammer test, a spring loaded mass has a fixed amount of energy imparted to it by extending the impact spring to a fixed position, this is achieved by pressing the plunger against the surface of the concrete under test. Upon release, the mass impacts on the plunger, rebounds and the distance traveled by the mass expressed as a percentage of the initial extension of the spring, is called the rebound number. The rebound distance is measured on an arbitrary scale marked from 10 to 100 (Kolek, 1958, Carino, 1974). Schmidt

standardized the hammer blow by developing a spring-loaded hammer and devised a method to measure the rebound. Several models of the device were built (Greene, 1954) and patented, with further developments.

12.1   Physical Principle and Theory

The Rebound Hammer (Proceq, 2007a) is principally a surface hardness tester. With this instrument the user presses a plunger against the surface under test and a spring then releases a mass to impact on the plunger. Inside the instrument a spring provides a defined impact energy for each measurement. After the impact the mass rebounds a certain distance and this is shown on the scale by a pointer. Before removing the instrument from the concrete element the impact mechanism can be locked by the locking button and the rebound value R be read. The position of the pointer indicates the rebound as a percentage of forward hammer travel. Equation 1 explains how the rebound value R is calculated:

$$R = 100 \cdot \sqrt{\frac{E_{reflected}}{E_{forward}}} = 100 \cdot \sqrt{\frac{1/2 D x_R^2}{1/2 D x_0^2}} = 100 \cdot \frac{x_R}{x_0} \tag{1}$$

where D is a spring constant, E_{forwar} is the energy before the impact, $E_{reflected}$ is the energy following the impact, x_0 is the displacement at triggering of impact and x_R is the displacement following the impact (rebound distance).

Figure 2.1 shows the moment of the impact of the hammer mass 14 on the plunger 1. Other main parts are impact spring 16, the pawl 13 which releases the hammer mass, and pointer 4.

The most suitable surfaces for testing by this method are vertical faces of the concrete structure, which means the impact is produced in horizontal direction. Impact directions up and down on horizontal surfaces plus at angles of 45° up and down are also possible. For these measurements a correction of the measured values due to gravity has to be considered.

The classic "R"-value is the mechanical travel of the hammer mass on rebound. It is affected by its friction on the guide rod, the friction of the drag pointer on the scale, the influence of gravity during its travel, the relative velocity between unit and mechanical parts. The R value is measured as characteristic of the energy that is not absorbed by the material under test.

Some years ago a development led to a new instrument that combines innovative ideas with the advantages of the classical rebound hammer. The new instrument (Proceq, 2007b) measures the velocity of the hammer mass immediately before and after the impact and calculates the quotient Q (Fig. 2.2, Eq. 2). Based on the same physics the measurement is not affected by friction between hammer mass and guide rod and the one of the pointer and there is no need to
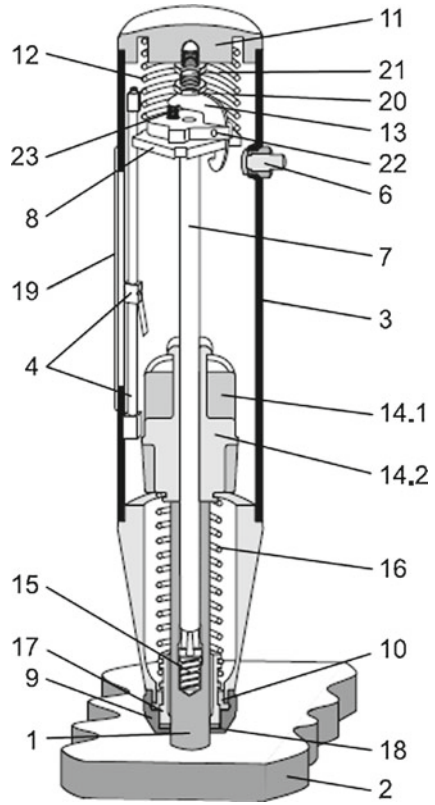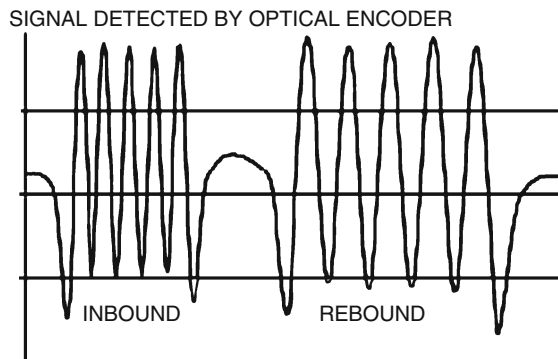
Fig. 2.1 Sectional view
of Concrete Test Hammer
Model

Fig. 2.2 Signal detection

SIGNAL DETECTED BY OPTICAL ENCODER

INBOUND   REBOUND

compensate for the impact direction. Equation 2 explains how the rebound value R is calculated:

$$Q = 100 \cdot \sqrt{\frac{E_{reflected}}{E_{forward}}} = 100 \cdot \sqrt{\frac{1/2mv_R^2}{1/2mv_0^2}} = 100 \cdot \frac{v_R}{v_0} \tag{2}$$

where the rebound value Q is expressed as a function of the respective kinetic energies before ($E_{forward}$) and after ($E_{reflected}$) the impact. These two quantities depend on the mass m of the hammer and on the respective velocities immediately before (v_0) and after (v_R) the impact.

An ergonomic housing accommodates the impact mechanism and the optical absolute velocity encoder that measures the velocity of the hammer mass. There are integrated electronics as well as the LCD that process the data and display the concrete strength plus all other information of the measurement series. The impact spring initiates an impact of the hammer mass on the plunger. According to the surface hardness of the concrete element the rebound velocity of the hammer mass is lower or higher.

12.2 Measuring Equipment and Handling

The Rebound Hammer is a portable instrument that can easily be operated by one person. Inside the cylindrical housing there is the impact mechanism that activates the plunger which protrudes from the housing on the front end. The plunger has to be pressed perpendicularly against the surface of the test specimen and the pressure has to be increased until the hammer impacts. Inside the instrument the impact spring provides a constant impact energy for each measurement, which is 2.207 N.m for the normal (Type N) hammer. After the impact the mass rebounds a certain distance and this is shown on the scale by a pointer. Before removing the instrument from the concrete element the impact mechanism can be locked by the locking button and the rebound value be read. The position of the pointer indicates rebound as a percentage of forward hammer travel.

The instrument is immediately ready for the next measurement. The plunger can be placed on the desired measuring spot which according to the standards should be at least 25mm away from the previous one. The instrument is pressed towards the concrete surface. This unlocks the impact mechanism and the instrument housing is moved away from the structure under the force of the loading spring. At the end position the concrete test hammer is automatically loaded and ready for the next impact. Because of the influence of surface condition on test results, if the surface is too rough it should be smoothened with a grinding stone.

For structures with low strength and wall thickness below 100mm the Model L with smaller impact energy was developed. The normal energy would damage the structure or the reading could be affected. The instrument is basically the same but

Fig. 2.3 Typical digital Rebound Hammer

Fig. 2.4 Measurement with
the new device developed
(Q measurement)

the impact energy is only 0.635 N.m, i.e. one third of the one of the standard Model
N. For both types there are also the versions NR and LR that register the readings as
a graph on a paper roll.

In modern versions of rebound hammer an electronic measuring unit has been
added to help ensure proper test results which can be recorded for later review or
uploaded to a personal computer. The scale is replaced by a displacement sensor
which measures the rebound value. Impact direction, carbonation depth can be
entered in addition to other options and the unit is capable of direct statistical analy-
sis as shown in Fig. 2.3.

With the new device (Q measurement, Fig. 2.4), the measuring procedure is the
same as with the classic rebound hammer. The user can perform test series of a
specified number of impacts. Manual cancellation of obvious outliers is possible.
Operation with the "one button" user interface is simple. To obtain a reading in units
of compressive strength the user can select the desired unit, the length of the series
and the averaging mode, carbonation depth (if applicable), conversion curve for

concrete mixture and form factor. At the end of the series the instrument will display the average Q value converted to the desired concrete compressive strength unit. The instrument is suitable for testing a wide variety of concrete, mortar, rock on site as well as in the laboratory. It is handy for difficult to access or confined test areas (i.e. working overhead) and especially convenient for testing on tunnel linings as measurements are independent of impact direction.

12.3   Calibration and Interpretation of Results

An initial test series at the Swiss Federal Materials Testing and Experimental Institute (EMPA) was successful and application was made to patent the instrument world-wide. A correlation was developed between the compressive strength of standard cubes and rebound number. The first successful reports appeared in 1951. The new method of non-destructive concrete testing was acclaimed throughout the world. DIN 4240 was published in 1962 dealing with the SCHMIDT Hammer and its use.

However, as other investigators began to develop correlations between strength and rebound number, it became evident that there was not a unique relationship between strength and rebound number (Kolek, 1959). This lead to the often-stated recommendation that a correlation should be developed using the same concrete and forming materials as used in construction. Without such a correlation, the rebound hammer is useful only for detecting gross changes in concrete quality throughout a structure (Carino, 1994). The issues of reliability of the rebound measurement and of calibration are key issues.

The rebound number is first very sensitive to the very local properties of concrete, i.e. to the fact that the impact occurs just above an aggregate or a volume of cement paste. Thus, a series of measurements must be performed in a limited area around the same point, whose values are averaged such as to obtain a representative value for R. For instance, ASTM C 805 requires that 10 rebound numbers be taken for a test.

The first correction corresponds to the direction of impact (horizontal, vertical up and down), for which the calibration curve (which expresses the estimated compressive strength as a function of rebound number) must be shifted, as shown on Fig. 2.5. The test hammer symbols in the diagram indicate the impact direction and the respective conversion curve. In many countries cubes of 150x150x150mm are used as test specimens for which conversion curves are available as well.

A common factor that influences the reading is the carbonation of the concrete which starts from the surface and penetrates into the structure. Rebound numbers on a carbonated surface can be as much as 50% higher than non-carbonated surfaces. Correction factors have been proposed by (Tanigawa et al., 1988) and in japanese and chinese guidelines (AIJ, 1983, JGJ/T 23-2001), but their values are very different and the more efficient way to compensate for this effect remains the calibration of the rebound values against the strength of core specimens taken from the structure.

Fig. 2.5 Conversion curve for the average compressive strength measured on cylinders (φ150, H300mm)
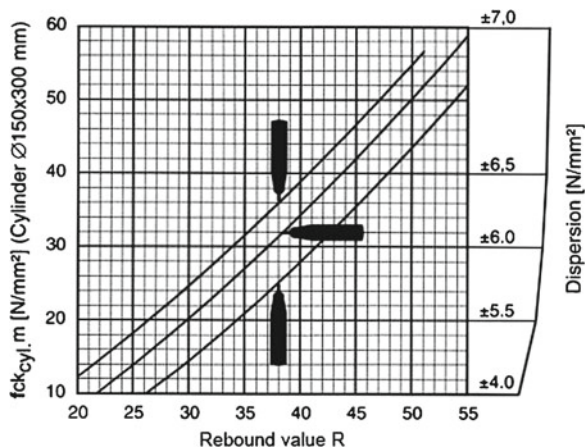
Many other factors have been recognized as influencing the rebound number, the most influent being (Evangelista et al., 2003):

– the moisture condition, a dry surface giving higher values,
– the surface texture, a smoother surface giving higher values than a rough one,
– the type of aggregate.

The influences of these factors are so great that it is very unlikely that a general calibration curve relating rebound hammer to strength, as provided by the equipment manufacturers, will be of any practical values, event by using a series of corrective coefficients. It is the reason why the EN 13791 has chosen a different approach for calibration: it gives a "basic curve" linking the rebound number and the estimated strength and the calibration process consists in shifting this basic curve accordingly to the results given by comparing the values of rebound number and true core strength measured at a given number of points. This calibration method does not explain why one has to shift the curve but is able to account for the effect of any influential factor.

On the innovative device which measures energy and gives a Q factor instead of R, the correlation between the Q value and the compressive strength of a concrete element is represented by another conversion curve which covers a large range of concrete strengths (from 10 MPa up to 100 MPa). The use of the device is easier because the effect of the direction of the test and that of the carbonation depth can be automatically corrected. The issue of calibration is however the same. A more precise derived compressive strength can be achieved by creating site specific (custom) conversion curves.

12.4   Reliability and Limitation of Results

Owing to its simplicity, speed and low cost the rebound hammer is, by far, the most widely used non destructive test device for concrete. Another main advantage of rebound measurement for strength estimation is that this technique has a more direct

Fig. 2.6 Test anvil with
hammer under test

link with mechanical properties of concrete than most others. But this simplicity can be misleading and results sometimes in careless handling. For instance, manual corrections for impact direction can occasionally be "forgotten". Such omissions are less likely with the improved electronic concrete test, since such corrections are made automatically, providing these have been switched on.

A periodic function test is indispensable, since concrete dust penetrates the instrument and can change the characteristics of the impact. A function test must be carried out on a calibrated test anvil Fig. 2.6 before and after important assignments. Every 1000 – 2000 test impacts, the instrument should be thoroughly cleaned and then checked on the test anvil. If the readings get smaller than the lower limit the mechanism of the hammer usually has to be cleaned which can be done by the user. If the readings persist to be too low the hammer needs re-calibration. This should be done by a certified service centre in order to perform the calibration in the right way.

The test anvil is standardized. EN 12504-2 specifies the steel block with a hardness of minimum 52 HRC, a mass of 16 ± 1 kg and a diameter of approximately 150 mm. Typical R-values are 81 for N-type and 75 for L-type hammers, tolerance is +/-2R. Each anvil is calibrated with selected Master Equipment and the calibration of Rebound hammers and anvils is traceable back to the Master Anvil.

According to the European standard a minimum of 9 dm^2 of concrete surface with 10 cm thickness is needed. The rebound hammer Model N can be used on surfaces of concrete elements of any direction that have a minimal thickness of 100mm and are fixed with the structure, or if the thickness is less the specimen must be rigidly supported or Model L must be used. Moreover, the temperature during the tests must be between 10 and 35°C.

Statistical evaluations of test results should also be performed according to national specifications and requirements.

The evaluation of concrete compressive strength using the rebound hammer gives in any case valuable information about the quality of concrete. Another application of this technique consists in the localization of the coring zone for optimizing the number of cores to be tested in a laboratory

However, there is a large variance in opinions as to the accuracy of estimating the compressive strength. In any case, the accuracy can be increased by performing a proper calibration, such as to reduce the main causes of bias. The FHWA guide (FHWA, 1997) states that for a properly calibrated device, the accuracy is +/- 15 to 20 percent for test specimens cast, cured and tested under laboratory conditions and that it is approximately +/- 30 to 40 percent for in place compressive strength. Malhotra considers that the uncertainty is more probably +/- 25% in a structure (Malhotra and Carino, 2004).

This variety of opinions is explained because experimental correlations and correlation curves have not been established in a standard context. The type of concrete, shape and size of reference specimens (cores taken from the structure or cubes or cylinders from the laboratory) have widely varied. More often carbonation and moisture have not been controlled. It results a wide variety of calibration curves, which are not strictly valid for extrapolation in a different context. It is the reason why another calibration approach is proposed by EN 13791, in which the exact correlation curve is not *a priori* known, but built on the basis of few additional destructive tests.

One also must note that since the rebound number is indicative of the near-surface properties of concrete (about 3 centimeters), it may be not indicative of the bulk concrete in a structure. It is influenced by local properties (air voids, higher content in cement, carbonation, effect of formwork and curing conditions…).

12.5   Guidelines for Use and Standards

The method is covered by several standard specifications including:

- ASTM C 805, Standard test method for rebound number of hardened concrete, in: Annual book of ASTM standard, ASTM C805-85, Detroit, 1994.
- BS 1881 - Part 202 - Recommendations for surface hardness tests by the rebound hammer, BSI, UK 1986.
- DIN 4240, Kugelschlagprüfung von Beton mit dichtem Gefüge, Richtlinien für die Anwendung, 4-1962.
- EN 12504-2, Testing concrete in structures – Part 2. Non destructive testing – determination of rebound number, 2001.
- EN 13791, Assessment of in-situ compressive strength in structures and precast concrete, CEN, Brussels, 28p., 2007.
- JGJ/T 23-2001, J 155-2001, Technical specification for inspection of concrete compressive strength by rebound method, 2001 (in Chinese).

Some guidelines are also available:

- AIJ, Architectural Institute of Japan, Manual of nondestructive test methods for the evaluation of concrete strength, p. 26, 1983 (in japanese)
- FHWA, Guide to non destructive testing of concrete, FHWA-SA-97-105, USDOT, Washington DC, 1997.
- Malhotra V.M., Carino N.J., Handbook on non destructive testing of concrete, CRC Press, 2004.

References

Carino N.J. (1994) Nondestructive testing of concrete: history and challenges, in ACI SP-144, Concrete Technology – Past, Present and Future, P.K. Mehta Ed., ACI, Detroit, MI, pp. 632–678.

Evangelista A.C., Shehata I., Shehata L. (2003) Parameters that influence the results of non destructive test methods for concrete strength, NDT-CE 2003, Berlin.

Greene G.W. (1954) Test hammer provides new method of evaluating hardened concrete, ACI J., vol 26, n. 3, pp. 249–256.

Kolek J. (1958) An appreciation of the Schmidt rebound hammer, Mag. Concr. Res., 10, 28, pp. 27–36.

Proceq S.A. (2007a) Product brochure Original Schmidt hammer.

Proceq S.A. (2007b) Product brochure SilverSchmidt hammer.

Tanigawa Y., Baba K., Mori H. (1988) Estimation of concrete strength by combined non destructive testing method, ACI SP 82, pp. 57–76.

13   Pull-out testing

Andrzej Moczko

This technique is the only not fully non destructive technique described in this section. It was however considered useful to describe it briefly, since (a) it is of common practice in structural assessment and (b) it provides an output directly correlated with mechanical properties of concrete. Thus, this test can bring valuable information on the material condition, either used alone or in combination with other (non destructive) techniques.

13.1   Physical principles and theory

The fundamental principle behind pull-out testing is that accurate estimation of the strength on-site can be obtained, as the peak-force (the pull-out force) correlates accurately to the concrete compressive strength measured by standard cylinders or cubes in the laboratory.

A metal insert is either cast into fresh concrete or installed into hardened concrete. When an estimate of the in-place strength is desired, the insert is pulled by means of a jack reacting against a bearing ring. The pullout strength is determined
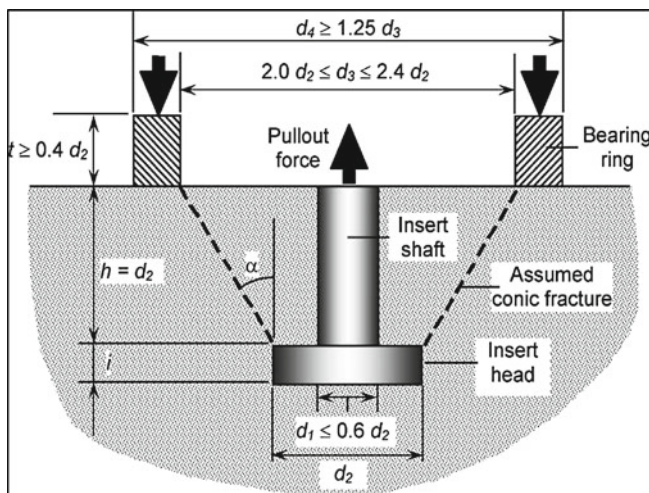
Fig. 2.1 General principles of the pull-out test

by measuring the maximum force required to pull the insert from the concrete mass. Alternatively, the insert is loaded to a specified load to verify whether a minimum level of in-place strength has been attained. It is essential to ensure that the dimensions of the pull-out test shall be determined according to Fig.2.1.

The diameter of the insert head ($d2$) is the basis for defining the test geometry. The insert head diameter shall be greater than or equal to 2/3 of the nominal maximum size of aggregate. A typical value is 25 mm. The thickness of the insert head and the yield strength of the metal shall be sufficient to prevent yielding of the insert during test. The sides of the insert head shall be smooth. The length of the pullout insert shaft shall be such that the distance from the insert head to the concrete surface (h) equals the diameter of the insert head ($d2$). The diameter of the insert shaft at the head ($d1$) shall not exceed 0.60 $d2$. The counter pressure ring shall have an inside diameter ($d3$) of 2.0 to 2.4 times the insert head diameter ($d2$), and shall have an outside diameter ($d4$) of at least 1.25 times the inside diameter. Usually diameter of such ring is assumed to be about 55 mm. The thickness of the ring (t) shall be at least 0.4 times the pullout insert head diameter. Finally, inserts are pulled out using a hydraulic pull machine reacting against a counter pressure ring and the force required to pull-out the insert is measured (Petersen, 1997, Petersen and Poulsen, 1993).

Internal rupture during pull-out test is a multistage process where three different stages, each with different fracture mechanisms, can be observed. In the first stage, at a level of about 30-40% of ultimate load, tensile cracking begins, starting from the notch formed by the upper edge of the insert's head. These cracks run out in the concrete at pronounced open angle (Fig. 2.2). The total length of these first cracks is typically 15-20 mm from the edge of the insert's head. In the second stage of internal rupture a multitude of stable microcracks are formed in the above mentioned truncated zone. These cracks run from the top of the insert's head to the

Fig. 2.2 Schematic damage
and cracking pattern during
the pull-out test
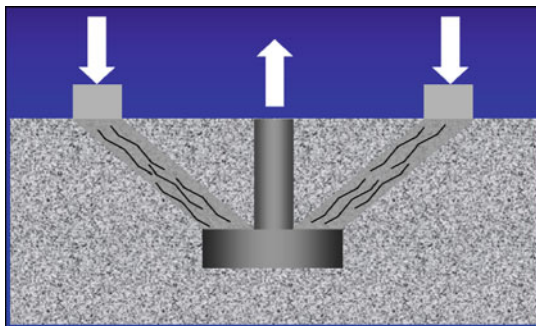
bottom of the counter pressure ring. The formation of this second cracking pattern
is similar to that of vertical microcracks inside a concrete cylinder or cubes during
ordinary uniaxial compression tests.

Finally, when the load reaches ultimate value, third stage of rupture occurs. This
forms a tensile/shear crack running all the way around from the outside edge of the
insert head to the inside edge of the counter pressure ring. Since the second micro-
cracking stage of rupture is responsible for and directly correlated with the ultimate
load in this testing procedure, it can be accepted that pull-out force is directly pro-
portional to the compressive strength of concrete (Krenchel, 1982, Krenchel and
Shah, 1985). Moreover, it can be observed that the failure obtained in such test is
caused by crushing of the concrete. This fracture mechanism has been also con-
firmed by nonlinear finite element analysis (Ottosen, 1981).

There are two basic categories of pull-out tests: one which involves an insert
having to be cast into the concrete and the other where the expanding ring insert is
fixed into a drilled hole and undercut groove in the hardened concrete.

The first procedure is mainly used to obtain a reliable estimation of the in-
place strength of concrete in newly cast structures, with following main
applications:

- determining whether in-place concrete strength is sufficient for early application
  of loads, such as due to formwork removal or application of prestressing.
- determining whether the in-place strength is sufficient for terminating curing and
  thermal protection.

The second pull-out procedure, based on the post-installed inserts, has been
developed for determining on site compressive strength of existing concrete struc-
tures. In this case following practical application can be considered:

- evaluation of the actual compressive strength in existing concrete structures
  during technical surveys,
- verification of in-place strength when strength of standard-cured specimens fails
  to meet acceptance criteria,
- testing of the residual strength of concrete elements prior to further loading,
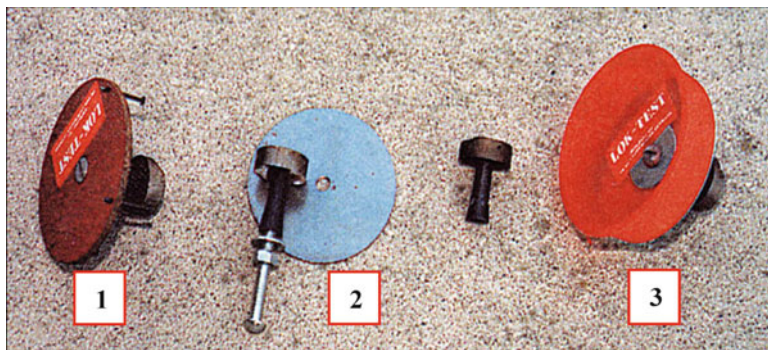- quality control of the structure after completion.

Fig. 2.3 Insert hardware

13.2 *Measurement equipment and handling*

In the case of testing focused on the estimation of the in-place strength of concrete in newly cast structures special inserts (Fig.2.2) have to be casted into the fresh concrete. Cast-in-place inserts shall be made of metal that does not react with cement. The insert shall consist of a cylindrical head and a shaft to fix embedment depth. The shaft shall be attached firmly to the center of the head. The insert shaft shall be threaded to the insert head so that it can be removed and replaced by a special bold relevant to pullout the insert. Such inserts can be installed as inserts nailed to formwork (Fig. 2.3 – type 1), as inserts attached to formwork cutouts (Fig.2.3 – type 2) or as floating inserts (Fig. 2.3 – type3). The inserts shall be embedded into the fresh concrete by means that ensure a uniform embedment depth and a plane surface perpendicular to the axis of the insert shaft.

Load is applied through a manually operated hydraulic pull-machine. The loading rate must be uniform, so that the nominal normal stress on the assumed conical fracture surface increases at a rate of 70 ± 30 kPa/s. For a pullout test system in which $d2 = 25$ mm and $d3 = 55$ mm, the specified stress rate corresponds to a loading rate of approximately 0.5 ± 0.2 kN/s. If the insert is to be tested to rupture of the concrete, the test is carried on until rupture occurs. If the insert is to be tested only to a specified load to verify a minimum in-place strength, the specified uniform rate is kept until the specified pullout load is reached. The specified load is maintained for at least 10 seconds. The pull-out force is recorded and correlated to compressive strength by means of a general calibration curve.

Application of pull-out technique for testing existing concrete structures needs different procedures of insert preparation. In the first stage, using special staff of equipment, a 18.4 mm diameter hole is drilled perpendicular to the surface, outside reinforcement disturbance. Next a recess (slot) is routed in the hole to a diameter of 25 mm and at a depth of 25 mm. A special split ring is inserted through the hole in the recess until it fits in the inside diameter of the recess and expanded by means of a special expansion tool (Fig. 2.4). Finally, the insert is pulled out using a pull

Fig. 2.4 Ring expansion
hardware

Fig. 2.5 Applying the
loading on the insert

machine reacting against a counter pressure ring (Fig. 2.5). As a result of the mea-
surements pull-out force is defined and similar procedure, as in the case of in place
casted inserts, is applied for determining concrete in-situ compressive strength.

13.3   Guidelines, references and standards

ASTM C900-06, Standard Test Method for Pullout Strength of Hardened Concrete.
ACI Committee 228, In-place Methods for Determination of Strength of Concrete,
    Technical Committee Document 228.1R-03, American Concrete Institute, PO
    Box 19150, Detroit, MI 48219, 2003, p. 44.
Canadian Standard CSA A23.2, Methods of Test and Standard Practices for
    Concrete, Test Procedure A23.2-15C – Evaluation of concrete strength in-place
    using the pullout test.
EN 12504-3: 2005, Testing Concrete in Structures, Part 3: Determination of „Pull-
    out" Force.
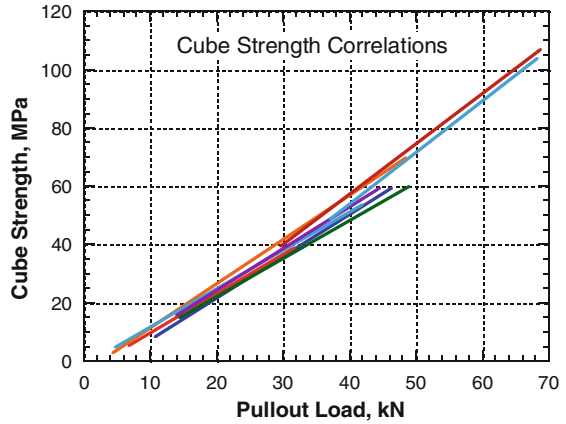
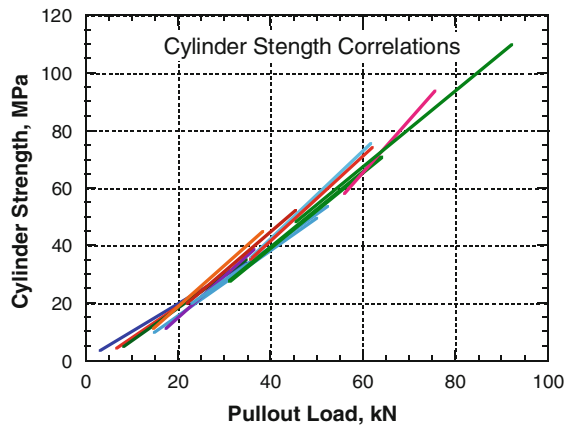**Fig. 2.6** Some examples of calibration curves for cubes

**Fig. 2.7** Some examples of calibration curves for cylinders

13.4 *Calibration and interpretation of results*

Several investigations have shown that the pull-out measurements provides an accurate estimate of in-place strength because the peak pullout force has a well-defined correlation to compressive strength measured using standard cylinders (Fig. 2.6) or cubes (Fig. 2.7).

More than 20 years of correlation experience from all over the world indicates close agreement, suggesting that one general correlation is applicable for all normal density concrete mixtures [(Bickley, 1982), (Carino, 1990), (Petersen and Poulsen, 1993), (Petersen, 1997)]. It is only for lightweight aggregate concrete and for mixes with maximum aggregate size larger than 40 mm that such relationships are not valid.

Fig. 2.8 General correlation
curves proposed by ACI
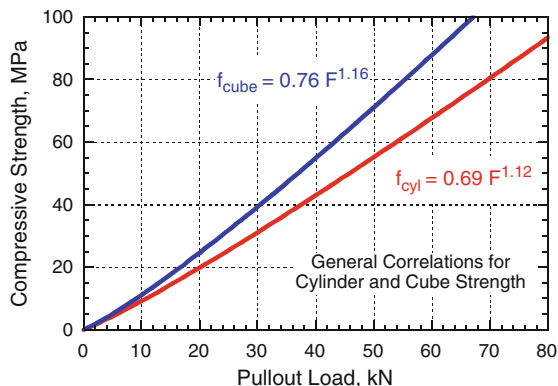
As an example, two following calibration equations can be assumed as a relevant approximation of the curves shown with relation to cube strength:

$$f_{c,cub} = 1.41\,P - 2.82 \quad \text{for strength under 50 MPa}$$
$$f_{c,cub} = 1.59\,P - 9.52 \quad \text{for strength over 50 MPa}$$

The general correlations shown in Fig. 2.8 is a more resent proposal of calibration suggested by (Carino, 1990) and recommended by equipment producer, providing sufficient accuracy for all normal density concrete mixtures. It is however necessary to mention that project specifications may require development of mixture specific correlations.

13.5   Reliability and limitation of results

Inserts shall be located in those portions of the structure that are critical in terms of exposure conditions and structural requirements. When pull-out tests are used for other purposes, the number of tests shall be determined by specification but at least 3 measurements for one testing area. Pull-out test locations shall be separated so that the clear spacing between inserts is at least seven times the pullout insert head diameter. Clear spacing between the inserts and the edges of the concrete shall be at least 3.5 times the head diameter. Inserts shall be placed so that reinforcement is outside the expected conical failure surface by more than one bar diameter, or the maximum size of aggregate, whichever is greater. It is not allowed to perform pull-out tests for frozen concrete.

Experience indicates that pull-out strengths are of lower value and more variable for manually-placed surface inserts than for inserts attached to formwork. In the case of post-installed inserts it is crucial to remove free-standing water from the hole at the completion of the drilling and undercutting operations. Protect the hole from ingress of additional water until completion of the test. Penetration of water into the failure zone could affect the measured pullout strength; therefore,

water must be removed from the hole immediately after drilling, grinding, and undercutting operations.

For concretes with a maximum aggregate size of 38 mm, tested by means of pull-out method, with assumption that the confidence level is equal to 95 % and for an average of at least 4 tests, the estimated compressive strength based on the general correlations indicated is within ± 6 % of the strength measured from standard specimen tests (cylinders or cubes). The average coefficient of variation for individual result is about 8% for normal density concrete.

If the range of tests results exceeds the acceptable range, further investigation should be carried out. Abnormal test results could be due to improper procedures or equipment malfunction. The user should investigate potential causes of outliers and disregard those test results for which reasons for the outlying results can be identified positively. If there are no obvious causes of the extreme values, it is probable that there are real differences in concrete strength at different test locations. These differences could be due to variations in mixture proportions, degree of consolidation, or curing conditions.

References

Bickley J.A. (1982) The Variability of Pullout Tests and In-Place Concrete Strength, Concrete International, ACI, Vol. 4, No. 4, April 1982, pp. 44–51.

Bickley J.A. (2009) A brief history of pull-out testing with particular reference to Canada – A personal journey, Proc. 10th ACI Int. Conf. on Recent Advances in Concrete Technology and Sustainability Issues, Seville, Spain, oct-2009, SP-261-20, pp. 277–286.

Carino N.J. (1990) Statistical methods to evaluate in-place test results, RILEM, Testing during concrete construction, Chapman & Hall.

Krenchel H. (1982) Lok-strength and Capo-strength of concrete, ABK publication, Serie I, 71, Structural Research Laboratory, Techn. Univ. of Denmark, Lyngby.

Krenchel H., Bickley J.A. (1987) Pull-out testing of concrete-Historical background and scientific level today, The Nordic Concrete Federation, No.6.

Krenchel H., Shah S.P. (1985) Fracture analysis of the pullout test, Materials and Structures, RILEM, Vol.18, No 108.

Malhotra V.M., Carrette G. (1980) Comparison of Pullout Strength of Concrete with Compressive Strength of Cylinders and Cores, Pulse Velocity and Rebound Number, ACI J., Vol. 77, No. 3, May–June 1980, pp. 161–170.

Ottosen N.S. (1981) Nonlinear Finite Element Analysis of a Pull-Out Test, Journal of the Structural Division, Proc. ASCE, Vol. 107, No ST4, USA.

Petersen C.G., Poulsen, E. (1993) Pull-out Testing by LOK-test and CAPO-test with particular reference to the in-place concrete of the Great Belt Link, Revised Edition, November 1993.

Petersen C.G. (1997) LOK-TEST and CAPO-TEST Pullout Testing – Twenty Years Experience, Proc. Int. Conf. NDT-CE, British Institute of Nondestructive Testing, U.K., J.H. Ed. by J.Bungey, Liverpool, 8–11 April 1997, pp. 77–96.

Soutsos M.N., Bungey J.H., Long, A.E. (2005) Pullout Test Correlations and In-Place Strength Assessment The European Concrete Frame Building Project, ACI Materials Journal, Vol. 12, No. 6, Nov-Dec 2005, pp. 422–428.

Stone W.C., Carino N.J., Reeve C.P. (1986) Statistical Methods for In-Place Strength Prediction by the Pullout Test", ACI Journal, Vol. 83, No. 5, Sept-Oct. 1986, pp. 745–755.

Yun C.H., Choi K.R., Kim S.Y., Song Y.C. (1988) Comparative evaluation of non-destructive test methods for in-place strength determination, ACI Special Publ., SP 122-6, 1988, Detroit, USA.